# ANALYSIS OF THE DYNAMICS OF VASOMOTION USING LASER DOPPLER FLOW

by

SHRUTHI ANANTH RAJ

Presented to the Faculty of the Graduate School of

The University of Texas at Arlington in Partial Fulfillment

of the Requirements

for the Degree of

MASTER OF SCIENCE IN BIOMEDICAL ENGINEERING

THE UNIVERSITY OF TEXAS AT ARLINGTON

August 2005

ACKNOWLEDGEMENTS

I wish to express my heartfelt gratitude to Dr. Martin H. Kroll, Director, Clinical Chemistry & Core Lab, Pathology & Laboratory Medicine, Veterans Affairs Medical Center, Dallas for providing me with an excellent opportunity to work under his able guidance. His tremendous enthusiasm towards research, commitment, and expertise in myriad subjects has influenced me a great deal.

I would like to thank Dr. Khosrow Behbehani, Professor and Director, Department of Biomedical Engineering at UTA and Dr. Karel J. Zuzak, Assistant Professor, Department of Biomedical Engineering at UTA for taking time off their busy schedules and assisting me with valuable suggestions.

I also take this opportunity to thank Krishnakumar Ramalingam and Ganesh Balakrishnan for helping me in this endeavor. My sincere thanks to all the faculty, staff and friends, who directly or indirectly, contributed towards my effort. The volunteers who participated in the skin blood flow study deserve special mention.

My parents, Mr. Ananth Raj and Mrs. Indira Raj, and my sisters, Shriya and Shamitha have constantly supported and encouraged me in word and spirit. I owe everything to their best wishes and God's blessings.

June 3, 2005

ABSTRACT

ANALYSIS OF THE DYNAMICS

OF VASOMOTION USING

LASER DOPPLER

FLOW

Publication No. _____

Shruthi Ananth Raj, M. S.

The University of Texas at Arlington, 2005

Supervising Professor: Martin H. Kroll

Vasomotion is a phenomenon caused by changes in the diameters of blood vessels. It is due to the contractile activity of small arteries and arterioles resulting in periodic changes of blood flow in the skin. These flow variations in the arteries are reflected by the Laser Doppler Flowmeter.

The goal of the skin blood flow (blood perfusion) study is to establish a method to analyze and quantify the pattern of vasomotion as detected using Laser Doppler Flow (LDF). Spectral analysis of the LDF signal reveals the presence of periodic components

in the vascular system. The study involves twelve subjects of which six subjects are normal and six subjects have a history of vascular diseases. Peaks occurring between frequencies 0 Hz – 0.2 Hz are isolated from the power spectrum and various prime number series are generated. The skew of the series is significantly different for normal and diseased subjects ($\alpha = 0.05$) and examination of peak height as a function of frequency (odds ratio = 4) is a distinguishing factor for the two subject populations.

The high level of order and structure seen in the microvasculature is elucidated by way of phase plane analysis and singular value decomposition (SVD). Normal subjects exhibit dynamic phase plots while diseased subjects have lesser complicated patterns. Statistical testing of the singular values shows significant differences between the two groups (F-test and Mann – Whitney test at $\alpha = 0.05$) suggesting the loss or change of one or more physiologic components in the vascular system of the diseased subjects.

TABLE OF CONTENTS

ACKNOWLEDGEMENTS..... iii

ABSTRACT ..... iv

LIST OF ILLUSTRATIONS..... ix

LIST OF TABLES..... xiii

Chapter

1. INTRODUCTION……. 1

1.1 Vasomotion……..... 1

1.1.1 Methods of study of vasomotion…….. 2

1.1.2 Previous studies of vasomotion…… 3

1.1.3 Resistance to blood flow…….. 5

1.2 Laser Doppler Flowmeters ..... 9

1.3 Theory of Spectral Analysis, Singular Value Decomposition and Phase Plane Analysis..... 12

1.3.1 Spectral Analysis……... 12

1.3.2 Singular Value Decomposition……. 14

1.3.3 Phase Plane Analysis……. 15

1.4 Vascular Diseases……. 23

1.4.1 Atherosclerosis…….. 24

1.4.2 Hypertension……. 26

1.4.3 Dyslipidemia……. 28

1.4.4 Diabetes Mellitus…….. 30

2. METHODS……..... 34

2.1 Instrumentation……..... 34

2.1.1 Theory of Laser Doppler Flow ..... 34

2.1.2 Periflux PF 3 Laser Doppler Perfusion monitor ..... 45

2.2 Operation…….. 53

2.2.1 Subject Demographics……... 53

2.2.2 Study Protocol……... 54

2.2.3 Experimental Set-Up……. 55

2.3 Data analysis using power spectrum…… 61

2.4 Data analysis using phase plane and SVD…….. 62

3. RESULTS……..... 67

3.1 Results of power spectrum analysis..... 67

3.2 Results of SVD and phase plane analysis..... 87

4. DISCUSSION……..... 97

4.1 Discussion of spectral analysis results..... 99

4.2 Discussion of SVD and phase plane analysis results..... 104

5. CONCLUSIONS AND RECOMMENDATIONS FOR FUTURE WORK.. 106

5.1 Conclusions…….. 106

5.2 Recommendations for future work…….. 108

Appendix

A. DATA ANALYSIS ALGORITHM……. ..... 110

B. CONSENT FORM FOR SUBJECTS OF VASOMOTION STUDY…….. 112

REFERENCES ..... 120

BIOGRAPHICAL INFORMATION..... 125

LIST OF ILLUSTRATIONS

Figure Page

1.1 Vasomotion ..... 2

1.2 Representation of vascular network with tubes ..... 6

1.3 A generalized microvascular network..... 8

1.4 Ticking of the pendulum in various stages..... 16

1.5 Momentum vs. position for the pendulum at maximum displacement…… 17

1.6 Momentum vs. position for the pendulum at zero displacement…… 18

1.7 Phase space trajectory for one cycle of the pendulum…… 18

1.8 Phase space trajectories for the pendulum with different starting displacements……. 19

1.9 Effect of friction and air resistance on the pendulum……. 19

1.10 Depiction of attractor point……. 20

1.11 Depiction of limit cycle……... 21

1.12 Depiction of torus…… 22

1.13 Schematic summary of the natural history, morphologic features, main pathogenic events and clinical complications of atherosclerosis in the coronary arteries…… 25

1.14 Hypothetical scheme for the pathogenesis of essential hypertension……. 27

1.15 Depiction of lipid fractions……. 29

1.16 Synthesis and release of insulin……... 31

2.1 Output field from a multimode laser……... 35

2.2 Block diagram of the differential operation set-up……. 42

2.3 PF 3 Block diagram…… 45

2.4 Front panel of Periflux PF 3……..…… 55

2.5 Rear Panel of Periflux PF 3…… 55

2.6 Light probe used in LDF and EKG pads…… 56

2.7 Obtaining and reviewing patient data……. 58

2.8 Experimental set-up for collection of blood perfusion data……... 59

2.9 Blood flow perfusion…….. 59

2.10 Vector formation for phase plots…… 63

2.11 Final matrix for SVD calculation…… 63

2.12 Flow chart for data analysis…… 66

3.1 Raw data of blood perfusion vs. time for N1..... 67

3.2 Raw data of blood perfusion vs. time for N2..... 68

3.3 Raw data of blood perfusion vs. time for N3..... 68

3.4 Raw data of blood perfusion vs. time for N4..... 69

3.5 Raw data of blood perfusion vs. time for N5..... 69

3.6 Raw data of blood perfusion vs. time for N6..... 70

3.7 Raw data of blood perfusion vs. time for D1 (Hypertension)..... 70

3.8 Raw data of blood perfusion vs. time for D2 (Diabetes mellitus)..... 71

3.9 Raw data of blood perfusion vs. time for D3 (Diabetes mellitus)..... 71

3.10 Raw data of blood perfusion vs. time for D4 (Diabetes mellitus)..... 72

3.11 Raw data of blood perfusion vs. time for D5 (Diabetes mellitus)..... 72

3.12 Raw data of blood perfusion vs. time for D6 (Hyperlipidemia)..... 73

3.13 Power spectrum of N1…… 73

3.14 Power spectrum of N2…… 74

3.15 Power spectrum of N3…… 74

3.16 Power spectrum of N4…… 75

3.17 Power spectrum of N5…… 75

3.18 Power spectrum of N6…… 76

3.19 Power spectrum of D1…… 76

3.20 Power spectrum of D2…… 77

3.21 Power spectrum of D3…… 77

3.22 Power spectrum of D4…… 78

3.23 Power spectrum of D5…… 78

3.24 Power spectrum of D6…… 79

3.25 Part of the raw original data from D1…….. 85

3.26 Reconstructed pattern for D1…….. 85

3.27 Phase plot of vector X1 vs. X2 for subject N1……..…….. 87

3.28 Phase plot of vector X4 vs. X5 for subject N1…… 87

3.29 Phase plot of vector X7 vs. X8 for subject N1…… 88

3.30 Phase plot of vector X10 vs. X11 for subject N1…… 88

3.31 Phase plot of vector X1 vs. X2 for subject D1…… 89

3.32 Phase plot of vector X4 vs. X5 for subject D1…… 89

3.33 Phase plot of vector X7 vs. X8 for subject D1…… 90

3.34 Phase plot of vector X10 vs. X11 for subject D1…… 90

3.35 Comparison of means for normal and diseased subjects……. 92

3.36 Polynomial curve fitting for subject N1……...…… 95

3.37 Polynomial curve fitting for subject D1……... 96

5.1 Progression of disease in an individual……107

LIST OF TABLES

Table Page

1.1 Quantitative parameters of the vascular system ..... 7

2.1 Subject demographics for normal subjects..... 54

2.2 Subject demographics for diseased subjects ..... 54

3.1 Sample frequencies and peaks found in subjects N1 and N2…….. 80

3.2 Sample frequencies and peaks found in subjects N3 and N4…….. 80

3.3 Sample frequencies and peaks found in subjects N5 and N6…….. 80

3.4 Sample frequencies and peaks found in subjects D1 and D2…….. 81

3.5 Sample frequencies and peaks found in subjects D3 and D4…….. 81

3.6 Sample frequencies and peaks found in subjects D5 and D6…….. 81

3.7 Prime numbers and series in normal subjects...……... 82

3.8 Prime numbers and series in diseased subjects…… 83

3.9 Sum of peaks at various frequencies; their ratios & outcomes…… 86

3.10 Singular values for normal subjects…….... 91

3.11 Singular values for diseased subjects…….. 91

3.12 Mean, SEM and t-test values…….. 92

3.13 Rankings for observations of singular values in normal and diseased group……. 93

3.14 Standard deviation and F-test results…….. 94

# CHAPTER 1

# INTRODUCTION

## 1.1 Vasomotion

The classical definition of vasomotion is the alteration in the caliber of a blood vessel. The phenomenon, also known as angiokinesis, can occur in vivo and in vitro. Local changes in smooth muscle constriction and dilation cause rhythmic oscillations in the vascular tone [1]. This oscillation of the vascular tone, generated from within the vascular wall results in vasomotion. It is not a consequence of heartbeat, respiration or neuronal input. Vasomotion may serve as a protective mechanism during ischemia and is present in many tissues.

The first detailed report of vasomotion in the bat wing was made more than 150 years ago [2]. Vasomotion has been studied using intravital microscopic techniques in different animals and tissues such as bat wings, cat mesentery, hamster cheek pouch, dog omentum, rabbit ear, cat tenuissimus muscle, rat spinotrapezius muscle, cat sartorius muscle, and rabbit tenuissimus muscle [3].

Vasomotion is a difficult phenomenon to measure as it is not possible to define specific amounts of tone in the oscillating vessel and thence determine concentration-response curves unambiguously. Another issue is that vasomotion is unpredictable and hard to reproduce. Experimental animals occasionally cease to exhibit vasomotion for

varying periods of time and in vitro experiments fail because vasomotion cannot be replicated.

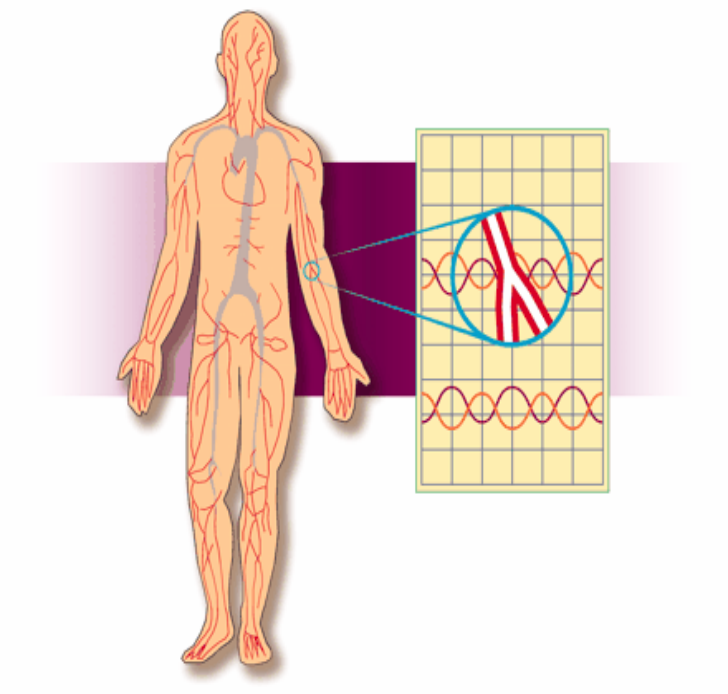

Figure 1.1 Vasomotion

*1.1.1 Methods of study of vasomotion*

- Vital microscopy: It is the traditional method in which the movements of blood vessels are directly observed. A skin window is implanted in the underlying tissue of the animal (awake) to inspect the blood vessels. In most cases, the animal is anesthetized [1].
- Pressure measurements: The pressure in the capillaries is obtained after direct cannulation to give a measure of the ratio of the pre- to post-capillary resistance.

The arteriovenous pressure difference is maintained constant during the measurement [1].

- Blood-cell velocity measurements: Maintaining a constant capillary diameter, the time taken by a cell to cover a certain distance along a capillary is measured which is proportional to the volume flow through the capillary. Since flow is determined by pressure gradient along the capillary, variations in flow reflect upstream conditions [1].
- Laser- Doppler flow measurement: When light from a strong, monochromatic source is back-scattered from moving objects, it undergoes a frequency shift (Doppler shift). An analysis of this back-scattered light from living tissues gives a relative measurement of blood cell movement and thus the average blood flow in a volume of tissue [1].

Investigators have characterized the dynamics of vasomotion as random or deterministic, usually chaotic or possibly periodic [24]. At the onset of this study, the type of dynamics was not decided.

### *1.1.2 Previous studies of vasomotion*

Even though microscopic techniques have been the standard for detection of vasomotion, new technology, represented by Laser Doppler Flow, facilitates the non-invasive observation of microvascular activity. Laser Doppler flow methods of measuring blood flow have been shown to be sensitive and specific enough to detect vasomotion similar to that observed by microscopic techniques [4]. Using the Laser

Doppler flow technique, investigators have shown that significant changes in blood flow patterns occur between normal subjects and those with peripheral arterial occlusive disease [5]. These observations have been confirmed by additional studies, showing the similarity between Laser Doppler devices and microscopic visual techniques [6]. Therefore, Laser Doppler flow represents a non-invasive technique for studying vasomotive activity in the microcirculation.

Vasomotion arises from the alternating constriction and relaxation of smooth muscle cells in arterioles rather than from a central source [7]. In recent years, studies have shown the endothelium to release Endothelium-Derived Relaxing Factors (EDRF) that causes smooth muscles in arterioles to relax, allowing increased blood flow [8]. The observations made with microscopic techniques have been simulated in the laboratory, using individual vessels, allowing the study of the effects of EDRF [8]. At present, the laboratory methods for assessing the effects of vasoconstriction and vasorelaxation by EDRF and other vasoactive agents entail the use of single-vessels dissected from laboratory animals.

Work by Griffith has shown the dynamics of vasomotion to demonstrate oscillatory behavior with some degree of periodicity [9]. This oscillatory behavior in individual arterioles probably forms the basis for the vasomotion. Oxidized Low Density Lipoprotein (LDL), a modified LDL, often found in subjects with increased risk for cardiovascular disease or stroke, inhibits EDRF (Nitric Oxide) mediated vasodilatation in coronary and peripheral arteries and in resistance arterioles [10]. Seifert showed distinctive differences in vasomotive patterns between normal subjects

and patients with peripheral arterial stenosis caused by atherosclerosis [5]. These studies imply that subjects with heart or vascular disease will demonstrate vasomotive patterns distinctly different from those of control subjects.

### *1.1.3 Resistance to blood flow*

The cardiovascular system is a form of circulation which collects blood in the large veins and forces it by the contraction of the heart through two vascular networks (pulmonary and peripheral) connected in series [11]. Arteries possess distensible properties and major pressure drop occurs in the arterioles. The flowing fluids develop internal friction resulting in resistance against flow. A pressure difference becomes necessary to overcome this resistance. The ratio of the change in pressure ($\Delta P$) and the resistance (R) gives the flow (Q) through the arteries.

$$Q = \Delta P/R \tag{1.1}$$

This is analogous to Ohm's law for electrical current. Flow is the volume ($\Delta V$) per time ($\Delta t$) flowing through the tube with a cross-sectional area (C).

$$Q = \Delta V/ \Delta t \tag{1.2}$$

The velocity (u) is the speed of individual elements which varies with the distance from the tubular axis and depends on the velocity profile. The mean velocity (U) multiplied by the cross-sectional area yields the flow.

$$Q = U * C \tag{1.3}$$

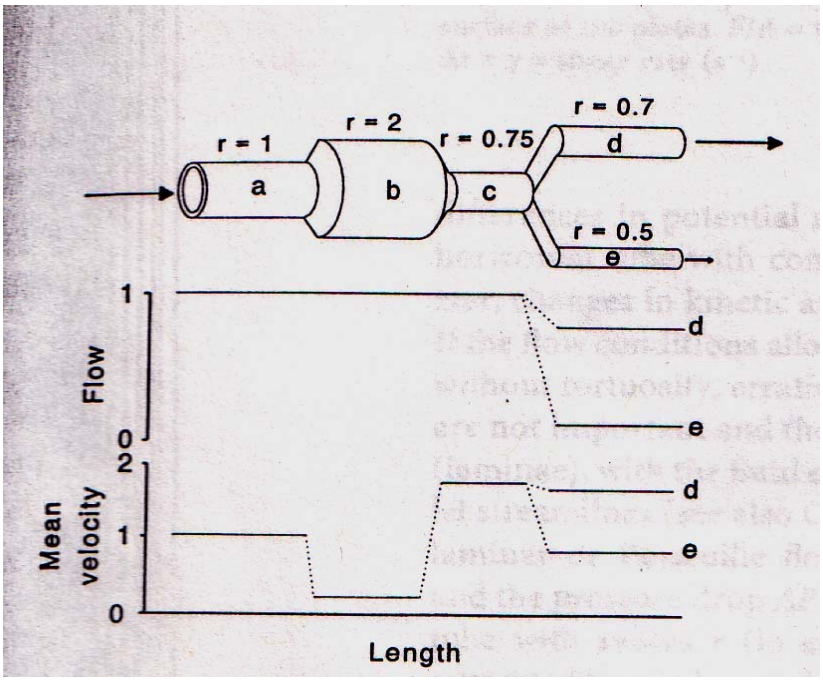


Figure 1.2 Representation of vascular network with tubes

The figure shows the continuity of flow through series-connected and parallel-connected tubes with different diameters (representing the vascular network). The flow through the tubes *a, b, c,* and *d* + *e* is identical, but the flow in *e* is approximately ¼ of flow in *d* since the diameter of *d* is *1.4* times that of *e*. This is in accordance with the Hagen-Poiseuille law which states that the conductance of a tube is proportional to the fourth power of radius.

In a system of series-connected tubes with various cross-sectional areas, the flow through the system is constant.

$$Q = U_1 * C_1 = U_2 * C_2 \qquad (1.4)$$

Thus, the velocity in tubular segments connected in series is inversely proportional to the cross-sectional area of the segments. The total resistance (R) is given by the sum of the resistances of the individual tubes.

$$R = R_1 + R_2 \ldots\ldots R_n \tag{1.5}$$

In parallel–connected tubes, since the individual tubular conductances add up to the total conductance, the total resistance is smaller than the lowest individual resistance.

Table 1.1 Quantitative parameters of the human vascular system

| Blood Vessels | Lumen diameter (mm) | Fraction of peripheral vascular resistance (%) | Intravascular blood volume[b] (%) | Total cross-sectional area ($cm^2$) |
|---|---|---|---|---|
| Aorta | 25 | 10 | 10 | 4 |
| Arteries | 3-10 | 10 | 10 | 50 |
| Arterioles | 0.03-0.2 | 50-55 | 10 | 700 |
| Capillaries | 0.04-0.02 | 30-35 | 4 | 4000 |
| Venoles | 0.01-0.1 | 5 | 70 | 3000 |
| Veins | 0.5-10 | 5 | 70 | 100 |
| Venacavae | 30 | 5 | 70 | 10 |
| Pulmonary artery | 25 | -- | 8 | 5 |
| Pulmonary capillaries | --[a] | -- | 8 | 5000 |
| Pulmonary veins | 12 | -- | 8 | 5 |

[a]No cylindrical capillaries around lung alveoli [11]

[b]Note that 8% of blood volume is in the four chambers of the diastolic heart [11]

The exact conditions do not exist in the vascular system for the Hagen-Poiseuille law, but it holds good for reasonable estimates of resistance to flow in the vascular system.

A generalized microvascular network with the terminal arteriole (ta), capillary (c), conducting lymphatic (l), terminal lymphatic bulb (tb) is shown in figure 1.3. The arrows show the direction of blood flow and lymph flow [11].

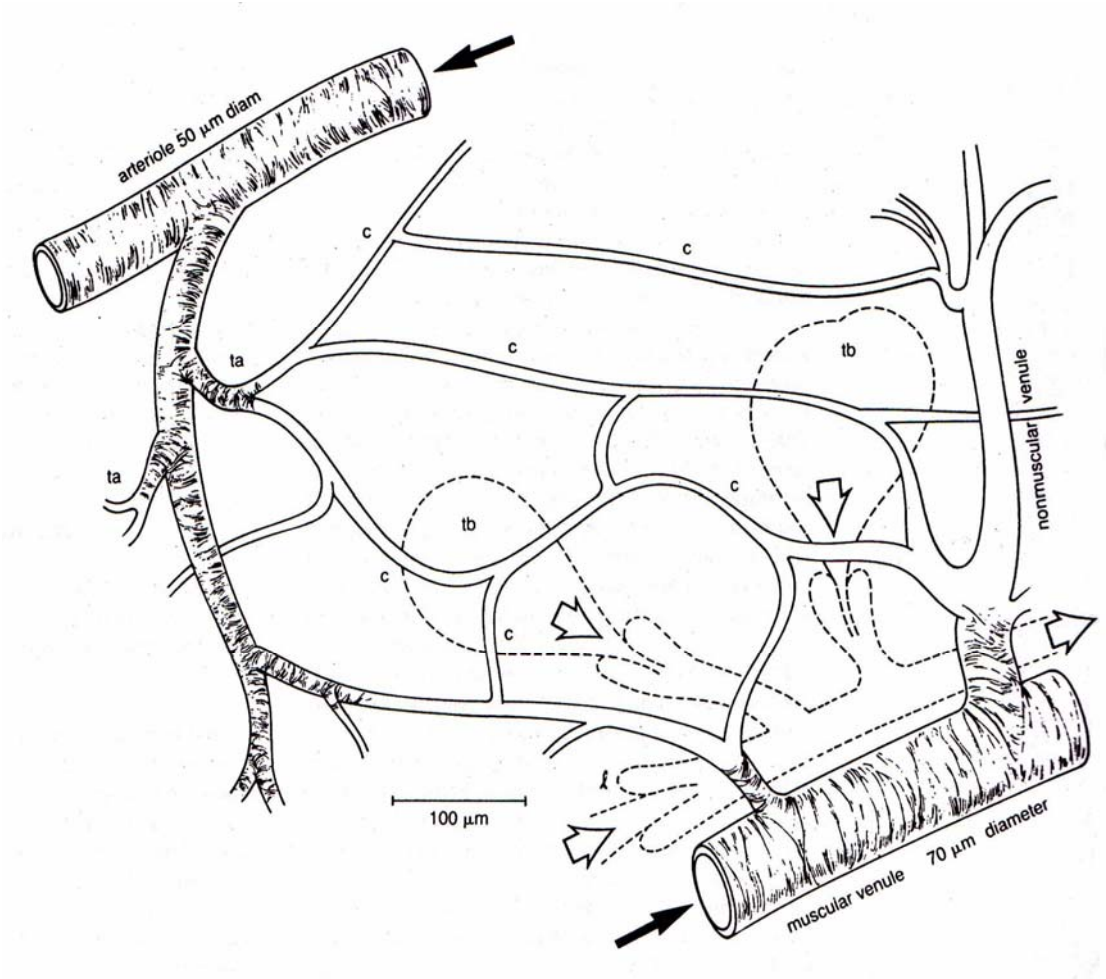


Figure 1.3 A generalized microvascular network

## 1.2 Laser Doppler Flowmeters

Laser Doppler flowmeters [12] are used to measure microvascular blood perfusion in tissues. The model used in this study is the Periflux PF3 from Sweden. In the LDF technique, a narrow beam of monochromatic light is generated by a low power laser. An optical fiber probe carries this beam to the tissue being studied. Light is partly absorbed and partly diffusely scattered by the illuminated tissue. Light hitting the static structures will remain unchanged but light hitting the moving blood cells will undergo a slight Doppler shift i.e., change in wavelength. The magnitude and frequency distribution of the Doppler shift are directly related to the number and velocity of blood cells but are virtually unrelated to the direction in which they move.

The measurement probe [12] incorporates three optical fibers, one of which carries the laser beam to the tissue. The two additional fibers capture and carry part of the illuminating beam which is back-scattered from the tissue to photodetectors where it is converted into electronic signals. A mixture of Doppler-shifted and non-shifted wavelengths make up back-scattered light. The Doppler shifted components are extracted from laser noise and other interfering frequencies by the double channel sensor in the flowmeter (a unique feature patented by Periflux). A cell-motion correlated signal called Flux which is free from background noise is thus produced.

| | | | | |
|---|---|---|---|---|
| Perfusion Or Blood Cell Flux | = | Number of blood cells moving in the measured volume | * | Mean velocity of these cells |

The Total Backscatter (TB) value is derived from the intensity of light picked up by the probe [12]. Light is reflected by hemoglobin at the wavelength of 632.8 nm. TB is related to tissue blood content and its value falls with the increasing erythrocyte number. The Concentration of Moving Blood Cells (CMBC) is proportional to the number of moving blood cells within the illuminated tissue volume [12]. Division of the Flux by CMBC gives the mean velocity of the moving blood cells.

Ordinary laser Doppler flowmeters underestimate the perfusion at high blood cell concentrations that may occur during routine clinical procedures. The Periflux has an integrated linearizer that ensures that the output signal is always proportional to blood cell Flux even at high blood cell concentrations in tissue. Flux represents the blood cell transport through the microvascular network i.e., from the arterial to the venous side and is integrated over the entire measured volume. In normal skin, this would be a hemisphere with a radius of 1 mm.

Laser Doppler flowmetry measurements are relative in nature. They are proportional to perfusion with a varying proportionality factor for different tissues. Calibration needs to be performed on the tissue on which the measurement is going to be done when one is utilizing the absolute perfusion number. This method, developed by Perimed allows the PF3 to display results as arbitrary digital units designated Perfusion Units (PU) which is directly related to a physical standard called *Motility Standard* [12]. It is based on the signal produced by the Brownian motion of a 0·5% suspension of 0·48μm diameter polystyrene microspheres at 20°C. When one is

studying the dynamics of perfusion, because the tissue elements and meter are constant, one is only interested in the change of perfusion and calibration is not necessary.

Laser Doppler flowmetry can be either noninvasive or invasive when desired and there are different probes for this purpose [12]. The angle and standard probes are used for surface measurements, hence suitable for skin blood flow measurements. For body cavities, the stainless steel probe is used whose position is guided by a micromanipulator. The needle probe is intended for deep tissue perfusion measurements whereas the bent tip probe is used to access nasal and oral mucosa. The other probes are endoscopic probe and suturable angle probe for use in the oral cavity. Different vascular depths can be reached by equipping the laser Doppler system with green, red and /or near-infrared laser light sources. The distance between the transmitting and receiving fibers also influences the measuring depth.

LDF has a variety of clinical applications [12]. In plastic and reconstructive surgery, it is used in monitoring perfusion in flaps and replanted digits. In angiology and vascular surgery, the degree and location of atherosclerosis in lower limb arteries can be evaluated at rest and during post-occlusive hyperemia by LDF. The effect of drugs on human and animal tissue perfusion is an important application of LDF in pharmacology. Vasoconstrictive or vasodilation responses in the microcirculation of skin (e.g. in diabetes) helps in assessment of functional and structural microangiopathy which is an aspect of internal medicine. In gastroenterology, combination with an endoscopic probe enables measurement of blood perfusion in the stomach, duodenum, colon and rectum. Other significant applications are in the areas of orthopedics,

dermatology, neurology and anesthesiology. The variations in microvascular blood flow can be followed during basal conditions or after provocations such as heat or occlusions.

## 1.3 Theory of Spectral Analysis, Singular Value Decomposition and Phase Plane Analysis

### *1.3.1 Spectral Analysis*

Any waveform can be analyzed as a combination of sine waves of various amplitude, frequency and phase. This method was developed by Fourier in 1807 and is called Fourier or spectral analysis. It is extremely useful as it breaks down the signal into constituent sinusoids of different frequencies.

Spectral estimation describes the distribution (over frequency) of the power contained in a signal, based on a finite set of data. The Fourier transform is a mathematical method that converts an input signal from the time domain to the frequency domain. The analog signal is converted into a discrete-time aperiodic signal by sampling with a period T. The angular sampling frequency is given by $\omega_s = 2\pi / T$. Theoretically, the signal in the time domain x(t) is written as a series of weighted Dirac functions [13]. Thus

$$x(t) = \sum_{n=-\infty}^{\infty} x(n)\partial(t - nT) \tag{1.6}$$

The Fourier transform of this equation is

$$X(\omega) = \int_{-\infty}^{\infty} x(t) e^{-j\omega t} dt \tag{1.7}$$

$$\text{Or} \quad X(\omega) = \int_{-\infty}^{\infty} \sum_{n=-\infty}^{\infty} x(n) \partial(t - nT) e^{-j\omega t} dt \tag{1.8}$$

Changing the order of integration and summation, we obtain

$$X(\omega) = \sum_{n=-\infty}^{\infty} x(n) e^{-j\omega nT} \tag{1.9}$$

If the data has N equally spaced samples, it can be evaluated using the fast Fourier transform (FFT) where N is usually a power of 2. The symmetry and periodicity properties of the complex exponential yields

$$W_N^{kn} = e^{-j(2\pi/N)kn} \tag{1.10}$$

where $W_N = e^{-j(2\pi/N)}$.

In the power spectrum, higher frequency components are located at greater distances from the origin. Evaluating the power spectrum is an excellent way to isolate periodic structural features in the data. As opposed to the frequency spectrum, the power spectrum does not show spatial or phase angle information.

Power spectra works with nonlinear dissipative systems; but in cases of chaotic systems, it may reveal limited information.

*1.3.2 Singular Value Decomposition*

Singular Value Decomposition (SVD) is an important noise reduction technique and was introduced as a complement to dynamical analysis by Broomhead and King [14]. SVD has many important applications in biology such as deconvoluting titrations involving a mixture of pH indicators, detecting structural intermediates, characterizing protein dynamics, expressing gene data, etc.

If A is an $r * d$ matrix with $r \rangle d$ (if $r \langle d$, the operation is carried out on the transpose), matrix A can be decomposed into a matrix product of the form

$$A_{r\times d} = W_{r\times d} * S_{d\times d} * U^{T}{}_{d\times d} \tag{1.11}$$

W and U are orthogonal matrices.

$$W^{T}{}_{d\times r} * W_{r\times d} = 1 \tag{1.12}$$

$$U * U^{T} = 1 \tag{1.13}$$

S is a diagonal matrix of non-negative elements that are the singular values of matrix A. By convention the singular values are denumerated in the descending magnitude.

$s_1 \geq s_2 \geq ..... \geq s_d \geq 0$

The decomposition can be affected through a number of numerical procedures. In dynamical analysis, the general theorem of Golub is applied to a very specific matrix A, namely $E^N$, the matrix formed by embedding scalar data ($v_i$) in an N-dimensional embedding space.

$$A_{r\times N} = E^N = \begin{bmatrix} x_1 \\ x_2 \\ . \\ x_r \end{bmatrix} = \begin{bmatrix} v_1 & v_2 & . & . & . & v_N \\ v_2 & v_3 & . & . & . & v_{N+1} \\ . & . & . & . & . & . \\ v_r & v_{r+1} & . & . & . & v_{r+N-1} \end{bmatrix} \quad (1.14)$$

Using the theorem, there are matrices W, S and U such that

$$E^N = W.\ S.\ U^T \quad (1.15)$$

Thus, $E^N.U = W.\ S$

S is the diagonal matrix of singular values (squares of the Eigen values) and matrix U is a rotation in N-space.

SVD is a variation of principal component embedding and provides an alternate coordinate system for phase space reconstruction with important properties. Since the U matrix in SVD is orthonormal, it is purely a rotation. Distances between trajectory points are preserved by such projection. The net effect is to align each vector along a variable coordinate axis, rendering clearer portraits of the phase plane. Also, it cleans noise out of the initial set of vectors.

*1.3.3 Phase Plane Analysis*

Phase plane analysis provides a qualitative approach for studying dynamic systems. Every biological system has various variables influencing its behavior and phase plane analysis provides an interesting mode for ascertaining the relation between the diverse variables in the system. It is a graphical method for "solving" the set of differential equations that represent the system. An actual numerical solution cannot be obtained for a system of differential equations using phase plane analysis, but it gives a

good idea of how the system behaves over time. For a system of n first-order ordinary differential equations, the 2n-dimensional space consisting of the possible values of $(x_1, \dot{x}_1, x_2, \dot{x}_2, \ldots\ldots x_n, \dot{x}_n)$ is called its phase space. If n = 1, phase space is known as phase plane. Phase space is useful for demonstrating and visualizing the changes in the dynamical variables of a system.

In order to get a clear picture of phase space, the pendulum system is considered [15]. It is one of the most regular systems which acts periodically i.e., it returns to its initial condition again and again. The path of the periodic system must always return to the same point in phase space no matter how complicated the returning path is [15].

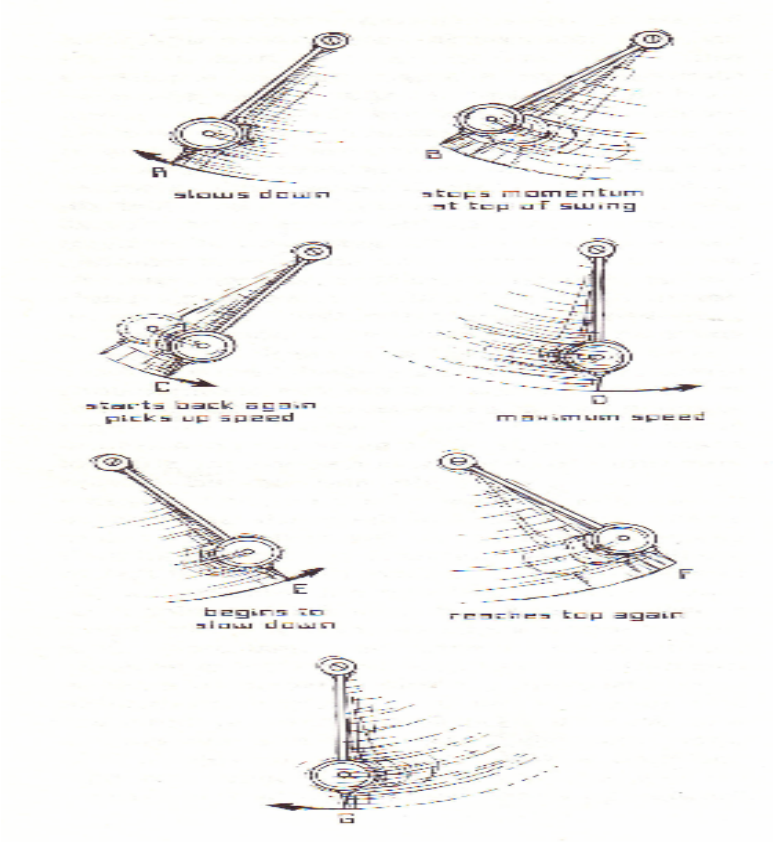


Figure 1.4 Ticking of the pendulum in various stages

The pendulum swings up to the left, slowing down as it moves, until for an infinitesimal second at the top of the swing it comes to rest and then returns, going faster. It reaches its maximum speed at the bottom of the swing and begins to slow down as it climbs to the right. The pendulum should go on swinging continuously in the absence of friction and air resistance. Since it swings back and forth in one direction, it has "one degree of freedom."

If we plot the instantaneous position *x* and velocity ν of the pendulum as a point in the plane (phase plane), with the horizontal and vertical axes representing x(t) and ν(t) respectively, we can generate phase plots. Each point in the x- ν phase plane represents an instantaneous state of motion (position and velocity) of the system. As the motion progresses, the representative point (phase point) traces out a path called the phase trajectory in the phase plane [15].

The top of the left swing is identified at B. The momentum (mass * speed) here is zero and the pendulum is at the farthest part of its swing (maximum displacement). The other point where the pendulum has zero momentum is at the right swing F.

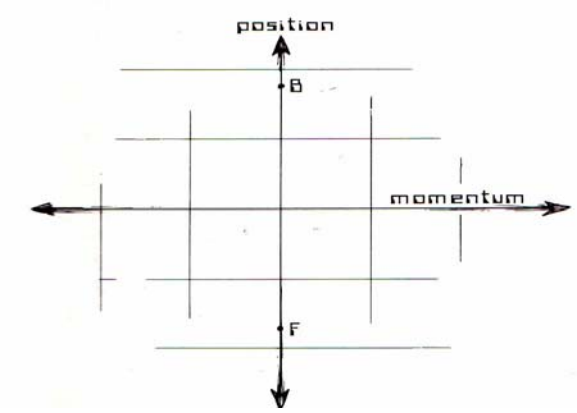


Figure 1.5 Momentum vs. position for the pendulum at maximum displacement

The two points where the pendulum is at its lowest point are D and G, with maximum momentum to the right and left respectively. Here, the displacement is zero and but its momentum is maximum.

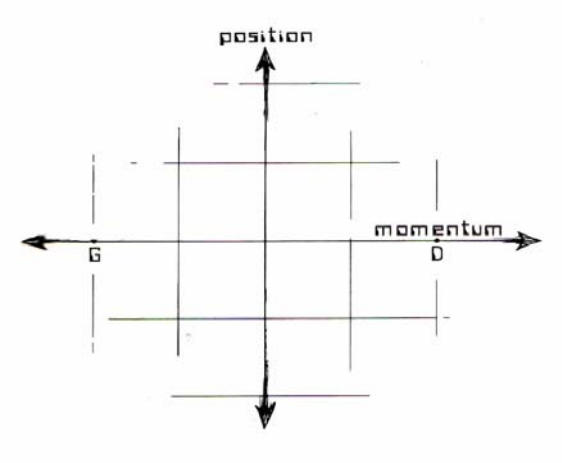


Figure 1.6 Momentum vs. position for the pendulum at zero displacement

The phase space trajectory representing the entire motion of the pendulum for one cycle is plotted. The phase map of a pendulum is a closed orbit because the plot repeats itself, cycle after cycle.

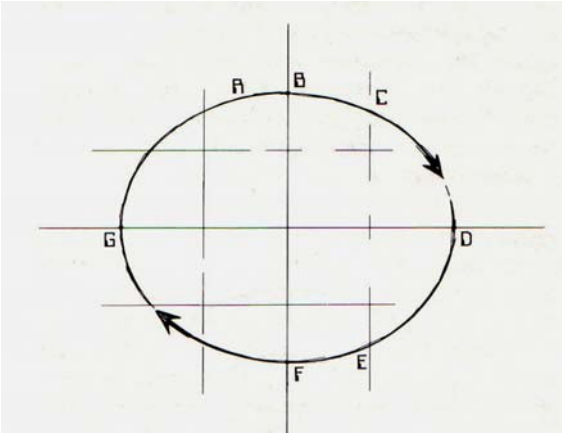


Figure 1.7 Phase space trajectory for one cycle of the pendulum

If the pendulum is given a stronger push at the start, the maximum displacement will be bigger and the trajectories for the pendulum can be drawn in the same phase map.

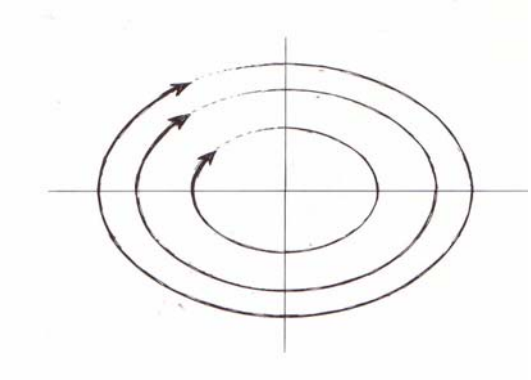

Figure 1.8 Phase space trajectories for the pendulum with different starting displacements

The above figures represent a pendulum in vacuum. Under ordinary circumstances, the pendulum eventually slows down due to friction and air resistance unless there is a motor to keep it going. This process of a periodic orbit's decay is represented by a phase space map. The central point shows the pendulum at rest (zero momentum and zero displacement).

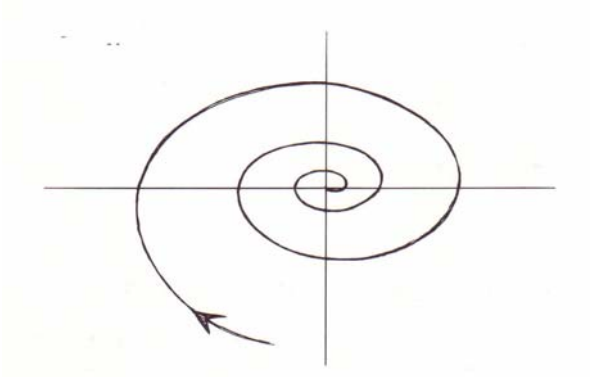

Figure 1.9 Effect of friction and air resistance on the pendulum

Also, every pendulum will eventually come to rest at this final displacement however great the initial displacement is.

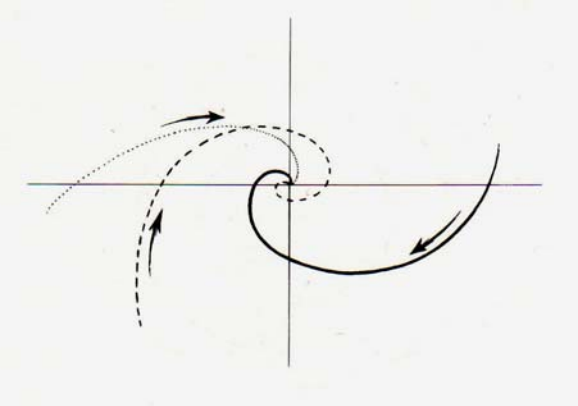

Figure 1.10 Depiction of attractor point

Since this point seems to attract trajectories to it, it is called an "attractor" point or a "fixed point attractor." An important concept in the world of order and chaos, an *attractor* is a region in phase space which exerts a magnetic appeal, pulling the system towards it.

Another important observation is that if the pendulum is given an additional push or momentarily damped, it eventually swings back to its original rhythm. The pendulum is drawn toward a cyclic path in phase space rather than being attracted to a fixed point. This path is called the "limit cycle."

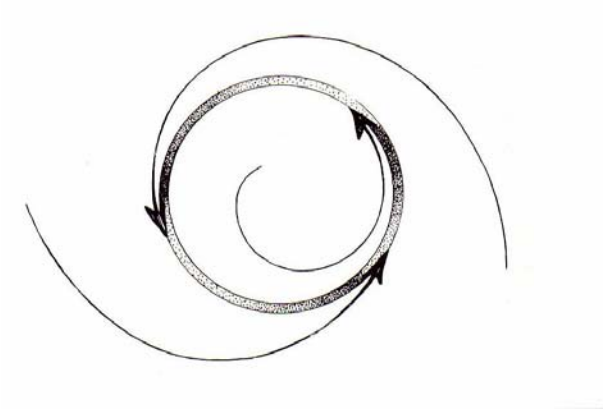

Figure 1.11 Depiction of limit cycle

An example for the limit cycle attractor is the predator-prey system formed in a lake stocked by trout and containing a few pike [15]. Initially, the pike have unlimited food supply of growing trout due to which the pike flourish and breed. As years go by, the pike number has ballooned at the expense of the trout. Since the food supply is reduced, the lake is overpiked and they begin to die out. Later, as the pike population drops, the trout multiply and stock the lake. Consequently, the pike numbers increase again. In this way, the oscillation between the predator (pike) and prey (trout) sets up a cycle. This situation is more complex than the pendulum because there is a collection of individuals, each one behaving randomly, yet all somehow creating a highly stable and organized system. The limit cycle is in a higher dimensional phase space.

The interaction of two predator-prey systems generates a doughnut-shaped figure called torus and plotting the dynamics of this larger two-cycle system creates a torus attractor. The advantage of the torus attractor is that any number of oscillators' combined motion can be represented on its surface thus making it multidimensional

(many degrees of freedom). If the periods or frequencies of two coupled systems are in a simple ratio, the twists around the torus join up exactly showing that the system is periodic.

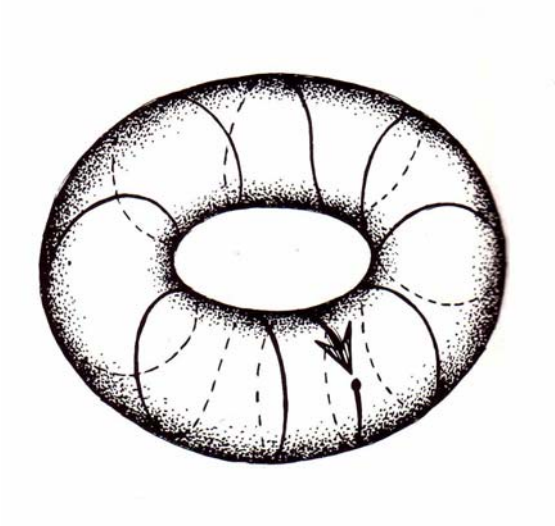

Figure 1.12 Depiction of torus

The problem with analyzing a system such as microvasculature as a dynamic system is that we do not possess a system of differential equations to describe our observations. Also, we do not know the character of the dynamic system as to whether it is linear or nonlinear, conservative or dissipative. Techniques devised for linear systems perform poorly with nonlinear systems. Furthermore, if the system is nonlinear and dissipative, most of the linear techniques fail. Phase plane analysis works well with linear, nonlinear, conservative and dissipative systems. It can provide insight into the structure of the equations describing the system as well as providing a qualitative understanding of the system dynamics.

Previous studies, such as work of Griffith, have shown that the behavior of afferent, muscular wall vessels possess both nonlinear and dissipative behavior. Also, there is no evidence that the microvasculature is reacting under a force (analogous to gravitational, spring or electrical force) or to a force field. Therefore, it is not possible to write down a simple set of differential equations in the form of a second-order differential linear system to describe the observed oscillations. Qualitative techniques provide a way to analyze the system.

## 1.4 Vascular diseases

Vascular diseases include any conditions that affect the circulatory system in the human body [16]. They affect arteries, veins and lymph vessels creating significant problems. The two principle mechanisms by which vascular abnormalities cause clinical disease are

- Narrowing or completely obstructing the lumens, either progressively (e.g. by atherosclerosis) or precipitously (e.g. by thrombosis or embolism)
- Weakening of the walls, leading to dilation or rupture

The arterial walls are generally thicker than the walls of the veins to withstand pulsatile flow and higher blood pressure in arteries. Arterial wall thickness gradually diminishes as the vessels become smaller, but the ratio of wall thickness to lumen diameter becomes greater. The basic constituents of the blood vessel walls are endothelial cells, smooth muscle cells (SMC) and extracellular matrix (ECM) including elastin, collagen and glycosoaminoglycans. The relative amount and configuration of

these basic constituents vary along the arterial system owing to local adaptations to metabolic and mechanical needs.

### *1.4.1 Atherosclerosis*

Arteriosclerosis is the term for thickening and loss of elasticity of arterial walls [16]. The most frequent pattern observed is atherosclerosis.

Atherosclerosis is characterized by lesions called fibrofatty plaques which protrude vascular lumens and weaken the underlying media. They develop primarily in elastic arteries (e.g. aorta, carotid and iliac arteries) and large and medium sized muscular arteries (e.g. coronary artery). Myocardial infarction (heart attack), cerebral infarction (stroke), aortic aneurysms and peripheral vascular disease (gangrene of the legs) are the major consequences of atherosclerosis.

In a typical case, the normal fatty streak occurs in the early 20's which gives rise to fibroatheroma and complicated lesions. These produce ischemia and infarctions (myocardial infarction and strokes).

Atherosclerotic plaques have three principle components which occur in varying proportions and configurations in different lesions.

- Cells, including SMC, macrophages and other leukocytes
- ECM, including collagen, elastic fibers and proteoglycans
- Intracellular and extracellular lipids

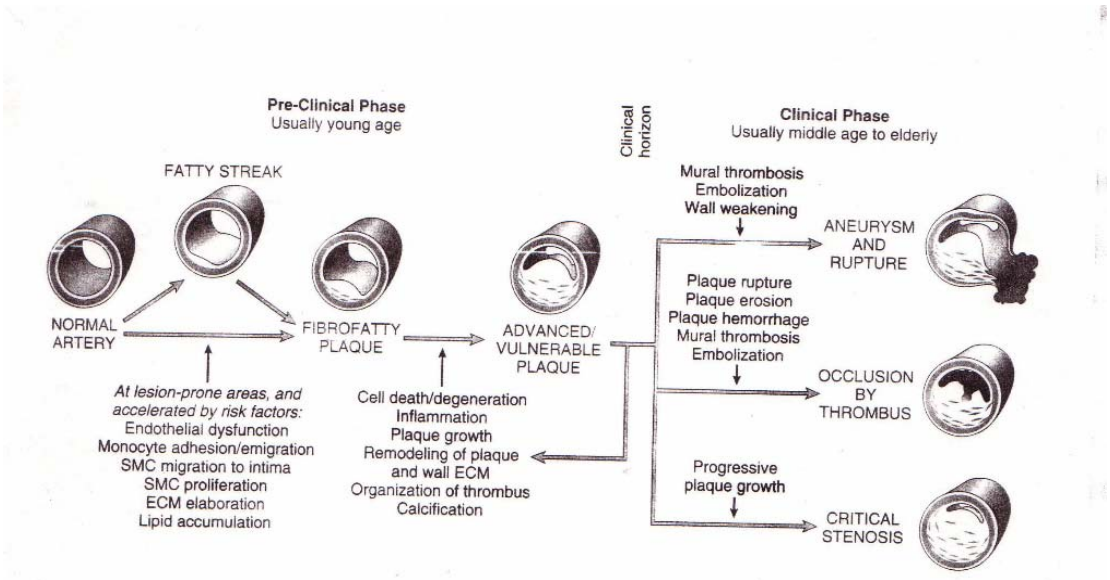


Figure 1.13 Schematic summary of natural history, morphologic features, main pathogenic events and clinical complications of atherosclerosis in coronary arteries [16]

Plaques continue to change and enlarge through cell death and degradation, synthesis and degradation of ECM and organization of thrombus undergoing calcification. The advanced lesion may undergo rupture, ulceration or erosion on the luminal surface. Hemorrhage, thrombosis and aneurysmal dilation are the other significant outcomes. Thrombosis causes ischemia of tissues and if there is complete occlusion of the vessels, infarction occurs (myocardial infarction, stroke, etc.).

Atherosclerosis is influenced by constitutional factors such as age, sex and genetics. The major risk factors are hyperlipidemia, hypertension, cigarette smoking and diabetes. Infarction is irreversible; the current thrust in medicine is prevention of the atherosclerotic process. To achieve this end, persons with clinically significant amount of atherosclerosis need to be identified before they are symptomatic or develop signs of the disease.

*1.4.2 Hypertension*

Hypertension is one of the vital factors for coronary artery disease and cerebrovascular accidents. It can lead to cardiac hypertrophy and potential heart failure, aortic dissection and renal failure [16]. The disease is complex and multifactorial with both genetic and environmental determinants. 95% of hypertension is idiopathic, called essential or benign hypertension and does not cause short-term problems. When controlled, it is compatible with long life and is asymptomatic unless complicated by a myocardial infarction or a cerebral accident. A small percentage, 5% of hypertensive people show a rapidly rising blood pressure which if untreated leads to death within a year. The clinical syndrome is characterized by severe hypertension, renal failure and retinal hemorrhage and is called accelerated or malignant hypertension.

The alteration of the relationship between cardiac output and total peripheral resistance causes arterial hypertension. Blood pressure is proportional to cardiac output and peripheral vascular resistance.

Blood pressure = Cardiac Output * Peripheral resistance

The level of blood pressure is determined by the interaction of multiple genetic, environmental and demographic factors. Cardiac output is dependant upon blood volume which is itself greatly influenced by sodium homeostasis in the body while peripheral vascular resistance is affected by neural and hormonal factors. Heart rate and contractility also influence cardiac output.

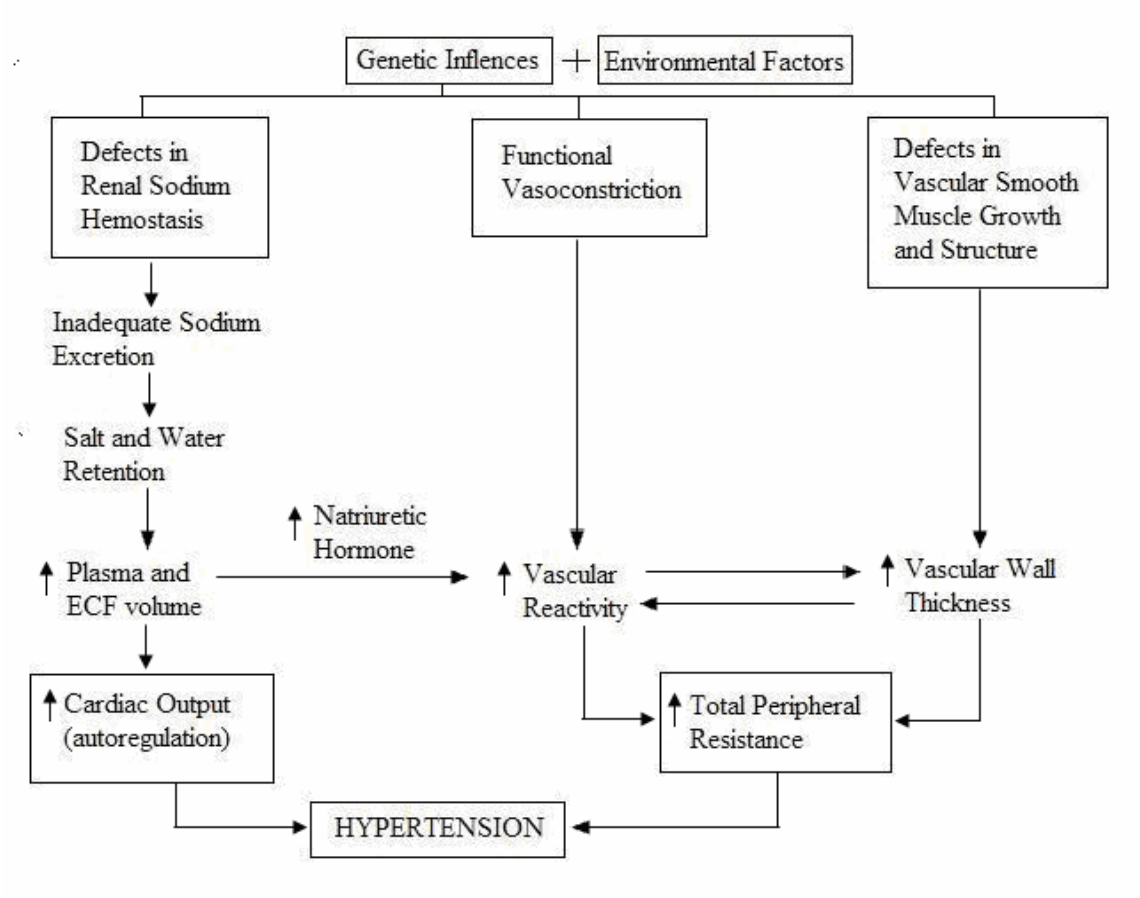


Fig 1.14 Hypothetical scheme for the pathogenesis of essential hypertension

The reduction of excretion of renal sodium, in the presence of normal arterial pressure may be the key event in initiating essential hypertension and also for the pathogenesis of hypertension. An increase in fluid volume as a result of decrease in sodium excretion would increase cardiac output and peripheral vasoconstriction thereby elevating blood pressure. When blood pressure is high, additional sodium would be excreted by the kidneys to equal intake and prevent fluid retention. Sodium excretion would become steady, but the blood pressure would also increase. The primary cause of

hypertension in an alternate hypothesis points to vasoconstrictive influences. This could cause structural thickening of the resistant vessels.

Exogenous factors implicated in hypertension are stress, obesity, smoking, physical inactivity and heavy consumption of salt. Hypertension causes degenerative changes in the walls of large and medium arteries that lead to aortic dissection and cerebrovascular hemorrhage. Thus, essential hypertension is multifactorial and results from the interaction of genetic and environmental factors influencing blood pressure.

Hypertension causes end-organ damage. It leads to renal failure, stroke, atherosclerosis and myocardial infarction. The effect of hypertension on arterioles is smooth muscle proliferation, narrowing of lumens and endothelial activation.

### *1.4.3 Dyslipidemia*

Dyslipidemia stands for the altered quantities of lipid fractions: elevated levels of Low Density Lipoproteins (LDL) or triglycerides, decreased levels of High Density Lipoproteins (HDL), either alone or in any combination.

Dyslipidemia activates the endothelium which leads to endothelial dysfunction. High blood pressure, diabetes and atherosclerosis (extreme form) are expressions of endothelial dysfunction. It is believed that endothelial dysfunction alters blood flow in the microcirculation and it is this microcirculation that we have measured.

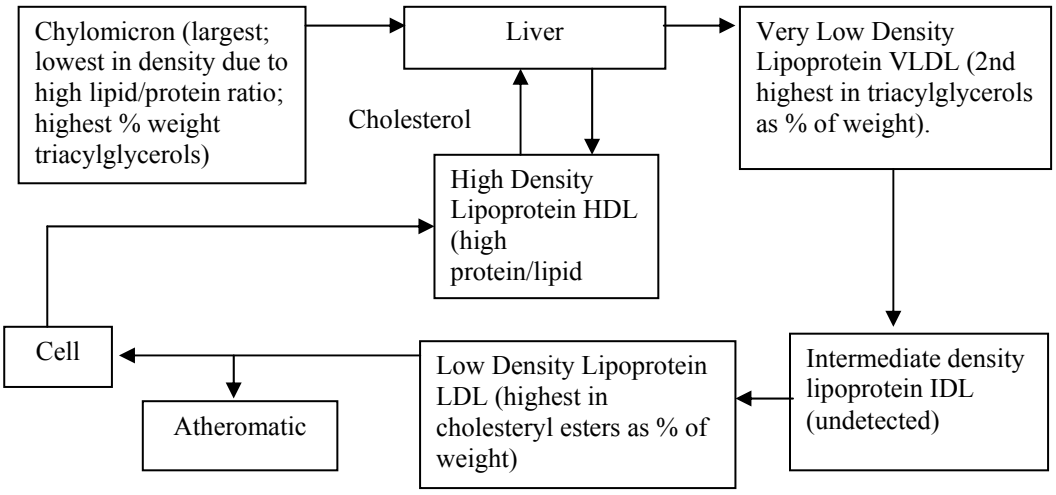


Figure 1.15 Depiction of lipid fractions

The major risk factors (cigarette smoking, low HDL, hypertension, family history, male sex and LDL) account for only about half of the variability in the coronary heart disease (CHD) risk in the USA population. The other factors are vital and they are called emerging risk factors. Persons with advanced subclinical coronary atherosclerosis are at greater risk for major coronary events than are persons with less severe atherosclerosis [37]. Tests are needed for atherosclerotic plaque burdens e.g. carotid sonography, coronary calcium. If we can identify blood flow patterns related to atherosclerotic burden, LDF would represent a noninvasive, reliable test.

*1.4.4 Diabetes Mellitus*

The islets of Langerhans are a microscopic cluster of cells in the endocrine pancreas weighing 1-1.5 gm and measuring 100-200 μm. They consist of four major cell types; β, α, δ and PP (pancreatic polypeptide) cells. The β cells produce insulin whose principal metabolic function is to increase the rate of glucose transport into certain cells in the body.

Diabetes Mellitus (DM) is a group of metabolic disorders characterized by high glucose levels which result from defects in insulin secretion or action or both (hyperglycemia). It is a leading cause of end-stage renal disease, adult-onset blindness and lower extremity amputations [36].

The normal values of blood glucose are in the range of 70-120 mg/dL. If an elevation in blood glucose is noted by any of the below mentioned three criteria, the person is termed diabetic.

- A random glucose > 200 mg/dL, with classical signs and symptoms
- A fasting glucose > 126 mg/dL on more than one occasion
- An abnormal oral glucose tolerance test in which the glucose is > 200 mg/dL two hours after a standard carbohydrate load

Depending on the pathogenesis of processes involved in the development of hyperglycemia, the majority of cases of diabetes fall into one of two broad classes.

Type 1 diabetes is characterized by an absolute deficiency of insulin caused by pancreatic β-cell destruction and accounts for approximately 10% of all cases.

Type 2 diabetes is caused by a peripheral resistance to insulin action and an inadequate secretory response by the pancreatic β-cells ("relative insulin deficiency"). Approximately 80% to 90% of patients have type 2 diabetes.

1.4.4.1 Regulation of insulin release

Preproinsulin is synthesized in the rough endoplasmic reticulum from insulin mRNA and delivered to the Golgi complex. A series of proteolytic cleavage steps in the golgi generate mature insulin and a cleavage peptide, C-peptide. Both insulin and C-peptide are then stored in secretory granules and secreted in equimolar quantities after physiologic stimulation.

The most important stimulus that triggers insulin synthesis and release is glucose itself which is depicted in the following figure.

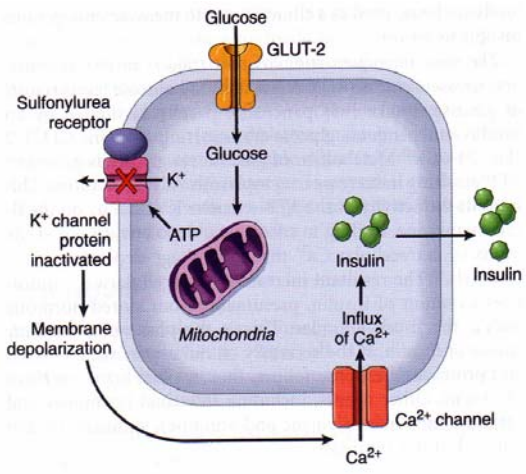


Figure 1.16 Synthesis and release of insulin

Uptake of glucose into pancreatic β cells results when there is a rise in blood glucose levels. This is facilitated by the glucose-transporting protein GLUT-2 which is insulin independent. Metabolism of glucose via glycolysis generates ATP, resulting in increase in cytoplasmic ATP/ADP ratios. The activity of the ATP-sensitive $K^+$ -channel on the β-cell membrane is inhibited, leading to membrane depolarization and influx of extracellular $Ca^{2+}$ through voltage-dependent $Ca^{2+}$ –channels. The resultant increase in intracellular $Ca^{2+}$ stimulates secretion of insulin from stored hormone within the β-cell granules. This is the phase of immediate release of insulin. A delayed and protracted response follows if the secretory stimuli persist and this involves active synthesis of insulin. Other agents, including intestinal hormones and certain amino acids (leucine and arginine), stimulate insulin release but not synthesis.

#### 1.4.4.2 Complications of diabetes

Diabetes exacts a heavy toll on the vascular system, involving both large and medium sized muscular arteries (macrovascular disease) as well as capillary dysfunction in target organs (microvascular disease) [36]. Macrovascular disease causes accelerated atherosclerosis among diabetics, resulting in increased risk of myocardial infarction, stroke and lower-extremity gangrene. The larger renal arteries are also subject to severe atherosclerosis with most damage exerted at the glomeruli level and microcirculation. Microvascular disease has profound effects in the retina, kidneys and peripheral nerves resulting in diabetic retinopathy, nephropathy and neuropathy.

Hyaline arteriosclerosis is the vascular lesion associated with hypertension. There is amorphous, hyaline thickening of the walls of the arterioles which causes narrowing of the lumen. It is related to the duration of the disease as well as the level of blood pressure in diabetics.

Diabetic microangiopathy causes diffuse thickening of basement membranes. This is obvious in the capillaries of the skin, skeletal muscle, retina, renal glomeruli and renal medulla. Nonvascular structures such as renal tubules, Bowman capsule, peripheral nerves and placenta may also display it. Inspite of the thickening of the basement membranes, diabetic capillaries are leakier than normal and plasma proteins. The microangiopathy underlies the development of diabetic nephropathy, retinopathy and some forms of neuropathy.

# CHAPTER 2

# METHODS

## 2.1 Instrumentation

### *2.1.1 Theory of Laser Doppler Flow*

Tissue blood flow has been measured by different methods in the past. The principles of these methods were based on were physical phenomena such as changes in electrical impedance or optical conductance, changes in surface temperature due to alterations in the degree of vascularization and clearance of radioactive tracers or heat. Laser Doppler Flowmetry is a novel technique which is noninvasive, easy to handle, versatile and sensitive with high reproducibility.

Stern first pointed the possibility to study circulation of the human skin by laser Doppler technique in 1975. Skin surface was illuminated with the light beam from a 15 mW He-Ne laser and selective irradiation of the cutaneous blood flow was accomplished. The reflected portion of the incident beam was found to be spectrally broadened by the Doppler Effect. Frequency shift of radiation scattered in moving red cells in the superficial blood vessels is the cause of this phenomenon. The following theory of LDF has been published by the inventors of the Laser Doppler flowmeter [17].

2.1.1.1 Laser output field

The total output field of general purpose multimode lasers is shown below.

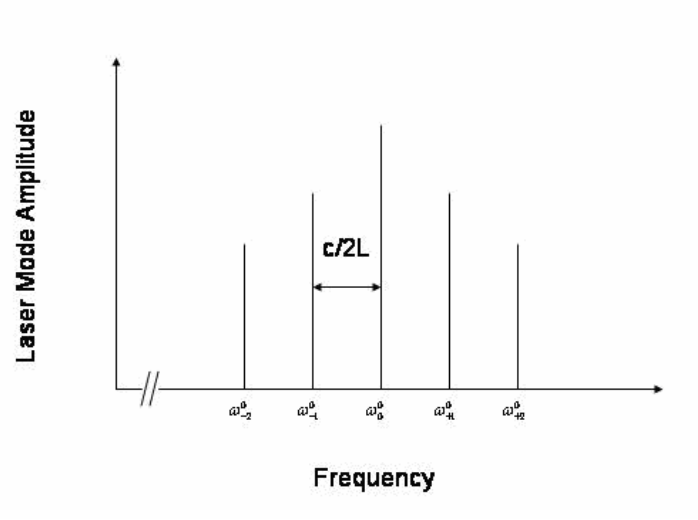


Fig 2.1 Output field from a multimode laser

$$E_{out}(t) = q \sum_{n=-N}^{N} \tilde{E}_n^0(\mathrm{t})\, e^{-j\omega_n^0 t} \tag{2.1}$$

q is a coupling factor, $\tilde{E}_n^o(t)$ is the complex time-dependant amplitude of the $n^{th}$ mode and $w_n^0$ is the mode frequency. The longitudinal modes are separated in frequency by $w_n^0 - w_{n-1}^0 = c/2L$, where c is the velocity of light and L is the optical path length of the laser cavity. The length of the laser cavity and the linewidth of the temperature-broadened neon resonance thus determine the number of modes.

The absolute value of the amplitude $\tilde{E}_n^o(t)$ of the individual modes may vary in the real multimode laser due to nonlinearities in the laser medium. The total laser output is fairly constant. The unstable amplitude conditions result in a slowly varying

frequency component in the light beating spectrum caused by mode interference of the different laser modes. This high amplitude noise interacts with the blood flow related Doppler signal due to which measurements are possible only during noise-free periods.

2.1.1.2 Reflected field

The laser beam is directed towards the tissue under study during measurement where absorption and scattering occur. The radiation is scattered in movable structures such as red blood cells as well as nonmoving soft tissue. Radiation emergent from the movable structures is shifted in frequency due to the Doppler Effect while that from the fixed tissue is unshifted in frequency. A portion of the total scattered radiation is impinged on the surface of the photodetector. The effective radiation penetration depth is approximately 1 mm in soft tissue. Hence, scattering and absorption take place in the primarily in the papilla region and the underlying corium (two dermal layers containing the intricate capillary network of the skin) [17].

The total field $E_\tau$ ($t$, $r$) reaching the position $r$ at the photosensitive area of the detector at time $t$ is given by

$$E_T(t,r) = \sum_{n=-N}^{N} \left( E_{Rn}(t,r) + E_{Sn}(t,r) \right) \tag{2.2}$$

$E_{Rn}(t,r)$ is the complex electromagnetic field produced by the n$^{th}$ laser-mode and scattered in nonmoving structures.

$$E_{Rn}(t,r) = \tilde{E}^{0}_{Rn}(t,r)\, e^{-j\omega_n^0 t} \tag{2.3}$$

This component of the total field corresponds to the reference beam in ordinary heterodyne light beating spectroscopy and is therefore unshifted in frequency. But it has a randomly fluctuating phase factor. If the laser is not stabilized, a time-dependent absolute value of the complex amplitude $\tilde{E}^{o}_{Rn}$ *(t, r)* is also present.

The complex electromagnetic field produced by the n$^{th}$ laser-mode and scattered in movable structures such as red cells is $E_{Sn}$ *(t, r)*. If the Doppler frequency shift is small in comparison with $\omega^{o}_{n}$, the field can be considered a narrow-band stochastic process and expressed in the form

$$E_{Sn}(t,r) = \tilde{v}_{n}\ (t,r)\, e^{-j\omega^{0}_{n}t} \tag{2.4}$$

$\tilde{\upsilon}_{n}$ *(t, r)* is the narrow-band complex amplitude of the field scattered in movable structures.

2.1.1.3 Photodetector Current

If the noise is neglected, the infinitesimal photocurrent *i (t, r)* produced by the field $E_{\tau}$ (*t, r*) at position *r* on the photosensitive area of the detector is proportional to the instantaneous intensity [17].

$$i(t,r) = C\left(E_{T}(t,r)\,E^{*}_{T}(t,r)\right) \tag{2.5}$$

C is the instrumentation constant which includes the quantum efficiency of the detector. Asterisk denotes the complex conjugate.

Inserting the expressions for the total field equations (2.2) - (2.4) in (2.5) gives

$$i(t,r) = C\left( \sum_{n=-N}^{N} \left( \tilde{E}_{Rn}^{0}(t,r) \right) e^{-j\omega_n^0 t} + \tilde{v}_n(t,r) e^{-j\omega_n^0 t} \right) \left( \sum_{m=-N}^{N} \left( \tilde{E}_{Rm}^{0*}(t,r) \right) e^{+j\omega_m^0 t} + \tilde{v}_m^{\,*}(t,r) e^{+j\omega_m^0 t} \right) \tag{2.6}$$

The spectral power of the photocurrent will be concentrated around discrete frequencies which are multiples of the mode-spacing frequency as a consequence of the narrow band nature of $E_{Sn}$ *(t, r)*. If the photodetector output signal is low-pass filtered, only terms with n = m in (6) need to be considered. The photocurrent is now expressed as

$$i(t,r) = \begin{aligned} & C \sum_{n=-N}^{N} \left| \tilde{E}_{Rn}^{0}(t,r) \right|^2 + C \sum_{n=-N}^{N} \left| \tilde{v}_n(t,r) \right|^2 + \\ & C \sum_{n=-N}^{N} \left( \tilde{E}_{Rn}^{0}(t,r) \tilde{v}_n^{\,*}(t,r) + \tilde{E}_{Rn}^{0*}(t,r) \tilde{v}_n(t,r) \right) \end{aligned} \tag{2.7}$$

The total photocurrent *i(t)* is given by the integral over the photosensitive area of the total radiation intensity impinging on it.

$$i(t,) = i_R(t) + i_S(t) + \eta C \left( \tilde{E}_R^0(t) \tilde{v}^*(t) + \tilde{E}_R^{0*}(t) \tilde{v}(t) \right) \tag{2.8}$$

The first term in (2.8) is the current produced by the beam unshifted in frequency. This component is *dc* current for a light source with stable mode amplitudes. The second term is the photocurrent corresponding to the self-beating term in a homodyne detection system. The third term corresponds to the heterodyne mixing of the frequency unshifted field and the frequency shifted field on the photosensitive area of the photodetector. According to the central limit theorem, random fluctuations in phase over the detector area will generate a total light beating current that obeys Gaussian

statistics (the Gaussian nature of the photocurrent ensues from the fact that the total light intensity striking the photodetector is produced by many independent scatterers). The introduction of the heterodyne efficiency η (|η| > 1) accounts for the effect of imperfect spatial coherence over the detector area [17].

If the flow under study is assumed to be stationary and no amplitude fluctuations are present in the multimode laser source, the first term in (2.8) is independent of time and the mean value of the photocurrent *i(t)* is written as

$$\langle i(t)\rangle = i_R + \langle i_S\rangle \tag{2.9}$$

The optical field is a Gaussian random process and hence the autocorrelation function of the low-pass filtered photocurrent is expressed as

$$\begin{aligned}\langle i(0)i(\tau)\rangle &= i_R^2 + 2\,i_R\langle i_S\rangle + \langle i_S\rangle^2 + \eta^2\langle i_S\rangle^2\left|g_S(\tau)\right|^2 \\ &+ \eta^2\, i_R\langle i_S\rangle\left(e^{+j\omega^0\tau}\, g_S(\tau) + e^{-j\omega^0\tau}\, g^*{}_S(\tau)\right)\end{aligned} \tag{2.10}$$

where $g_S(\tau)$ is the normalized autocorrelation function for the optical field scattered in movable structures.

The photocurrent spectrum $P_i\ (\omega)$ can be calculated according to the Wiener-Khintchine theorem from the photocurrent autocorrelation function.

$$p_i(\omega) = \frac{1}{2\pi}\int_{-\infty}^{+\infty}\langle i(0)i(\tau)\rangle\, e^{-j\omega\tau}d\tau \tag{2.11}$$

The heterodyne part of the light beating spectrum is identical in shape to the corresponding optical spectrum while the homodyne part will generally give rise to

frequency broadening. The standard deviation (rms value) of the photocurrent is calculated according to

$$\sigma_i^{\,2} = \langle i(t)^2 \rangle - \langle i(t) \rangle^2 \tag{2.12}$$

Making $\tau = 0$ in (2.10) and inserting (2.9) in (2.12) gives

$$\sigma_i^{\,2} = \eta^2 \left( \langle i_S \rangle^2 + 2 i_R \langle i_S \rangle \right) \tag{2.13}$$

And

$$i(t) \in N\left( i_R + \langle i_S \rangle, \sigma_i \right) \tag{2.14}$$

If a major portion of the radiation incident on the skin is scattered in nonmoving tissue, $i_R >> (i_S)$ and the homodyne part of the photocurrent may be neglected. Hence, $(i_S)$ can be considered proportional to $i_R$ and

$$\langle i_S \rangle = k^2 i_R \tag{2.15}$$

$k^2$ is a constant related to the density of moving scatterers. The heterodyne beating of the unshifted and shifted frequency beam alone helps us to determine the photocurrent and

$$i(t) \in N\left( i_R, \sqrt{2}\eta k\, i_R \right) \tag{2.16}$$

The instantaneous value of $i(t)$ is given by

$$i(t) = i_R \left(1 + A(t)\right) \tag{2.17}$$

where *A(t)* is Gaussian distributed and

$$A(t) \in N\left(0, \sqrt{2}\eta k\right) \tag{2.18}$$

The effect of mode interference on the photodetector current is expressed as a noise component *S(t). i(t)* with zero mean value, superimposed on the detector current *i(t)*. If the wide-band noise of the laser beam $(N_L(t))$ and the photodetector dark current and shot noise $(N_D(t))$ are considered, the total photocurrent $i_N(t)$ can be written as

$$i_N(t) = i(t)\,(1 + S(t))(1 + N_L(t))(1 + N_D(t)) \tag{2.19}$$

where $N_L(t) \in N(0, \sigma_L)$ ($\sigma_L^2$ is the variance of the wide-band laser beam noise) and $N_D(t) \in N(0, \sqrt{2e\Delta f / i_R})$ (e is the electron charge and Δf is the sampling bandwidth). Inserting (2.17) in (2.19) gives

$$i_N(t) = i_R(1 + A(t))\,(1 + S(t))(1 + N_L(t))(1 + N_D(t)) \tag{2.20}$$

2.1.1.4 Instrumentation of the device

The light from a laser source (Spectral Physics model I 20, 632.8 nm, 5 mW) is transmitted through an optical plastic fiber (Dollan - Jenner, φ 1.5 mm) to the skin area. A portion of the back-scattered radiation is gathered by afferent optical fibers and detected in a differential operation set-up.

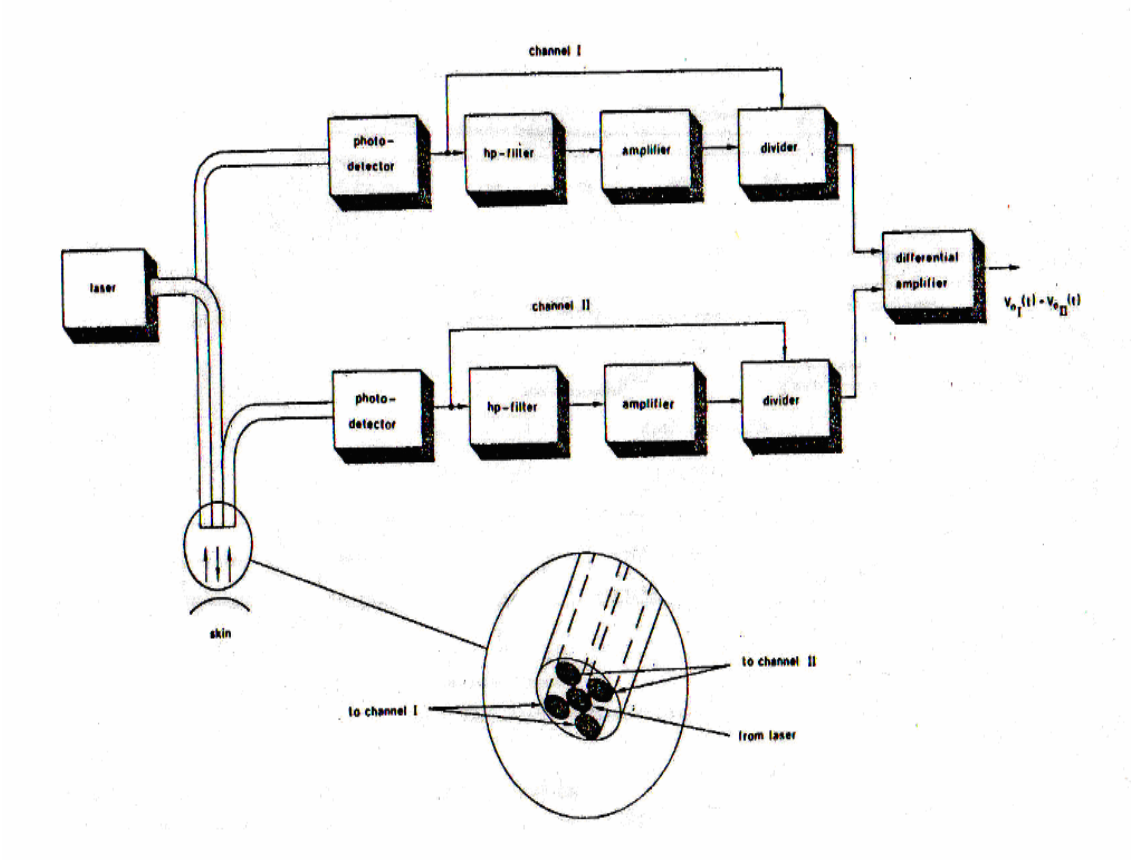


Fig 2.2 Block diagram of the differential operation set-up

2.1.1.5 Operation

In the differential detection set-up, the scattered radiation from the skin is gathered by four optical fibers symmetrically distributed around a central fiber transmitting the illuminating light beam from the laser to the probe. The proximal ends of the gathering fibers are connected in pairs to the photosensitive surface of the detector of each channel. The photodetector utilized is an integrated op-amp with a p-i-n diode as a photosensitive element (United Detector Technology UDT – 450). This detector was chosen because of its high quantum efficiency at the particular wavelength

and low cost in comparison with photomultiplier tubes. The detector response is flat from *dc* to more than 100 kHz. If the value of the feedback resistor is $R_f$ and thermal noise is neglected, the detector output signal is

$$V_D(t) = R_f i_N(t) \tag{2.21}$$

The blood flow related signal is separated from the dc component by high-pass filtering the photodetector output signal in an active three-pole Butterworth filter with the 3 dB point at 75 Hz (0.3 dB ripple). After amplification by a factor *F* in a low-noise linear amplifier (Texas Instruments TL 072), the remaining *ac* component is normalized by dividing it with the output signal from the photodetector. The analog divider (Burr-Brown BB 4291H) output signals $V_{01}(t)$ and $V_{011}(t)$ can be approximated by

$$V_{01}(t) \approx F_1\left(A_1(t) + S(t) + N_L(t) + N_{D1}(t)\right) \tag{2.22}$$

And

$$V_{011}(t) \approx F_{11}\left(A_{11}(t) + S(t) + N_L(t) + N_{D11}(t)\right) \tag{2.23}$$

By properly balancing the channels ($F_1 = F_{11} = F$), the difference is given by

$$V_{01}(t) - V_{011}(t) = F\left(A_1(t) - A_{11}(t) + N_{D1}(t) - N_{D11}(t)\right) \tag{2.24}$$

The rms value of the output signal from the differential amplifier

$$rms\left(V_{01}(t) - V_{011}(t)\right) = F\sqrt{4\eta^2 k^2 + 2e\Delta f\left(\frac{1}{i_{R1}} + \frac{1}{i_{R11}}\right)} \tag{2.25}$$

(2.25) is independent of both $(S(t)^2)$ and $\sigma_L^2$, corresponding to the mode interference noise and the wide-band beam noise in the laser respectively.

In the differential technique, the common mode terms such as large amplitude mode interference noise can be suppressed to a negligible level. Simultaneously, an increase in the signal-to-noise ratio (by a factor of 4) is obtained due to suppression of wide-band laser beam amplitude noise. These improvements significantly increase the sensitivity of the device, which is now determined primarily by the photodetector noise current. The blood flow related signal is extracted from the photocurrent power spectrum by subtraction of the photodetector noise power [17]. The output signal from the instrument is highly stable and continuous recordings of regional skin blood flow can be performed in the laboratory as well as at the bedside.

The thickness and optical properties of epidermis may affect the amplitude of the heterodyne component of the photocurrent spectrum. Spectral broadening is primarily caused by multiple scattering and homodyne scattering while frequency shifts towards lower frequencies have their origin in the angular dependence between the incident beam direction and the propagation direction of individual cells. Further, the LDF is insensitive to the direction of flow. Separate studies of the red cell velocities in the ascending and descending capillaries of the papilla cannot be done due to this directional ambiguity. If a frequency shifted reference beam is mixed with the scattered light from the skin on the photosensitive area of the detector, directional sensitivity can be achieved.

*2.1.2 Periflux PF 3 Laser Doppler Perfusion monitor*

2.1.2.1 Principle of operation

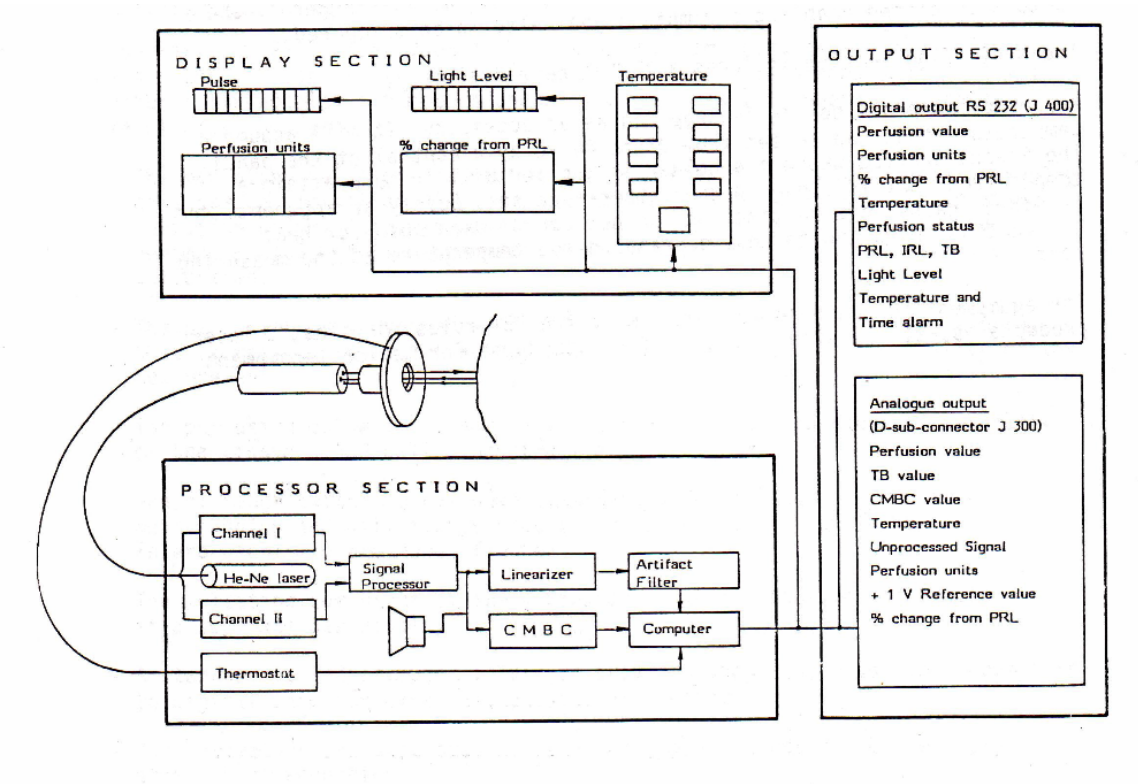


Figure 2.3 PF 3 Block diagram

The PF 3 consists of three sections

- The processor section contains the laser, optical fibers, signal processing circuits producing the various measuring signals in the analog form and a computer converting the signals into digital form, controlling the digital display and supplying data to the computer interface.

- The display/control section contains the controls necessary for operating the instrument and the various analog and digital displays.
- The output section contains the RS 232 interface which delivers the measurement parameters as standardized digital values for external computer handling and two outputs give out the same parameter as analog voltages.

2.1.2.2 The processor section

PF 3 measures the microvascular blood cell perfusion through tissue utilizing the Doppler shift i.e., the frequency change that light and other radiations of wave nature undergo when they interact with objects in motion (red blood cells here).

Wave movements are characterized by the equation

$$v = f * \lambda \tag{2.26}$$

where

v is the propagation velocity

f is the wave frequency

λ is the wavelength

Therefore, when frequency changes, there is a proportional change in wavelength. This is perceived as a color change in case of light and change in pitch in case of sound.

The laser output field has already been explained in the theory of laser Doppler flow. The backscattered light is a mixture of different wave frequencies, namely the original wave frequencies and the Doppler shifted frequencies. This is brought to the photodetector where it is converted into electric signals, which will have a mixture of

frequencies as the light. Such a mixture will give rise to new signals with frequencies constituting the difference between (and the sum of) the component frequencies. The electric circuits cannot contain the light frequency and sum frequency because they are very high ($10^{15}$ Hz). These signals with therefore leak away and disappear. The frequency differences which lie within the frequency range of 0-12 kHz, appear as the Doppler signal at the photodetector output. The stochastic signal is still a well defined function of the velocities, and the number of blood cells moving through the part of the illuminated volume that the returning fibers "see" in the human skin. This is a hemisphere of about 1 mm radius [12].

2.1.2.3 Double channel arrangement

The double channel arrangement in the Periflux produces a clean, cell-motion correlated Doppler signal effectively suppressing noise from other sources [12]. A standard low-power laser is used. The extracted signal is subsequently processed to compensate for variations in laser intensity and for transmission differences in the fibers. Finally, it is subjected to an electronic transformation corresponding to the mathematical relation between the unprocessed Doppler signal and the tissue perfusion.

The algorithm used for transforming the primary signal into a perfusion reading is expressed as

$$V_{out} = \left\langle K \int_{\omega_l}^{\omega_\mu} \omega \cdot P(\omega) d\omega \right\rangle \tag{2.27}$$

where $\omega$ is the Doppler frequency

$V_{out}$ is the output signal, proportional to the perfusion i.e. the blood cell transport through the measuring volume.

$P(\omega)$ is the total power spectral density of the difference amplifier output signal

$\omega_{\mu}$ is the upper cut-off frequency

$\omega_{l}$ is the lower cut-off frequency

K is the proportionality constant

2.1.2.4 Linearizing the perfusion value

The Periflux is equipped with an additional electronic processor called the linearizer [12]. This eliminates a systemic error that would make the LDF underestimate the degree of blood perfusion at elevated tissue blood cell concentration. When the photon (light quantum) hits a blood cell, it becomes scattered while passing through the measuring volume. As the tissue blood cell concentration increases, the probability that the photon will hit the blood cells more than one time during its passage also increases. It is this multiple scattering that causes the underestimation.

Under hyperemic conditions, increased cell concentrations may occur in inner organs such as brain, ling, liver, spleen, testis, kidney and the alimentary tract including the mucous membranes of the oral cavity. They can occasionally be observed during hyperemia caused by highly potent vasodilators (e.g. dorsal side of the hand), but rarely occurs in the skin.

The entire Doppler signal is fed to the linearizer network for the perfect functioning of the linearizer. For this, the instrument is in the WIDE BAND mode. It is indicated by the wide band led being lit, which means that the frequency range of the Doppler signal is large enough to include all Doppler frequencies that may occur in clinical use.

#### 2.1.2.5 The perfusion value

The perfusion value appears as a voltage at the computer output and is represented in perfusion units (PU). It constitutes the blood cell transportation through the microvascular bed i.e. of perfusion. The LDF reacts to all movements of definite structures (mainly RBCs) within its measuring volume and these movements are relative to the instrument probe's head. RBCs dominate in contribution to these movements, but there are contributions from other components such as thrombocytes and leucocytes which form a part of blood flow. Muscle cells, vessel walls and various membranes not related to blood flow are other additions. Tests have shown that contributions as a rule are insignificant [12].

The diffuse scattering of light within the tissue makes the signal virtually independent of the direction of cell movement. A blood cell moving in one direction will typify another one moving with the same speed in the opposite direction. The PF 3 does not react to flow of fluids with uniform refractive index such as pure blood plasma.

The PF 3 perceives signals in the skin from a tissue depth of 1.5 mm which means that only microvessels e.g. capillaries, arterioles and venules contribute to the

reading. When measuring tissue other than skin, larger vessels may pass through the measuring volume, but their influence is negligible as their walls are too thick and tight to permit more than limited amounts of light to pass in and out.

The perfusion value expressed in PU cannot be directly translated into units of physiological definition such as the number of blood cells flowing through a cubic mm of tissue per second. The same blood flow will give different perfusion readings in different kinds of tissue. When comparing flow measurements, there is considerable physiological variation in peripheral perfusion between different healthy subjects. There is also ample variation in the same subject over local tissue areas, even at small distances and over time. Due to the relative character of the LDF measurement, direct comparisons between measurements of different individuals and at different occasions have a limited value.

The blood cell perfusion is a product of two quantities:

- The number of blood cell within the measuring volume
- The mean velocity of these cells

Consequently, perfusion can be varied by changing either of these factors. In practice, both deviate simultaneously.

#### 2.1.2.6 The Motility Standard

The perfusion value can be calibrated using a PF 100 Motility Standard. It consists of a small bottle containing about 2.5 $cm^3$ of a colloidal suspension of latex particles (0·5% suspension of 0·48μm diameter polystyrene microspheres at 20°C)

whose Brownian motion is used as the Motility Standard [12]. The bottle has two caps, one with holes to accommodate various probe heads and is contained in a thermal insulator.

The Motility Standard produces a standard motility of 250 PU at standard temperature of +22$^{o}$C which corresponds to a standard motility voltage of 2.5 V at the analogue perfusion output with ± 5% statistical variation. The variation is mainly due to random variations in the Brownian motion.

If the outside temperature range is 18 – 26 $^{o}$C and the room temperature is t $^{o}$C, a correction is applied to the perfusion value produced by the standard. The formulae are:

Corrected Standard Motility = 250 + (t – 22) 4 PU

Corrected Standard Motility Voltage = 2.5 + (t – 22) 0.04 V

2.1.2.7 Design of the movement artifact filter (MAF)

The MAF is an electronic circuit that can be switched into the signal line before the indicating displays and the perfusion outputs [12]. Its main component is a slew-rate filter which is sensitive to the time-derivative, i.e. the slope rate or steepness of the perfusion signal. It reacts as soon as the signal rises faster than a predetermined (limit) rate. The limit rate is so chosen that it exceeds the steepest slope rate observed in physiologic phenomena by a good margin. The limit rate may be exceeded when a movement artifact develops. This will trigger the slew-rate filter, activating an electronic circuit which locks the perfusion display and outputs the value that was present when the disturbance started.

#### 2.1.2.8 Measurement depth of the laser Doppler perfusion measurements

The penetration depth of radiation is defined as the depth below the skin surface at which the light intensity decreases to about 37% of its value at the skin surface. For 632.8 nm He-Ne laser light and Caucasian skin, this distance is 1.5 mm [18]. This depth is a typical value because the absorption properties of skin are dependent on factors like tissue hematocrite (blood content), degree of oxygenation, pigmentation, etc.

The depth sensitivity is the degree to which light back-scattered from a certain depth contributes to the Doppler signal. It depends on wavelength and tissue properties and also relates to the geometrical dimensions of the probe and to what depth the bulk of the Doppler signal is originally generated. If the distance between the efferent and afferent fibers is increased, the depth sensitivity will increase due to the fact that the rays that are eventually picked up have traversed a longer way and penetrated deeper into the tissue. A too wide separation will give a weak Doppler signal completely obscured by thermal noise.

The average distance between the afferent and efferent fibers in the probe is in the order of 250 μm. The scattering volume in normal skin constitutes a hemisphere with a radius of 1 mm. The blood vessels in the periphery of this sphere give a lower contribution to the total output signal than those in the center of the sphere. The penetration depth and depth sensitivity may be significantly larger in tissues with less pronounced properties. Also, since the depth sensitivity of normal skin may include capillaries, shunts, small arteries as well as veins, both the nutritional flow and thermoregulatory flow contribute to the total output signal [12].

## 2.2 Operation

### *2.2.1 Subject Demographics*

Adult subjects between the ages of 20-65 were chosen for the study of vasomotion in the forehead. The study was approved by IRB and all subjects were recruited from Dallas Veteran Affairs Medical Center or Johns Hopkins School of Medicine (no subjects were enlisted from the University of Texas at Arlington). An assessment of clinical impact form was filled out which is a part of the human studies protocol. All subjects had to sign a consent form which included the purpose of the research study, benefits if any, remuneration, etc (please see appendix B).

In the preliminary studies, 12 subjects were examined of which, 6 subjects were normal and 6 subjects were diagnosed with vascular diseases known to affect the endothelium (atherosclerosis, hypertension, hyperlipidemia, heart failure and diabetes mellitus). The selected (diseased) subjects were mentally competent and ambulatory patients. Diabetes mellitus directly affects the endothelium causing endothelial dysfunction and is strongly associated with atherosclerosis and hypertension. For controls, subjects without these disorders (normal) were chosen. Subjects with other major diseases such as thyroid disease or severe lung disease were avoided. Patients treated for cancer were acceptable. Patients with sickle cell anemia were excluded, because sickle cells alter the vasomotive pattern. Also, patients with rashes over the foreheads were excluded.

Table 2.1 Subject demographics for normal subjects

| Subject # | Disease | Gender | Age (years) | Weight (Kg) | BMI ($Kg/m^2$) | Height (m) |
|---|---|---|---|---|---|---|
| N1 | None | F | 32 | 50 | 20.81 | 1.55 |
| N2 | None | M | 32 | 68 | 21.46 | 1.78 |
| N3 | None | M | 47 | 76 | 26.29 | 1.7 |
| N4 | None | F | 50 | 52 | 21.64 | 1.55 |
| N5 | None | M | 46 | 80 | 25.25 | 1.78 |
| N6 | None | F | 50 | 71 | 24.57 | 1.7 |
| Mean | | | 42.83 | 66.17 | 23.34 | 1.68 |
| Standard Deviation | | | 8.54 | 12.46 | 2.31 | 0.10 |
| Range | | | 32-50 | 50-80 | 20.81-26.29 | 1.55-1.78 |

Table 2.2 Subject demographics for diseased subjects

| Subject # | Disease | Gender | Age (years) | Weight (Kg) | BMI ($kg/m^2$) | Height (m) |
|---|---|---|---|---|---|---|
| D1 | Hypertension | F | 46 | 105 | 46.67 | 1.5 |
| D2 | Diabetes Mellitus | F | 48 | 100 | 32.65 | 1.75 |
| D3 | Diabetes Mellitus | M | 61 | 96 | 34.01 | 1.68 |
| D4 | Diabetes Mellitus | F | 55 | 82 | 25.88 | 1.78 |
| D5 | Diabetes Mellitus | F | 43 | 82 | 28.04 | 1.71 |
| D6 | Hyperlipidemia | F | 24 | 80 | 30.11 | 1.63 |
| Mean | | | 46.17 | 90.83 | 32.89 | 1.68 |
| Standard Deviation | | | 12.67 | 10.82 | 7.37 | 0.10 |
| Range | | | 24-61 | 80-105 | 25.88-46.67 | 1.5-1.78 |

*2.2.2 Study Protocol*

The experiment was conducted at the Dallas Veteran Affairs Medical Center, USA or at the Johns Hopkins School of Medicine. The blood flow in the skin of the forehead was measured for each subject and the pattern of perfusion versus time evaluated. The perfusion patterns were assessed for differences and compared between the diseased and control groups. The subjects' disease status was determined by the subjects' history or medical record (Clinical Patient Records).

*2.2.3 Experimental Set-Up*

The instrument used for the experiment is the Periflux PF 3 (Perimed, Sweden). It is a user-friendly device, whose front and rear panels are shown.

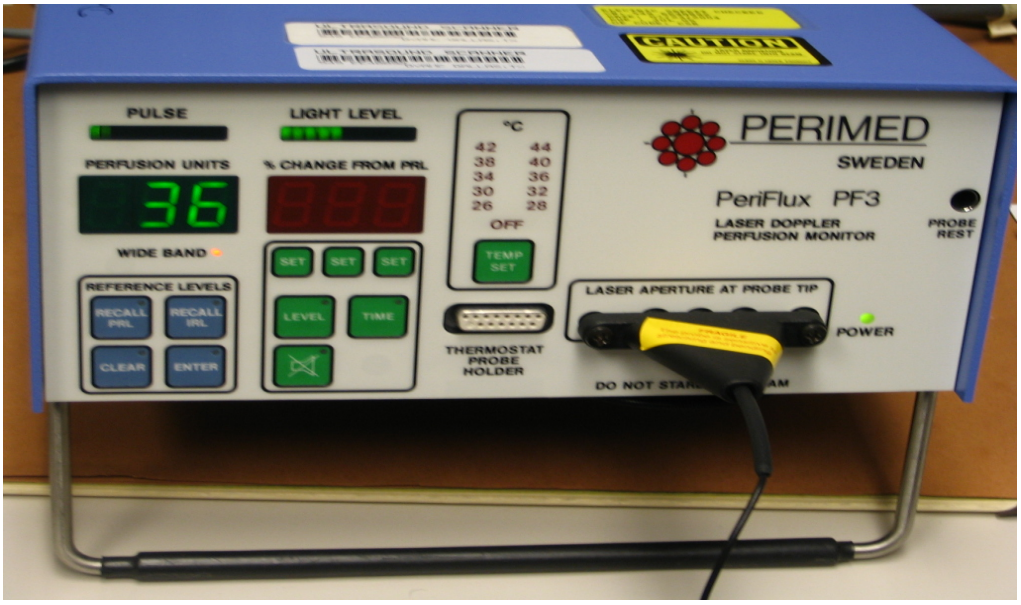


Figure 2.4 Front panel of Periflux PF 3

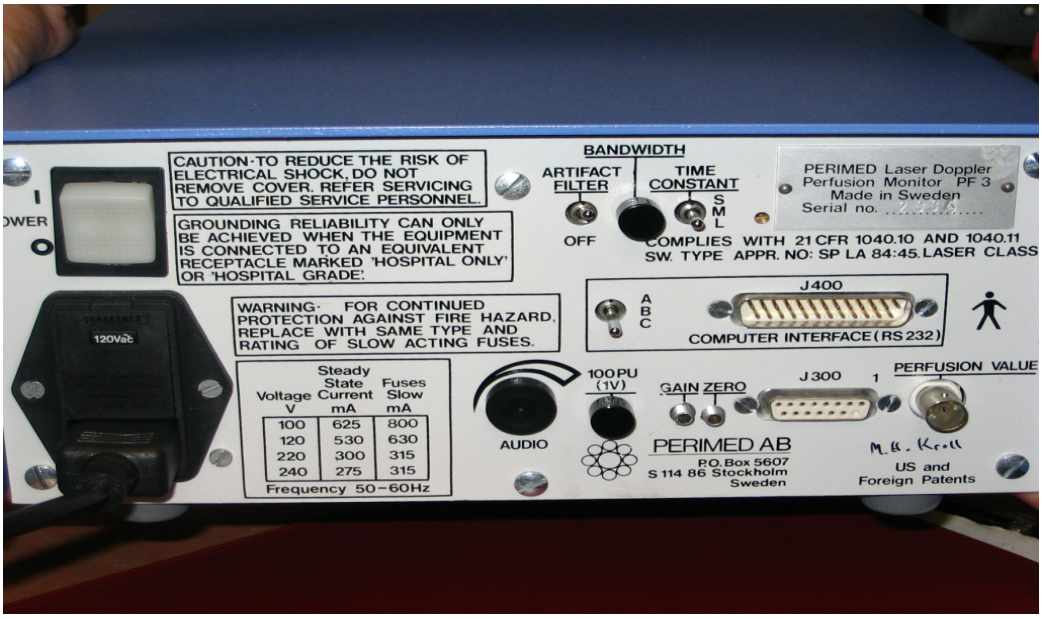


Figure 2.5 Rear Panel of Periflux PF 3

The momentary value of microvascular perfusion is continuously presented on a digital display, calibrated to read the perfusion in arbitrary perfusion units. The perfusion value is linear over the entire measuring range irrespective of the tissue blood cell concentration. The digital display is auto-ranging and reads the momentary perfusion while the pulsating component of the perfusion value is displayed in analog form at a separate display. The resolution of the instrument is 0.05 perfusion units.

A standard RS 232 computer interface provides the major measuring parameters in digital form for external computer processing. The parameters are also accessible at analog outputs for conventional strip chart recording. The equipment is designed to comply with the FDA rules for class 2 laser products as well as with the IEC safety standards for medical equipment. The standard probe PF 308 with the connector used for the measurement of LDF, the probe holder PF 104 and EKG pads for proper adhesion on the skin are shown in figure 2.6.


Figure 2.6 Light probe used in LDF and EKG pads

PF 308 is a multipurpose probe with a fiber separation of 0.25 mm, length 33 mm and diameter 6 mm. The radiation emitted from the probe is a 2 mW He-Ne laser (Siemens LGR 7621 S) with a wavelength of 632.8 nm and less than 1 mW in intensity at the probe tip. The Doppler shift frequency range has a lower limit of 20 Hz and an upper limit of 12 kHz (set to WIDE BAND mode).

The Periflux PF 3 LDF is connected to the desktop computer for serial asynchronous communication with a PF 321 parallel cable. The connector is J400 in the LDF and PS/2 port in the computer and both the devices are connected to a regulated power supply. In the PF 3, the artifact filter is in the ON position and the time constant is set at M. The baud rate and data block switch is set at position C. The transmitted type of data block is Type 2 (with perfusion values). The probe PF 308 is attached to PF 3 using the connector and the probe tip is fastened to the probe holder PF 104. The records can be printed out by hooking PF 3 through the J300 port to a recorder, but this output was not utilized in this study.

The software used for evaluating LDF data, developed by Gastrosoft Inc., Sweden, is called Perisoft (Version 5.10C2 © Copyright 1987-1995) and is executed in the DOS environment. A newer version of Perisoft, executable in the WINDOWS environment, was also used. A typical screen in which patient records can be obtained and reviewed is shown in figure 2.7.

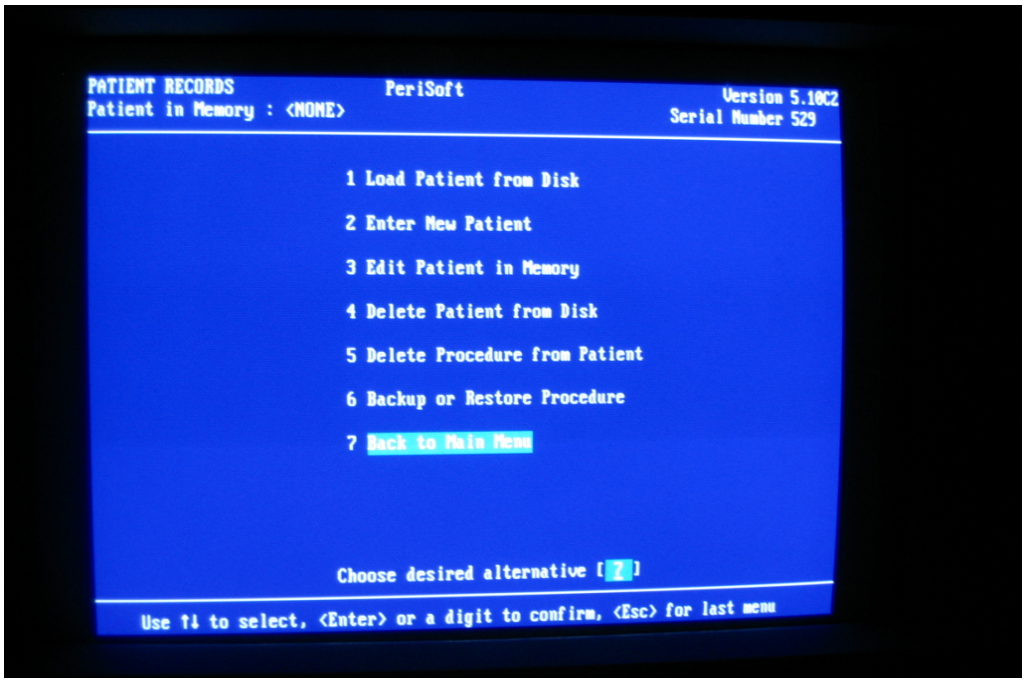


Figure 2.7 Obtaining and reviewing patient data

After loading the software into the computer, the Periflux is switched ON and allowed to warm up for 30 minutes. One may calibrate the instrument; one inserts the head of the probe into the probe rest hole and pushes it toward the static surface (delrin disc) present inside until it stops. The probe is then retracted till zero or until a figure is shown on the perfusion units display. The device is now ready for use.

The subject is asked to relax and be calm and is seated in a chair for collection of perfusion data. The probe holder PF 104 is attached to the centre of the forehead which should be clean and free of any type of residue (sweat, oil, etc). An EKG pad is used for good adhesion to the skin. The probe PF 308 is then fixed into the holder. To prevent occlusions of the blood flow, pressure between the probe and tissue is avoided.

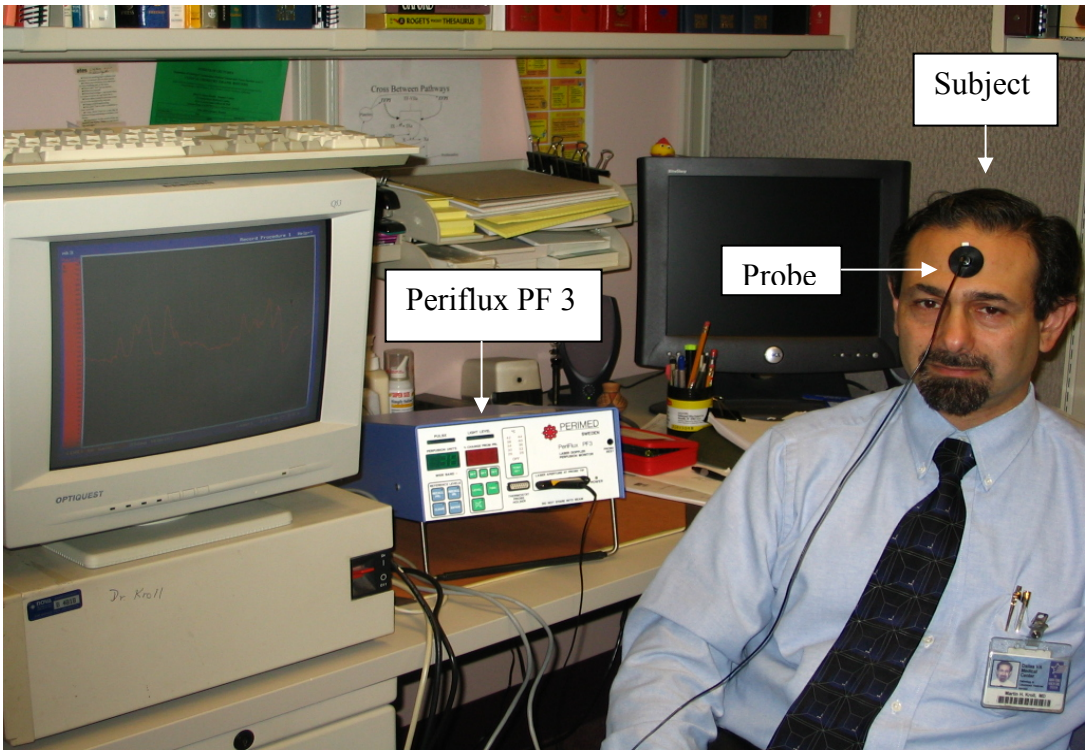


Figure 2.8 Experimental set-up for collection of blood perfusion data

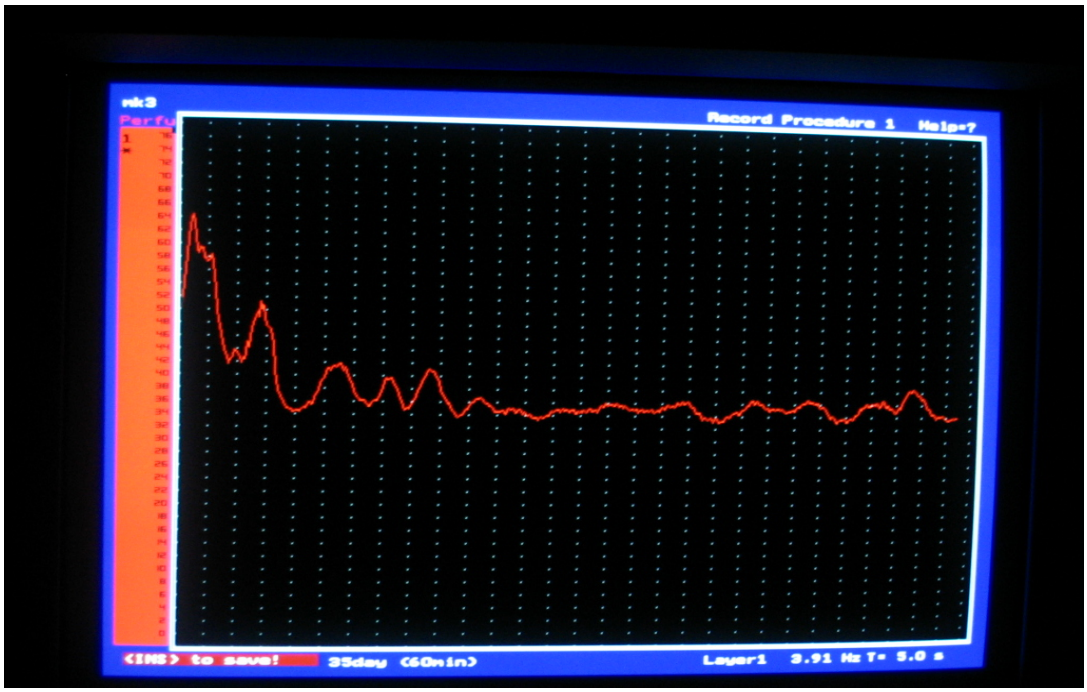


Figure 2.9 Measurement of blood perfusion

The probe tip is in contact with the tissue so that artifacts are minimized. The blood flow perfusion data is collected for a period of 10.42 minutes. It is very important that there is no alteration in the probe-tissue distance during measurement. Movements of the probe relative to the tissue or vice versa must be avoided because they will result in false indications. As soon as perfusion is stopped, a text file is generated which is stored in a folder called Peridata. This text file can be imported into MS Excel and Matlab environments for further analysis.

It is not necessary that the probe tip be in contact with the tissue because the measurements can be made as long as there is a reading on the perfusion unit's display. Normally, this occurs at skin-probe distances of up to 4 mm. However, when the distance becomes larger, the divergent beam emerging from the probe tip will illuminate a larger tissue area. The return fibers collecting the back-scattered light will also receive light from a larger area. The perfusion value is not essentially changed, but the measurement will be integrated over a larger tissue area thus collecting information from more microvessels. Hence, when using a large tip-tissue distance, the measurement will be less susceptible to variations over the tissue areas that depend on local variations in the microvascular bed [12]. Also, measurements made with different skin-probe distances are not comparable.

The condition of the probe's optical fibers can be checked by directing the probe's connector piece towards a strong light source and observing the fiber ends in the probe tip. All three fiber ends should light with about the same intensity.

## 2.3 Data analysis using power spectrum

The text file generated after collecting the blood perfusion data was imported into Microsoft Excel (Microsoft Corporation, Redmond, VA). This gave the momentary perfusion value and made the raw data easier to work with. A power spectrum analysis computer algorithm (power_spectrum.m; please see appendix A) was developed in the MATLAB (Mathworks Inc., Natick, MA) environment to check if the power spectrum of the normal and diseased subjects would differ. Since the data had N equally spaced samples, it was evaluated using the Fast Fourier transform (FFT) where N is usually a power of 2. The data was truncated at 5000 points (10.42 minutes) for uniformity among the subjects. No windowing was used. The overall mean was subtracted from the raw data to remove the DC offset and it was normalized by dividing it with the overall standard deviation. The sampling frequency was set at 8 Hz.

The spectral data was deconstructed in the JMP (SAS Institute Inc., Cary, NC) environment for identifying the peaks and the associated frequencies. Only the peaks between the frequencies 0 Hz - 0.2 Hz were picked out because major activity was observed in this region. The frequencies obtained were divided by resolution frequency (0.0019531 Hz) and the corresponding ratios were tabulated. These ratios were further divided by the basic primes (3, 5, 7, 11, 13, 17 and 19) and those frequencies at which integer ratios were obtained were categorized into separate series. The mean, standard deviation and skew of the series generated by the prime number 3 were computed for all the subjects in MS Excel and t – test was performed on the skew.

The peaks occurring between the frequencies 0.02 Hz – 0.08 Hz and 0.11-0.16 Hz were summed and their ratio was calculated in both the subject groups. With 1.0 as the threshold value, ratios less than 1.0 for diseased subjects were true positives (TP); greater than 1.0 were false negatives (FN). Ratios greater than 1.0 for normal subjects were true negatives (TN); less than 1.0 were false positives (FP). The odds ratio (OR) was then computed.

| Subjects | Disease + | Disease - |
|---|---|---|
| Test + | TP | FP |
| Test - | FN | TN |

$$OR = [TP/FP] / [FN/TN] \tag{2.28}$$

## 2.4 Data analysis using phase plane and SVD

The raw data was divided by the overall mean and multiplied by 10 for uniformity in the subject population. Eleven pseudo vectors were generated (lag phase of 11) in the MS Excel environment and every vector was plotted against its preceding vector to generate phase plots. The Whitney theorem for embedding data was used. The lag phase helps us to look at slower frequencies in the system.

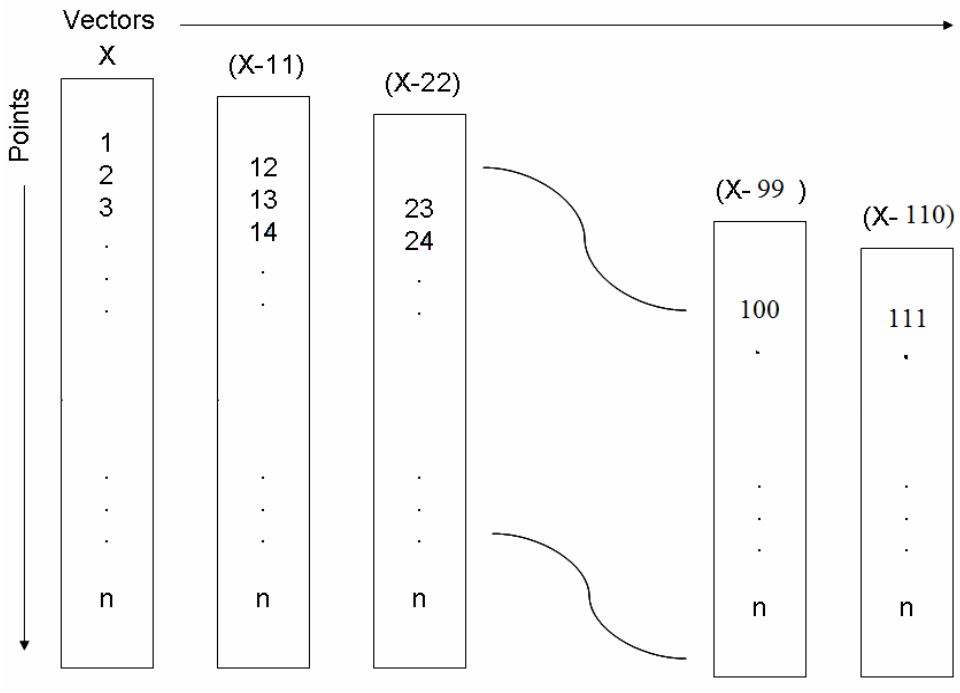


Figure 2.10 Vector formation for phase plots

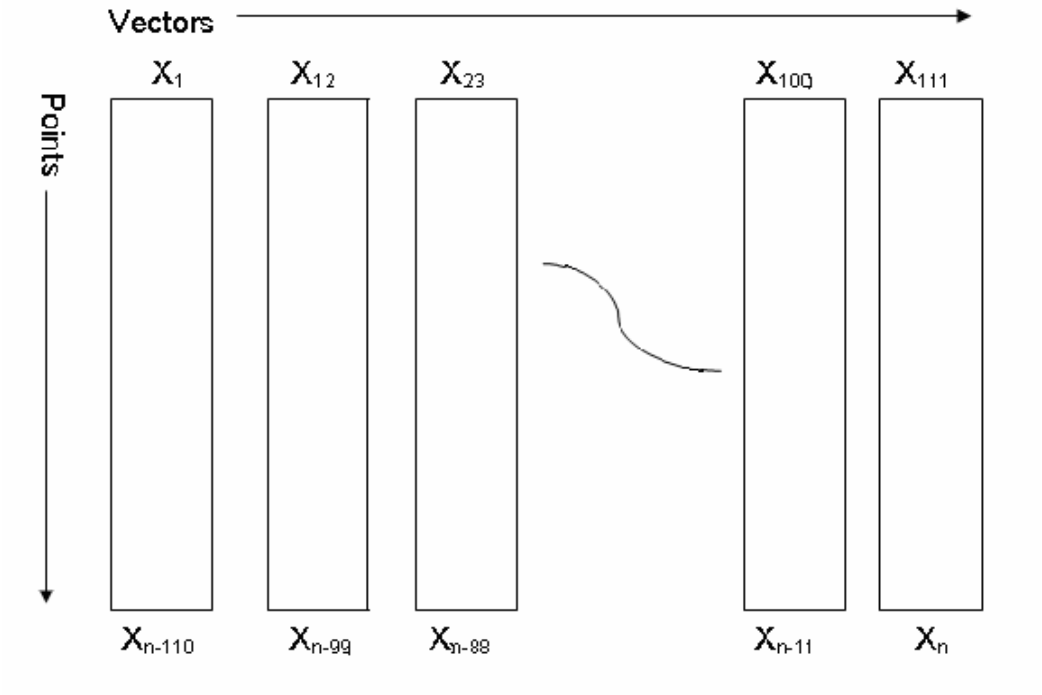


Figure 2.11 Final matrix for SVD calculation

The raw data was also imported into Matlab and SVD was calculated. The singular values (S1, S2, ... , S11) were tabulated in MS Excel and the mean $\left(\overline{X}\right)$ and standard deviation $\left(\overline{Y}\right)$ for each row for normal and diseased subjects were computed. Let $X_i$ be the $i^{th}$ row and N be the number of subjects.

$$\overline{X} = \frac{\sum_{i=1}^{N} X_i}{N} \tag{2.29}$$

$$\overline{Y} = \sqrt{\frac{\sum_{i=1}^{N} \left(X_i - \overline{X}\right)^2}{N}} \tag{2.30}$$

The standard error of mean (SEM) and the combined SEM (CSEM) were also calculated for both the control and diseased groups.

$$SEM = \frac{\overline{Y}}{\sqrt{N}} \tag{2.31}$$

$$CSEM = \sqrt{(SEM_{normal})^2 + (SEM_{diseased})^2} \tag{2.32}$$

The t–test was then performed. If the resultant p-value was greater than $t_{critical}$ at $\alpha = 0.05$, the two groups were considered significantly different from each other.

The F-test (variance ratio test) was also performed where the variances of the normal ($s_1$) and diseased groups ($s_2$) were used.

$$F = \frac{s_2^2}{s_1^2} \text{ or } F = \frac{s_1^2}{s_2^2}, \text{ whichever is larger.} \tag{2.33}$$

If the calculated ratio of sample variances (i.e. F) was greater than $F_{critical}$ at $\alpha$ = 0.05 for any of the singular values, the two groups were considered significantly different from each other.

The difference between the singular values S3 and S4 and S10 and S11 for both subject populations was computed and the Mann – Whitney nonparametric test was performed. The lowest numeral was given rank 1 (lowest to highest value). The Mann – Whitney statistic was calculated by,

$$U = n_1 n_2 + \frac{n_1(n_1+1)}{2} - R_1 \tag{2.34}$$

where $n_1$ and $n_2$ are the number of observations in normal and diseased groups respectively and $R_1$ is the sum of ranks of the observations in the normal group. If $U_{calculated}$ was greater than $U_{critical}$ at $\alpha$ = 0.05, the two groups were considered significantly different from each other.

The flowchart describing the data analysis is shown in figure 2.12.

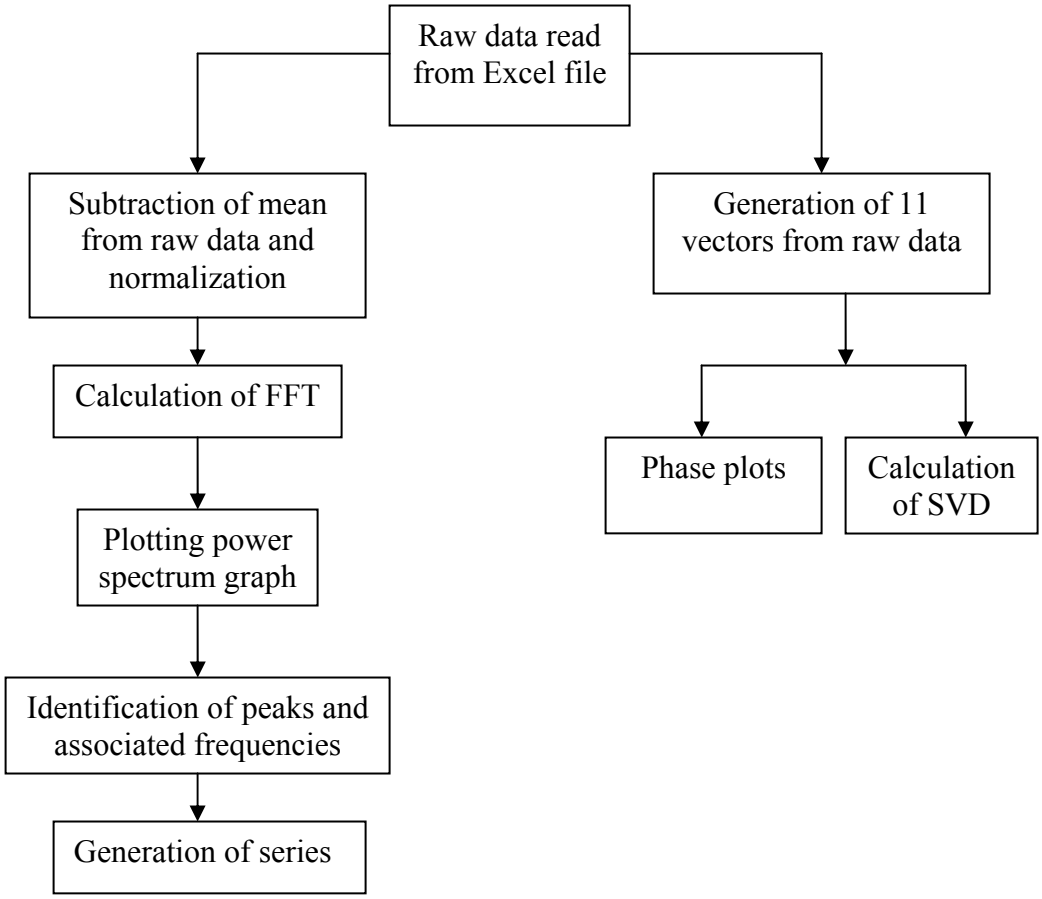


Figure 2.12 Flow chart for data analysis

CHAPTER 3

RESULTS

## 3.1 Results of power spectrum analysis

The raw data of perfusion vs. time for all normal and diseased subjects is shown in figure 3.1 – 3.12.

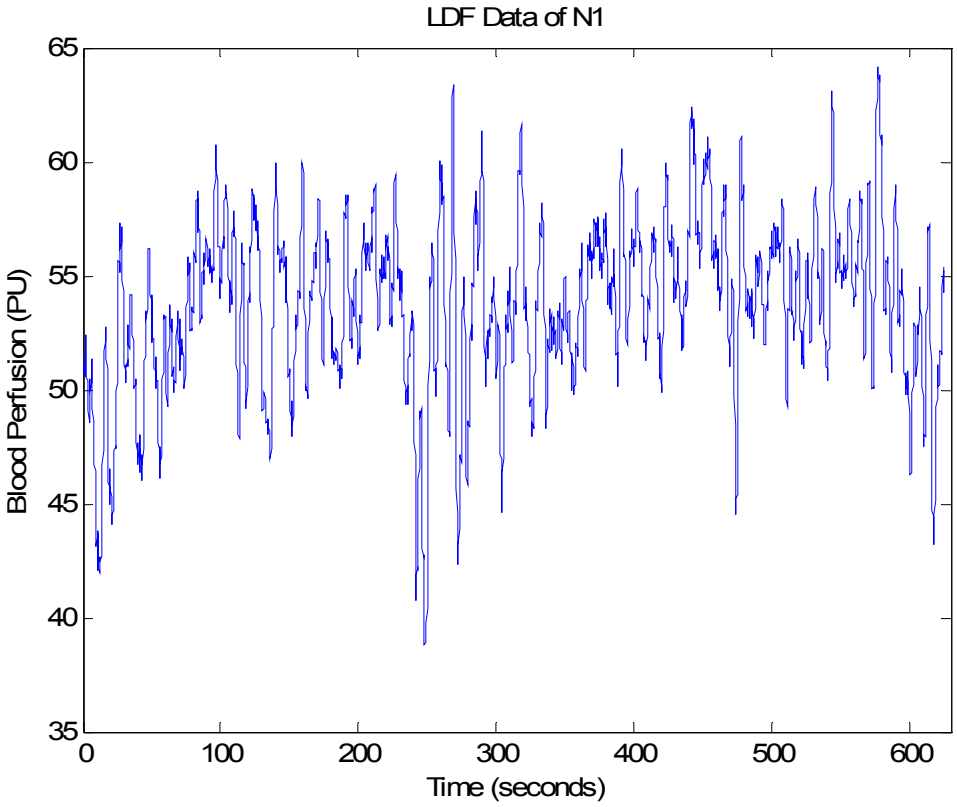


Figure 3.1 Raw data of blood perfusion vs. time for N1

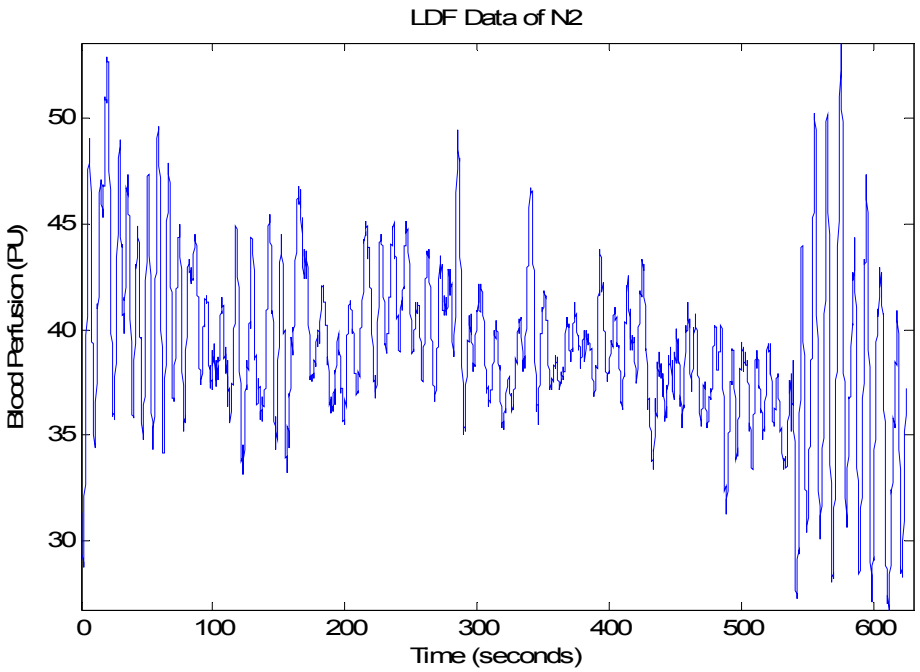


Figure 3.2 Raw data of blood perfusion vs. time for N2

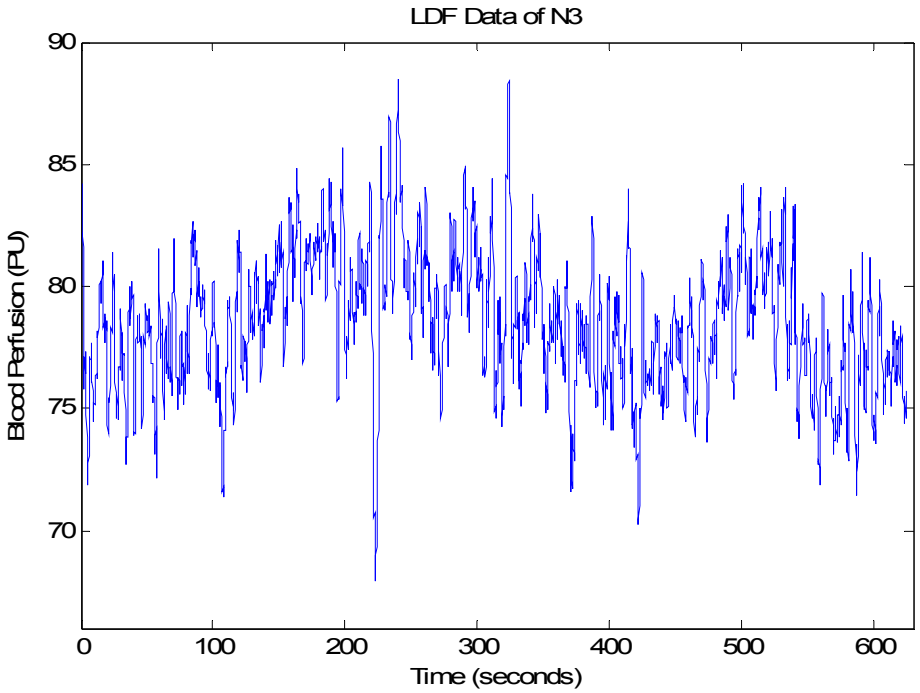


Figure 3.3 Raw data of blood perfusion vs. time for N3

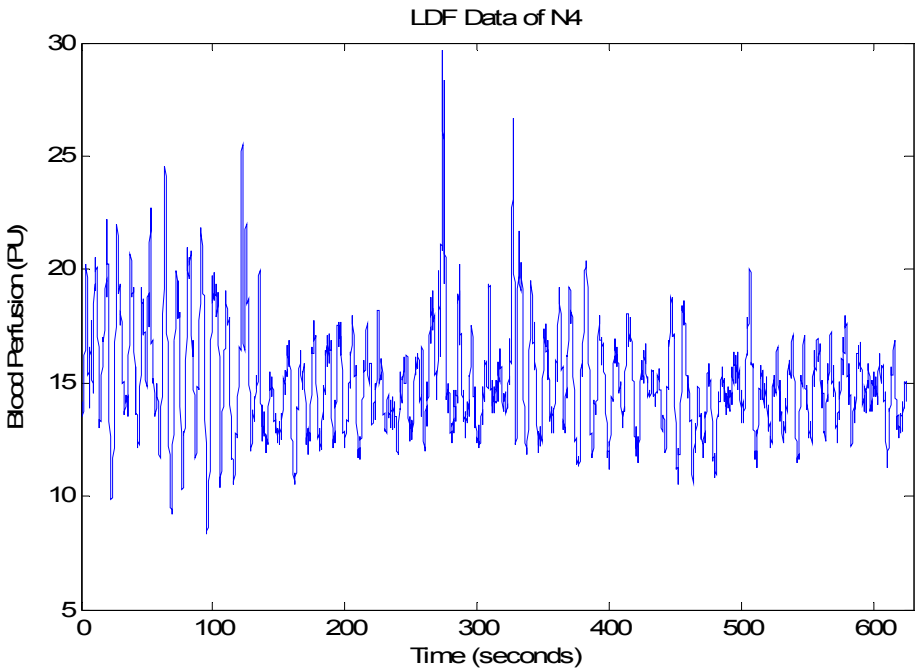


Figure 3.4 Raw data of blood perfusion vs. time for N4

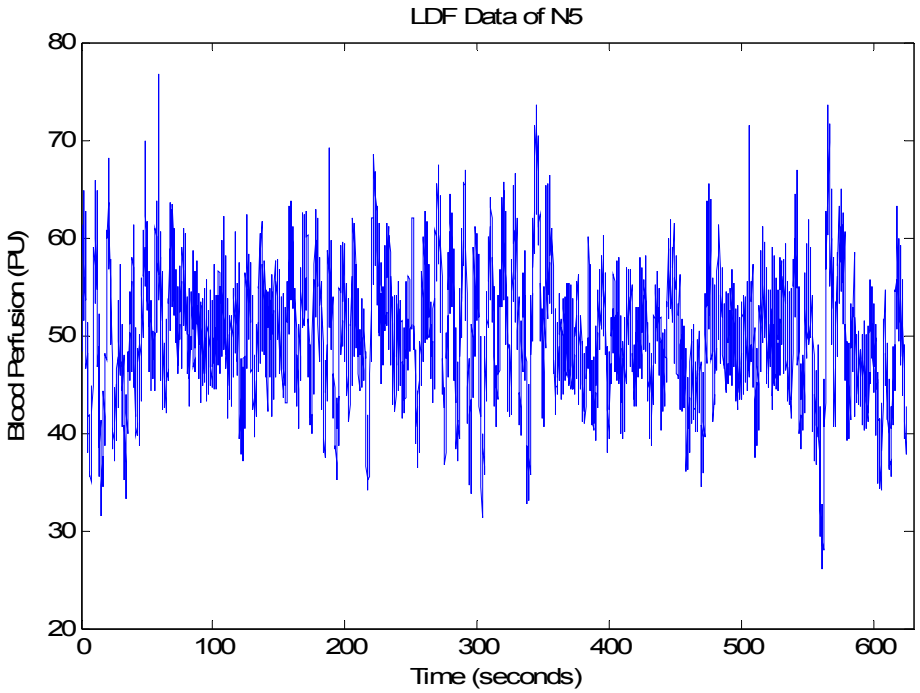


Figure 3.5 Raw data of blood perfusion vs. time for N5

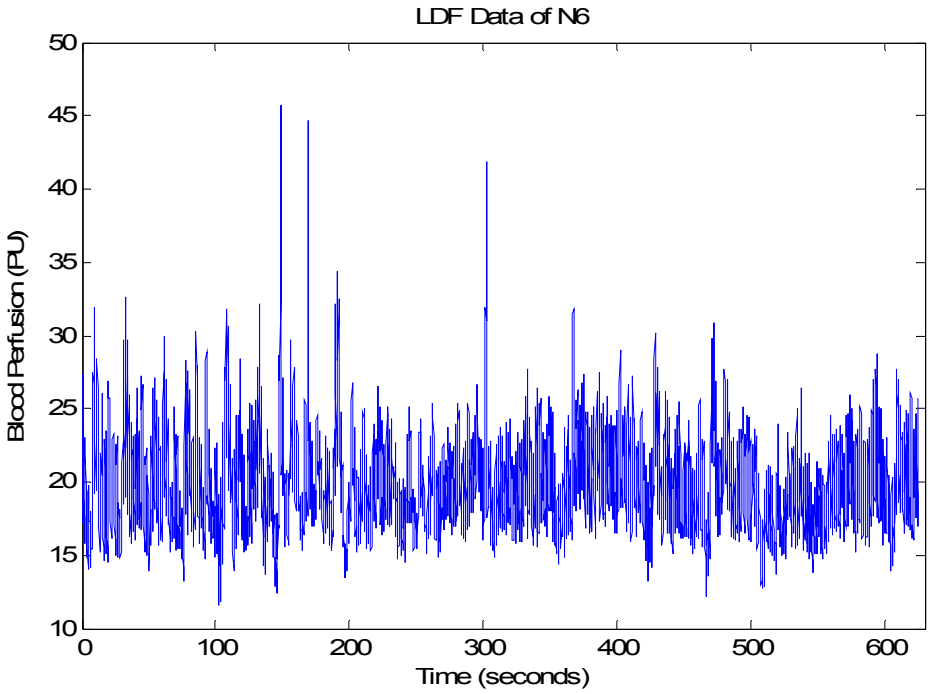


Figure 3.6 Raw data of blood perfusion vs. time for N6

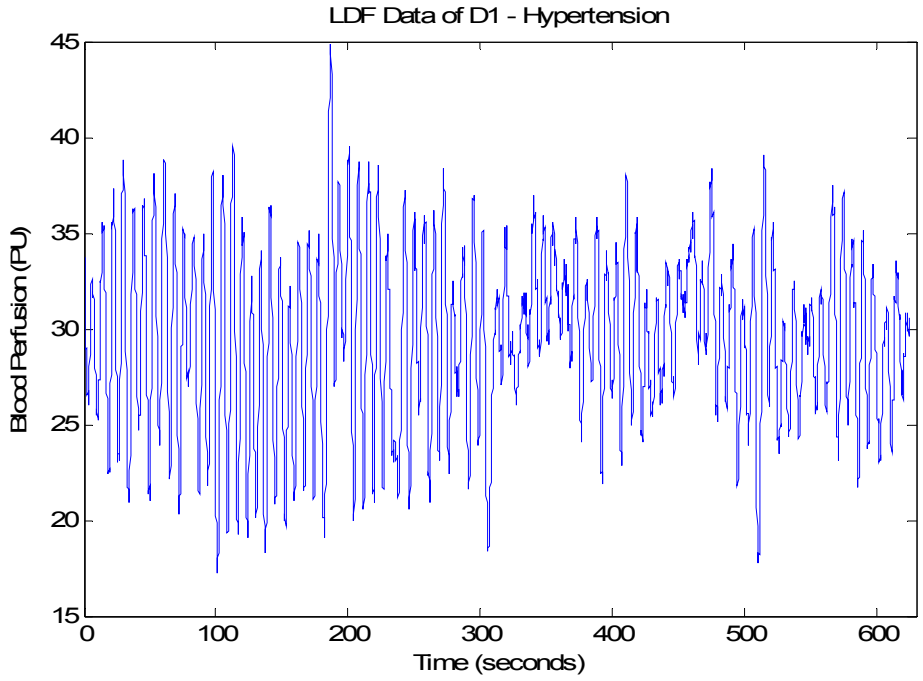


Figure 3.7 Raw data of blood perfusion vs. time for D1 (Hypertension)

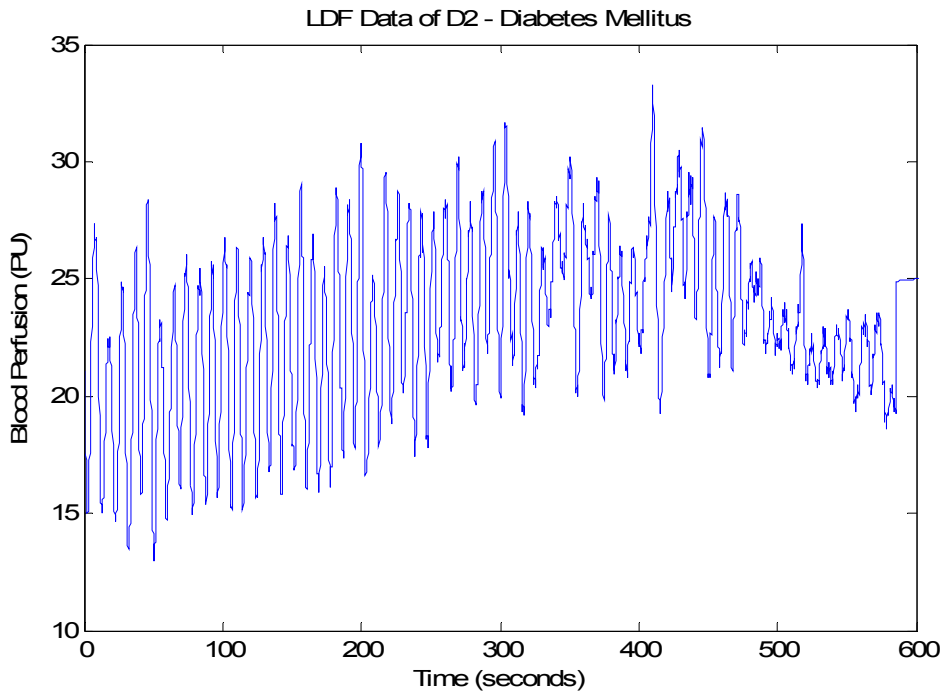


Figure 3.8 Raw data of blood perfusion vs. time for D2 (Diabetes mellitus)

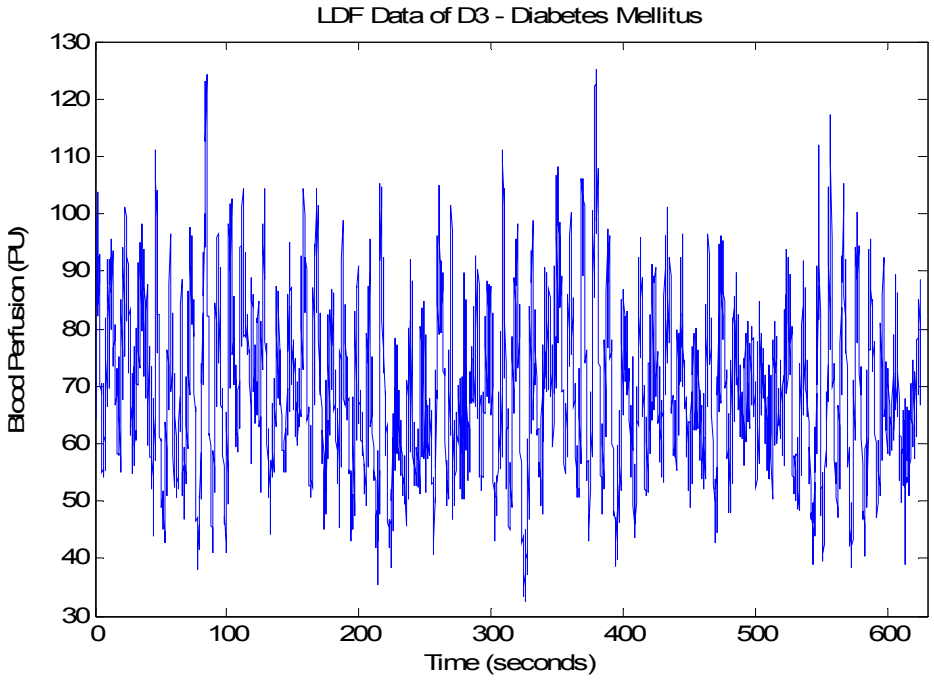


Figure 3.9 Raw data of blood perfusion vs. time for D3 (Diabetes Mellitus)

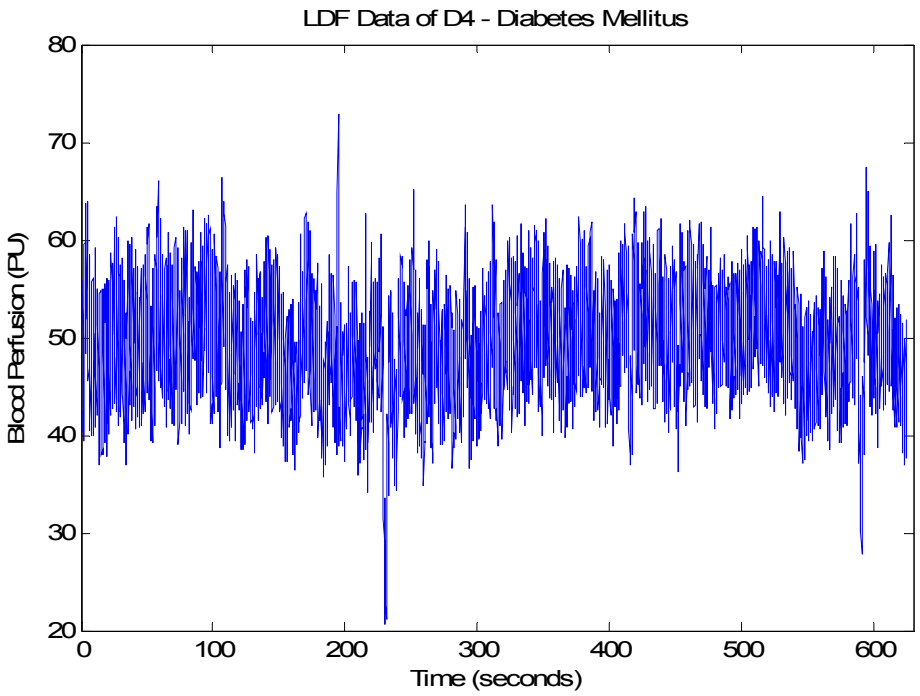


Figure 3.10 Raw data of blood perfusion vs. time for D4 (Diabetes Mellitus)

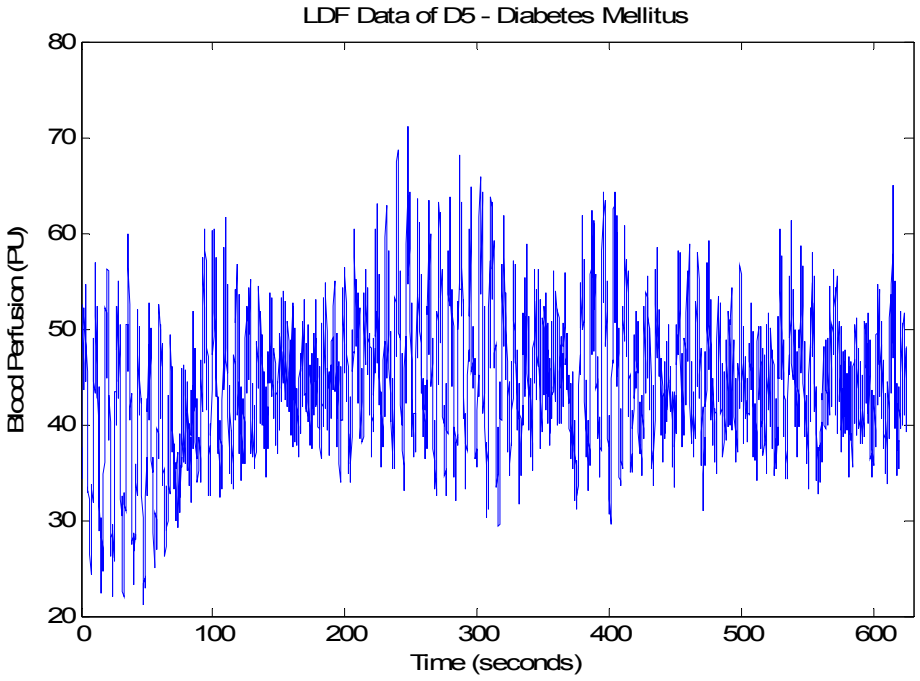


Figure 3.11 Raw data of blood perfusion vs. time for D5 (Diabetes Mellitus)

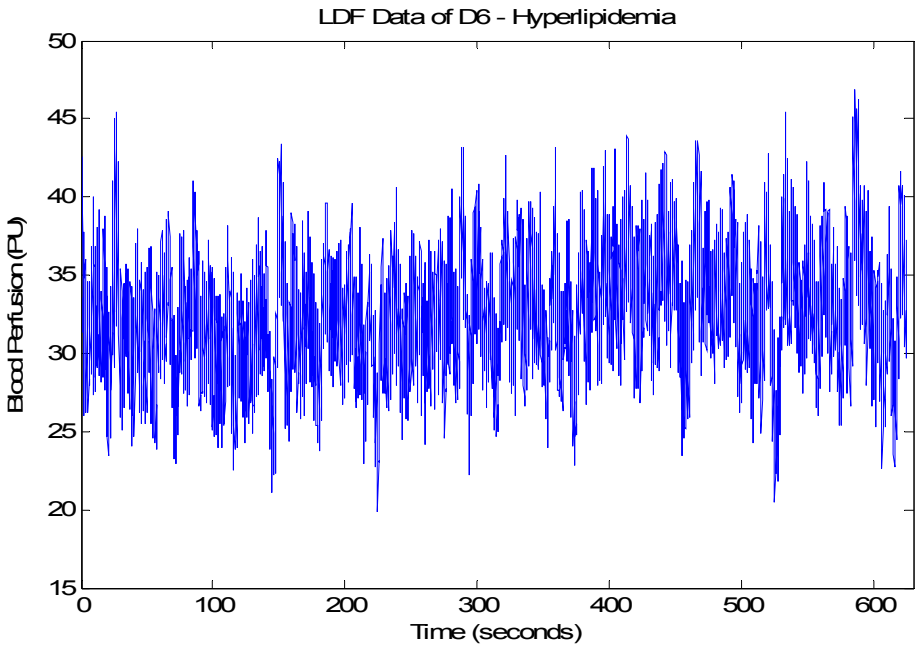


Figure 3.12 Raw data of blood perfusion vs. time for D6 (Hyperlipidemia)

The power spectra of all normal and diseased subjects are shown in figures 3.13 – 3.24.

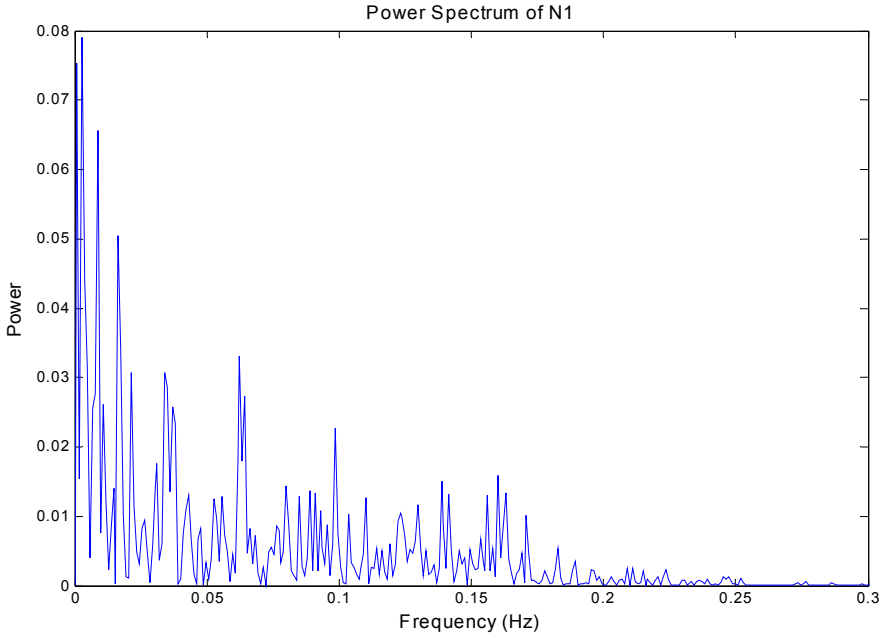


Figure 3.13 Power spectrum of N1

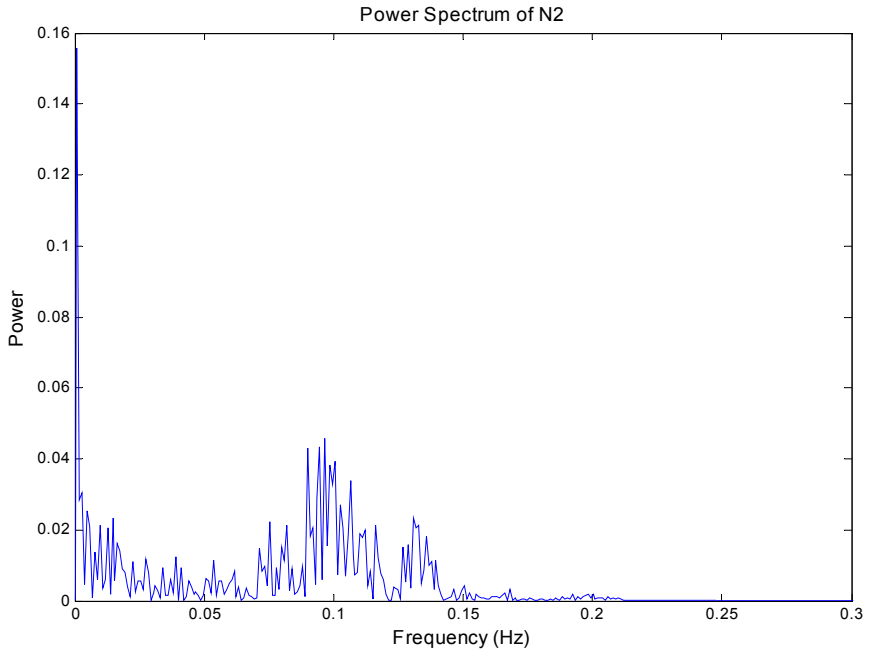


Figure 3.14 Power spectrum of N2

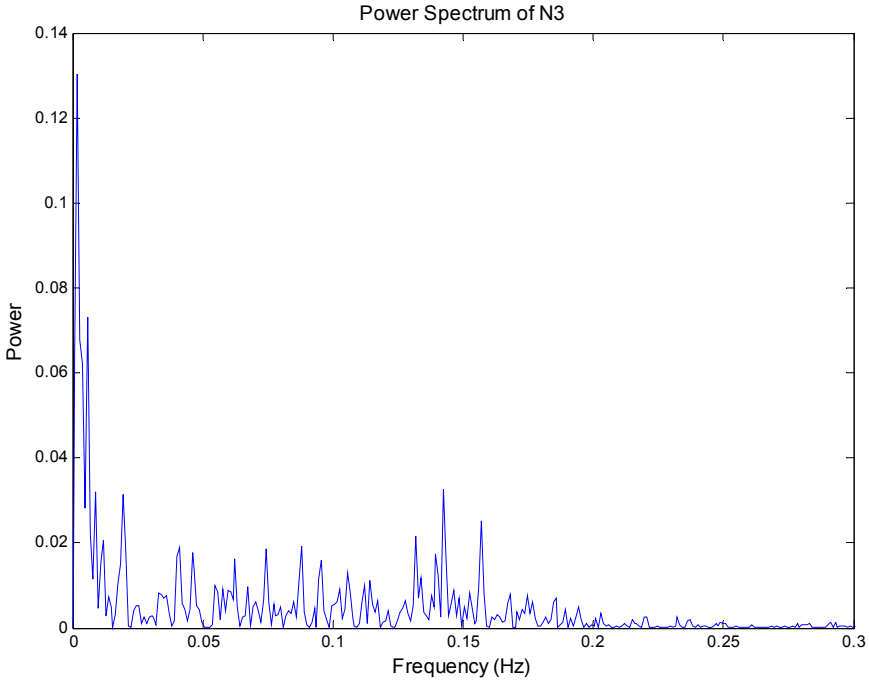


Figure 3.15 Power spectrum of N3

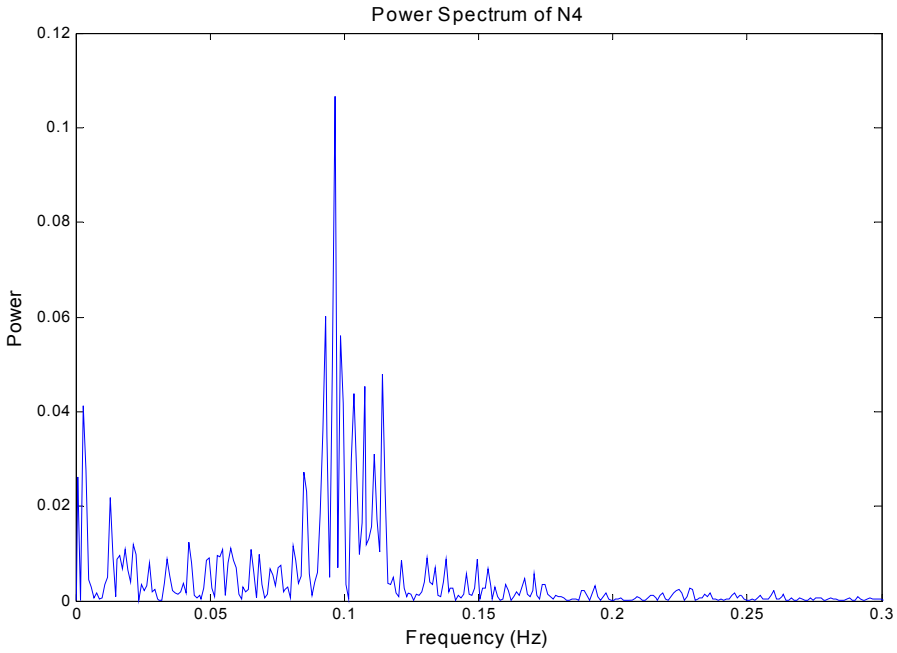


Figure 3.16 Power spectrum of N4

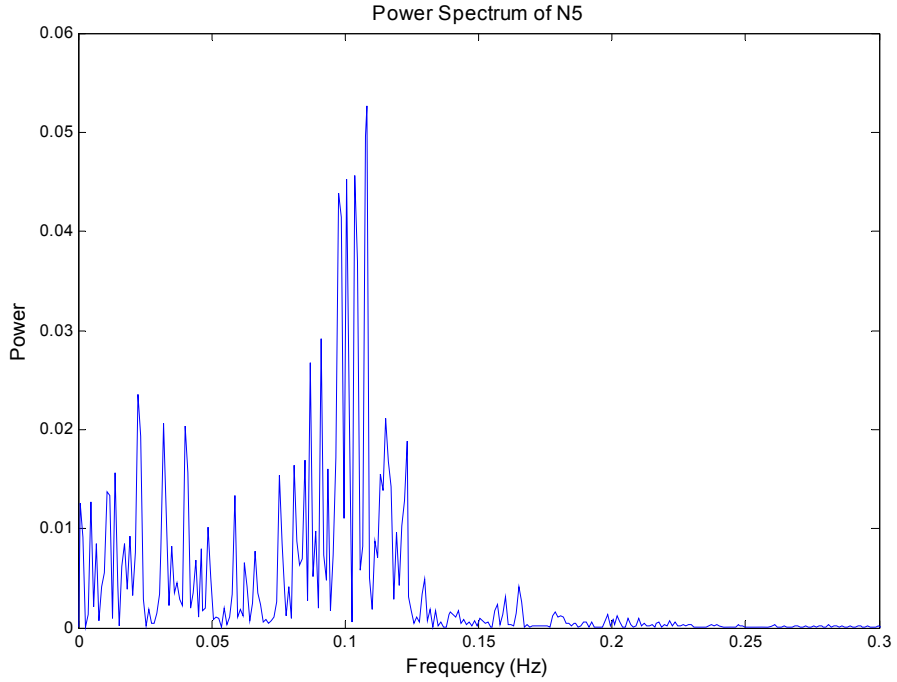


Figure 3.17 Power spectrum of N5

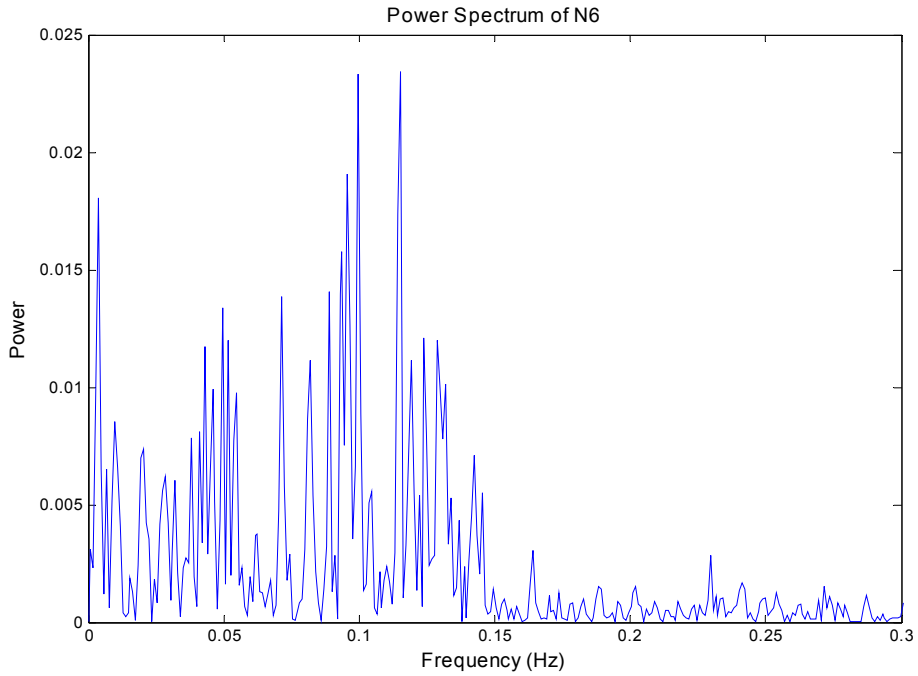


Figure 3.18 Power spectrum of N6

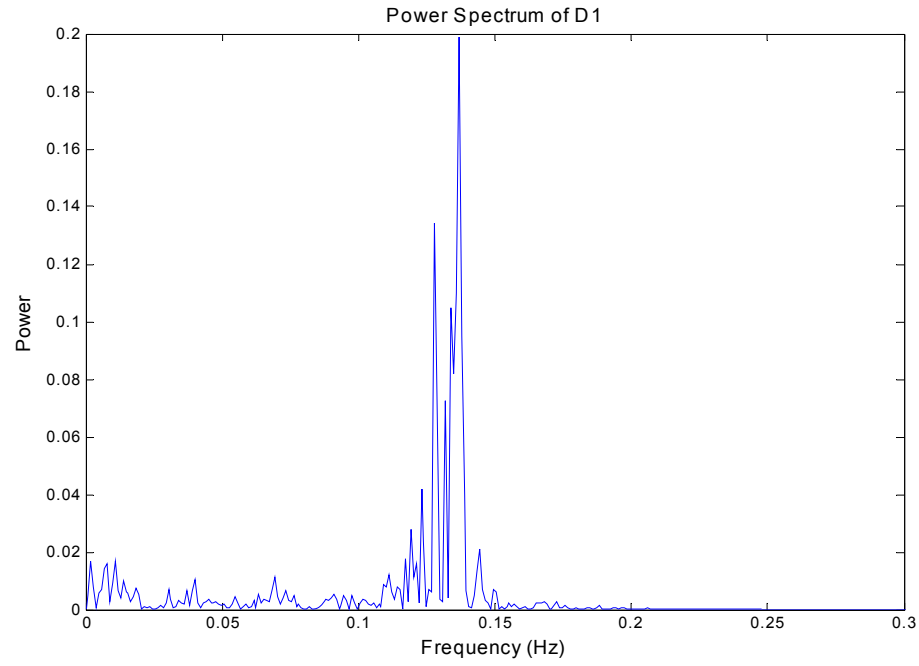


Figure 3.19 Power spectrum of D1

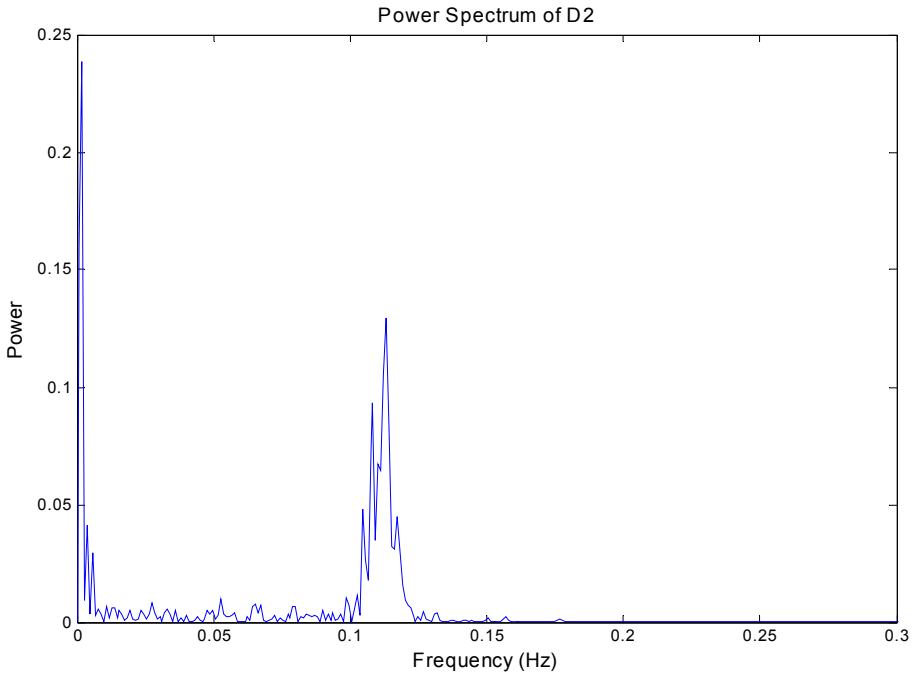


Figure 3.20 Power spectrum of D2

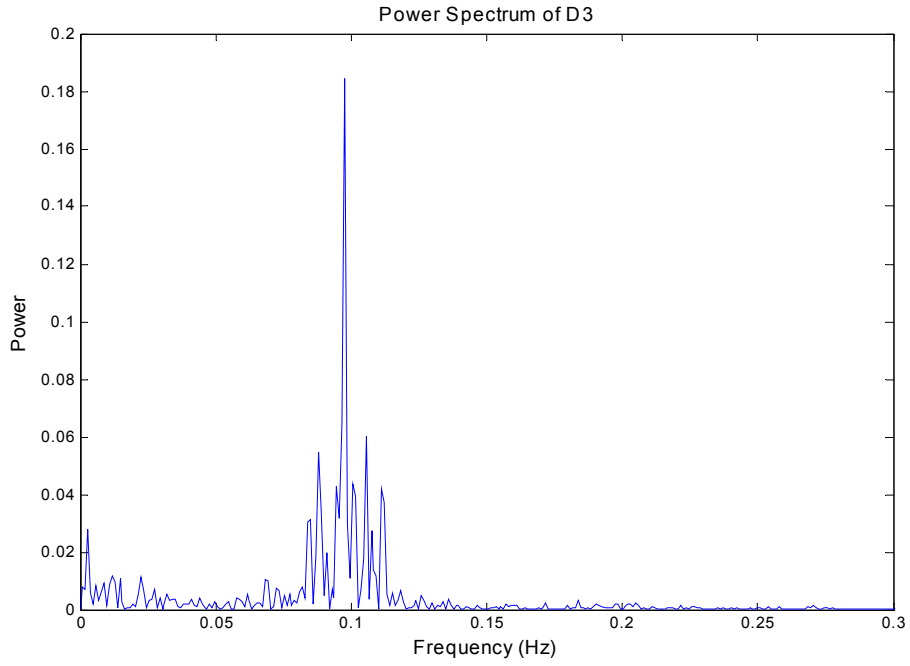


Figure 3.21 Power spectrum of D3

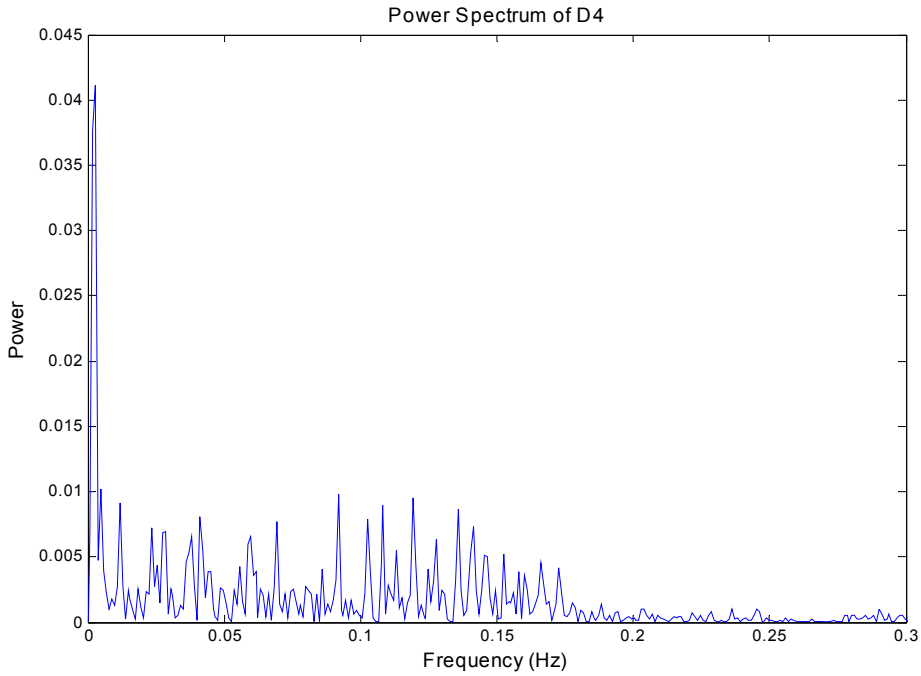


Figure 3.22 Power spectrum of D4

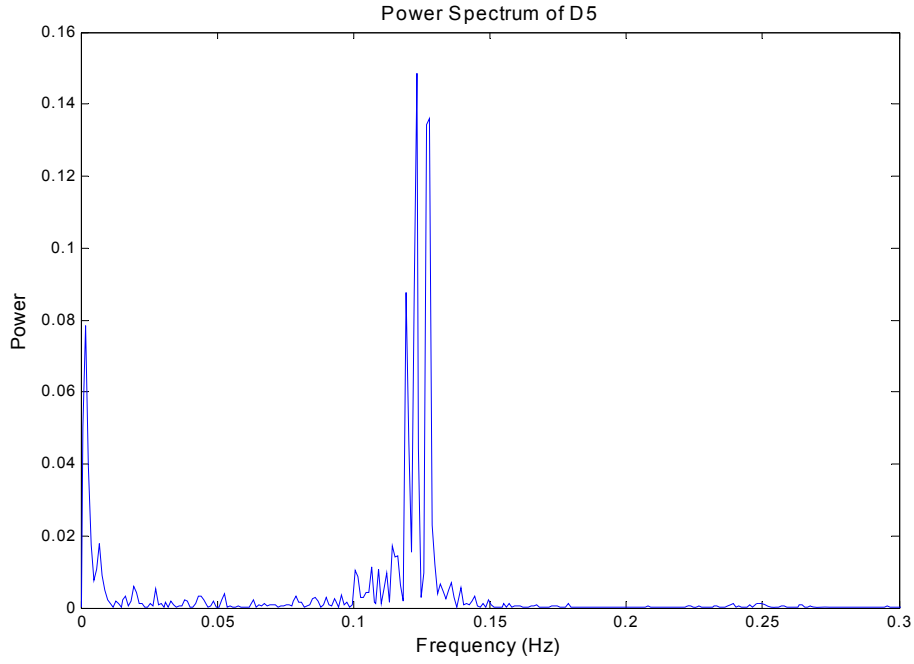


Figure 3.23 Power spectrum of D5

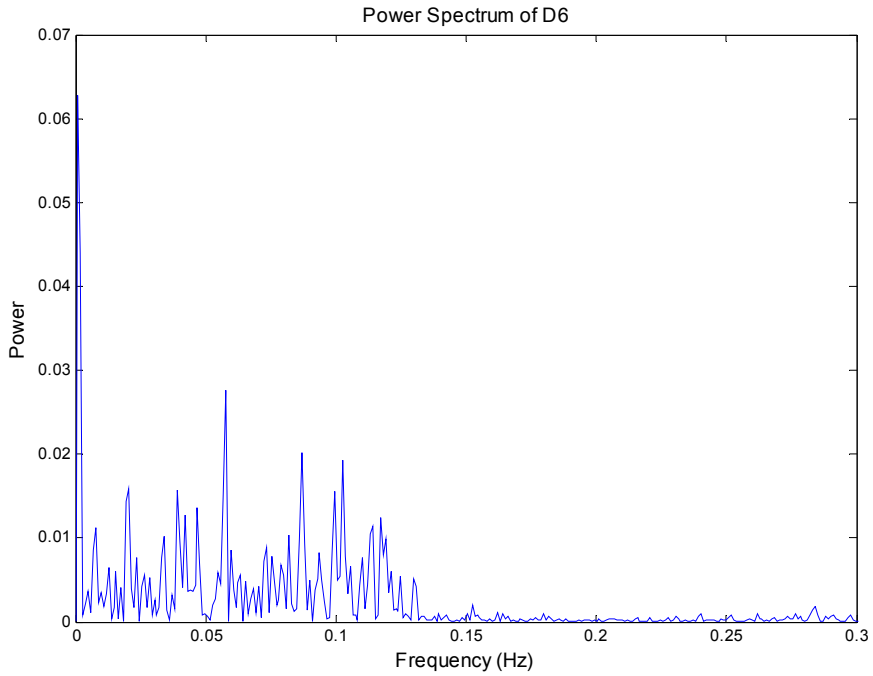


Figure 3.24 Power spectrum of D6

It was observed that the power spectra had multiple frequencies with a highly variable pattern. Major activity was present in the areas of < 0.5 Hz [Tables 3.1 – 3.6]. These frequencies are not to be confused with the pulse because the frequencies associated with pulse are > 1 Hz for most people. From the power spectra in figures 3.13 – 3.24, it is observed that the prominent peaks all occur between 0 Hz and 0.2 Hz. Only the first 10 frequencies from every subject have been tabulated. All frequencies were divided by the resolution r = 0.0019531 Hz. There is the possibility that some of the observed frequencies could be the result of beats, but review of the original data (Figures 3.1 – 3.12) in light of the spectra (Figures 3.13 – 3.24) do not show any evidence of beats.

Table 3.1 Sample frequencies and peaks found in subjects N1 and N2

| Subject N1 | | | Subject N2 | | |
|---|---|---|---|---|---|
| Frequency (f) | Amplitude | f/r | Frequency (f) | Amplitude | f/r |
| 0.0029297 | 0.078982 | 3 | 0.0048828 | 0.025312 | 5 |
| 0.0087891 | 0.065603 | 9 | 0.0078125 | 0.013652 | 8 |
| 0.010742 | 0.026053 | 11 | 0.0097656 | 0.021303 | 10 |
| 0.014648 | 0.014086 | 15 | 0.012695 | 0.020518 | 13 |
| 0.016602 | 0.050407 | 17 | 0.014648 | 0.023307 | 15 |
| 0.021484 | 0.030717 | 22 | 0.016602 | 0.016262 | 17 |
| 0.026367 | 0.009365 | 27 | 0.022461 | 0.011126 | 23 |
| 0.03125 | 0.017652 | 32 | 0.025391 | 0.0056175 | 26 |
| 0.03418 | 0.030745 | 35 | 0.027344 | 0.011799 | 28 |
| 0.037109 | 0.025764 | 38 | 0.03125 | 0.0043561 | 32 |

Table 3.2 Sample frequencies and peaks found in subjects N3 and N4

| Subject N3 | | | Subject N4 | | |
|---|---|---|---|---|---|
| Frequency (f) | Amplitude | f/r | Frequency (f) | Amplitude | f/r |
| 0.0019531 | 0.13044 | 2 | 0.0029297 | 0.041127 | 3 |
| 0.0058594 | 0.07315 | 6 | 0.0078125 | 0.0017284 | 8 |
| 0.0087891 | 0.03215 | 9 | 0.012695 | 0.021818 | 13 |
| 0.011719 | 0.020771 | 12 | 0.016602 | 0.0095216 | 17 |
| 0.013672 | 0.007298 | 14 | 0.018555 | 0.010748 | 19 |
| 0.019531 | 0.031529 | 20 | 0.021484 | 0.011869 | 22 |
| 0.025391 | 0.005305 | 26 | 0.027344 | 0.0081161 | 28 |
| 0.027344 | 0.002517 | 28 | 0.03418 | 0.008798 | 35 |
| 0.030273 | 0.002977 | 31 | 0.040039 | 0.0037456 | 41 |
| 0.033203 | 0.008307 | 34 | 0.041992 | 0.012454 | 43 |

Table 3.3 Sample frequencies and peaks found in subjects N5 and N6

| Subject N5 | | | Subject N6 | | |
|---|---|---|---|---|---|
| Frequency (f) | Amplitude | f/r | Frequency (f) | Amplitude | f/r |
| 0.0048828 | 0.012707 | 5 | 0.0039063 | 0.018046 | 4 |
| 0.0068359 | 0.008541 | 7 | 0.0068359 | 0.0065355 | 7 |
| 0.010742 | 0.0137 | 11 | 0.0097656 | 0.0085408 | 10 |
| 0.013672 | 0.015668 | 14 | 0.015625 | 0.001908 | 16 |
| 0.017578 | 0.008444 | 18 | 0.020508 | 0.0073828 | 21 |
| 0.019531 | 0.009317 | 20 | 0.024414 | 0.0018249 | 25 |
| 0.022461 | 0.023496 | 23 | 0.02832 | 0.0062159 | 29 |
| 0.026367 | 0.001822 | 27 | 0.032227 | 0.0060419 | 33 |
| 0.032227 | 0.020596 | 33 | 0.038086 | 0.0078697 | 39 |
| 0.035156 | 0.0082 | 36 | 0.041016 | 0.0081148 | 42 |

Table 3.4 Sample frequencies and peaks found in subjects D1 and D2

| Subject D1 | | | Subject D2 | | |
|---|---|---|---|---|---|
| Frequency (f) | Amplitude | f/r | Frequency (f) | Amplitude | f/r |
| 0.0019531 | 0.01702 | 2 | 0.0019531 | 0.23865 | 2 |
| 0.0078125 | 0.016134 | 8 | 0.0039063 | 0.04098 | 4 |
| 0.010742 | 0.016715 | 11 | 0.0058594 | 0.029503 | 6 |
| 0.013672 | 0.0099908 | 14 | 0.0078125 | 0.0053746 | 8 |
| 0.018555 | 0.0076389 | 19 | 0.010742 | 0.0065245 | 11 |
| 0.030273 | 0.0071244 | 31 | 0.013672 | 0.0062352 | 14 |
| 0.03418 | 0.0030924 | 35 | 0.015625 | 0.0048876 | 16 |
| 0.037109 | 0.0067866 | 38 | 0.019531 | 0.0048705 | 20 |
| 0.040039 | 0.010535 | 41 | 0.023438 | 0.0049347 | 24 |
| 0.044922 | 0.0034733 | 46 | 0.027344 | 0.0084742 | 28 |

Table 3.5 Sample frequencies and peaks found in subjects D3 and D4

| Subject D3 | | | Subject D4 | | |
|---|---|---|---|---|---|
| Frequency (f) | Amplitude | f/r | Frequency (f) | Amplitude | f/r |
| 0.0029297 | 0.02795 | 3 | 0.0029297 | 0.041167 | 3 |
| 0.0058594 | 0.0082721 | 6 | 0.0048828 | 0.010179 | 5 |
| 0.0087891 | 0.0090576 | 9 | 0.0087891 | 0.0017383 | 9 |
| 0.011719 | 0.011844 | 12 | 0.011719 | 0.0091319 | 12 |
| 0.014648 | 0.011018 | 15 | 0.014648 | 0.0024126 | 15 |
| 0.022461 | 0.011108 | 23 | 0.018555 | 0.0025582 | 19 |
| 0.027344 | 0.0070446 | 28 | 0.023438 | 0.0072297 | 24 |
| 0.029297 | 0.0039322 | 30 | 0.025391 | 0.0043423 | 26 |
| 0.032227 | 0.0054509 | 33 | 0.02832 | 0.0069786 | 29 |
| 0.035156 | 0.0034132 | 36 | 0.030273 | 0.0025487 | 31 |

Table 3.6 Sample frequencies and peaks found in subjects D5 and D6

| Subject D5 | | | Subject D6 | | |
|---|---|---|---|---|---|
| Frequency (f) | Amplitude | f/r | Frequency (f) | Amplitude | f/r |
| 0.0019531 | 0.078362 | 2 | 0.0048828 | 0.0036715 | 5 |
| 0.0068359 | 0.017717 | 7 | 0.0078125 | 0.011277 | 8 |
| 0.012695 | 0.0019086 | 13 | 0.0097656 | 0.0035205 | 10 |
| 0.016602 | 0.0031952 | 17 | 0.012695 | 0.0064635 | 13 |
| 0.019531 | 0.005814 | 20 | 0.015625 | 0.006001 | 16 |
| 0.027344 | 0.0052004 | 28 | 0.017578 | 0.0040529 | 18 |
| 0.03125 | 0.0015244 | 32 | 0.020508 | 0.015905 | 21 |
| 0.033203 | 0.0020281 | 34 | 0.023438 | 0.0077328 | 24 |
| 0.038086 | 0.0022441 | 39 | 0.026367 | 0.0056164 | 27 |
| 0.043945 | 0.0032373 | 45 | 0.02832 | 0.0053157 | 29 |

When the frequencies isolated from the power spectra were divided by the resolution frequency (0.0019531 Hz), many prime numbers were obtained. These were further categorized into series with each subject having at least three prime number series which are shown in tables 3.7 and 3.8. In the normal subjects prime numbers were obvious (e.g. 3, 5, etc.) whereas in diseased subjects, prime numbers were present as multiples (e.g. 6, 9, 15, etc.).

Table 3.7 Prime numbers and series in normal subjects

| Subject | Prime Number | Series |
|---|---|---|
| N1 | 3 | 1,3,5,9,17,18,19,22,26,29,31,39,42,51,54 |
| | 11 | 1,2,4,6,17 |
| | 17 | 1,3,4,7,8,9,11 |
| N2 | 3 | 5,14,15,16,19,21,28,30,33,35,39,42,44,50,52 |
| | 5 | 1,2,3,7,8,9,11,13,16,18,21,26,30,34 |
| | 13 | 1,2,4,5,9,10,11,12 |
| N3 | 3 | 2,3,4,14,23,2,4,29,30,35,36,39,40,45,47,50,52,62 |
| | 5 | 4,18,19,21,23,24,27,30,35,38 |
| | 7 | 2,4,6,8,14,15,22,23,25 |
| N4 | 3 | 1,17,26,27,29,33,38,39,47,51,57,66 |
| | 13 | 1,6,9, |
| | 19 | 1,5,6,9 |
| N5 | 3 | 6,9,11,12,15,20,27,29,31,32,37,42,45,61 |
| | 5 | 1,4,9,10,12,20,27 |
| | 7 | 1,2,8,11,13,18,19,23,29 |
| N6 | 3 | 7,11,13,14,17,23,28,31,32,34,44,45,51,54,56,58,61 |
| | 5 | 2,5,22,25,27,28,40 |
| | 7 | 1,3,6,8,12,13,14,20,24 |

Table 3.8 Prime numbers and series in diseased subjects

| Subject | Prime Number | Series |
|---|---|---|
| D1 | 3 | 20,21,25,26,31,38,39,40,42,45,51,53,59 |
| | 7 | 2,5,8,9,18,20, |
| | 19 | 1,2,6 |
| D2 | 3 | 2,8,15,17,18,23,27,32,35,37,40,45 |
| | 5 | 4,9,21,24,26,27 |
| | 7 | 2,4,7,15,22,23 |
| D3 | 3 | 1,2,3,4,5,10,11,12,14,15,17,21,28,29,30,31,36,38,43,50 |
| | 5 | 3,6,9,14,18,20,22,30 |
| | 7 | 4,6,7,8,9,10,11,12,19,23 |
| D4 | 3 | 1,3,4,5,8,13,14,19,30,33,35,37,51,52,54,59,63 |
| | 5 | 1,3,10,11,13,16,18,21,25,29,32,34,37 |
| | 13 | 2,3,5,12,14 |
| D5 | 3 | 13,15,18,23,27,39,42,45,51,53,57,61,67 |
| | 7 | 1,4,14,16,18,23 |
| | 13 | 1,3,5,9,11 |
| D6 | 3 | 6,7,8,9,16,24,25,27,28,32,34,35,36,39,40,52,56,62 |
| | 5 | 1,2,7,8,13,14,15,21,24,26,34 |
| | 13 | 1,5,9,10,11,12 |

Since 3 was a prime number commonly found in all subjects, the mean, standard deviation and skew of the amplitudes and frequencies of this series was computed.

| Skew | Normal | Diseased |
|---|---|---|
| Mean | 0.102869 | -0.20164 |
| SD | 0.129337 | 0.19344 |
| SEM | 0.052802 | 0.078972 |
| CSEM | 0.094998 | |
| t-test | 3.205395 | |

$$t_{calculated} > t_{critical} = t_{0.01(2),10} = 3.169$$

This result shows that the amplitudes in the power spectra of the diseased subjects tend to skew towards the left side i.e. higher frequencies > mean frequency, while those in the normal subjects skew towards the right side i.e. lower frequencies < mean frequency.

Using the peak amplitudes and their respective frequencies from the power spectra of the subject, the original waveforms were reconstructed. The mathematical formula used for reconstruction was a sum of sine waves whose basic form was

$$X = A * \sin(2\pi * t * f) \tag{3.1}$$

where **X** is the reconstructed wave

**A** is the amplitude (from power spectrum)

**t** is the time in seconds

**f** is the frequency in Hertz (from power spectrum)

The reconstructed wave was constructed using the formula

$$X = \sum_{i=1}^{n} X_i = \sum_{i=1}^{n} A_i * \sin(2\pi * t * f_i) \tag{3.2}$$

Some reconstructed patterns (a short segment of the entire pattern) are demonstrated in figure 3.25 and 3.26. The number of peaks used for reconstruction was minimal. If too many close frequencies were used, they produced beats. The reconstructed waves are not exact replicas of the original LDF signals. But the very fact that an image close to the original can be reproduced indicates that vasomotion data is a combination of sine waves with varying amplitudes and frequencies.

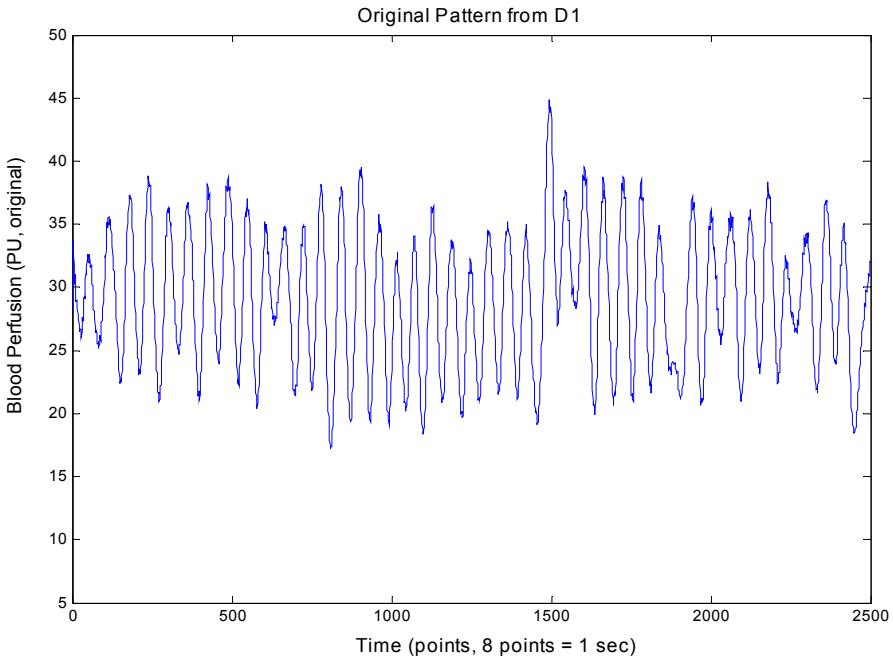


Figure 3.25 Part of the raw original data from D1

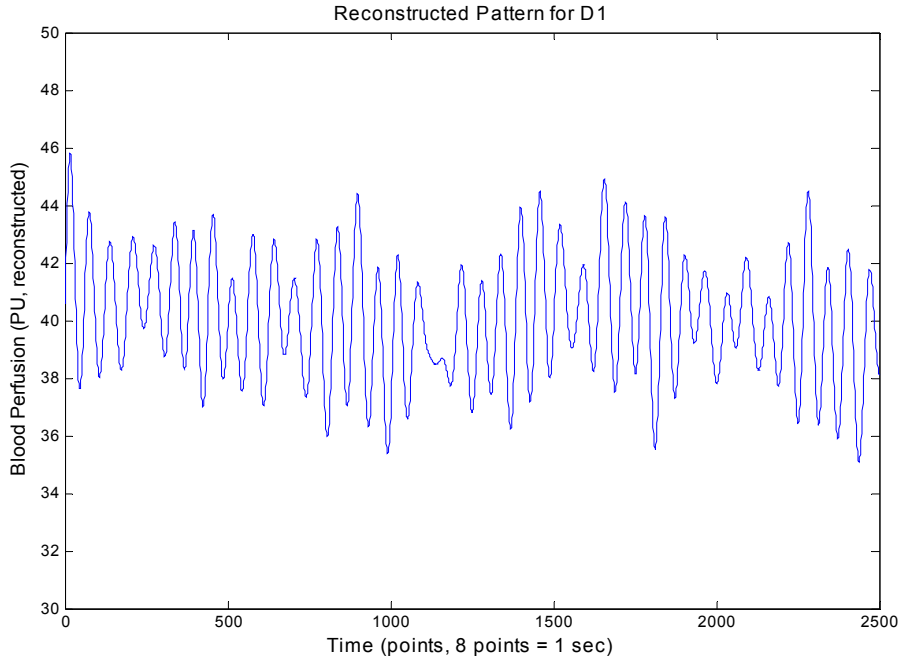


Figure 3.26 Reconstructed pattern for D1

Table 3.9 Sum of peaks at various frequencies; their ratios & outcomes

| Subject # | Sum of peaks occurring between frequencies 0.02-0.08 Hz (X1) | Sum of peaks occurring between frequencies 0.11-0.16 Hz (X2) | X1/X2 | Outcome |
|---|---|---|---|---|
| N1 | 0.2570516 | 0.122917 | 2.091262 | TN |
| N2 | 0.1635148 | 0.146318 | 1.11753 | TN |
| N3 | 0.1400217 | 0.1825271 | 0.767128 | FP |
| N4 | 0.1166001 | 0.1413521 | 0.824891 | FP |
| N5 | 0.1503849 | 0.0619181 | 2.428771 | TN |
| N6 | 0.1155279 | 0.10417844 | 1.108943 | TN |
| D1 | 0.0722123 | 0.6645174 | 0.108669 | TP |
| D2 | 0.0808077 | 0.1887484 | 0.428124 | TP |
| D3 | 0.0689848 | 0.0744669 | 0.926382 | TP |
| D4 | 0.0740734 | 0.0668558 | 1.107958 | FN |
| D5 | 0.026321 | 0.4267129 | 0.061683 | TP |
| D6 | 0.1711317 | 0.06489964 | 2.636867 | FN |

| Subjects | Disease + | Disease - |
|---|---|---|
| Test + | 4 | 2 |
| Test - | 2 | 4 |

$$OR = [4/2] / [2/4] = 4$$

The sum of peaks occurring between frequencies 0.02 Hz and 0.08 Hz and those occurring between frequencies 0.11 Hz and 0.16 Hz are tabulated in table 3.9. An odds ratio of 4 is obtained for the sample populations.

## 3.2 Results of SVD and phase plane analysis

The vectors were created as described in section 2.4 and phase diagrams were plotted.

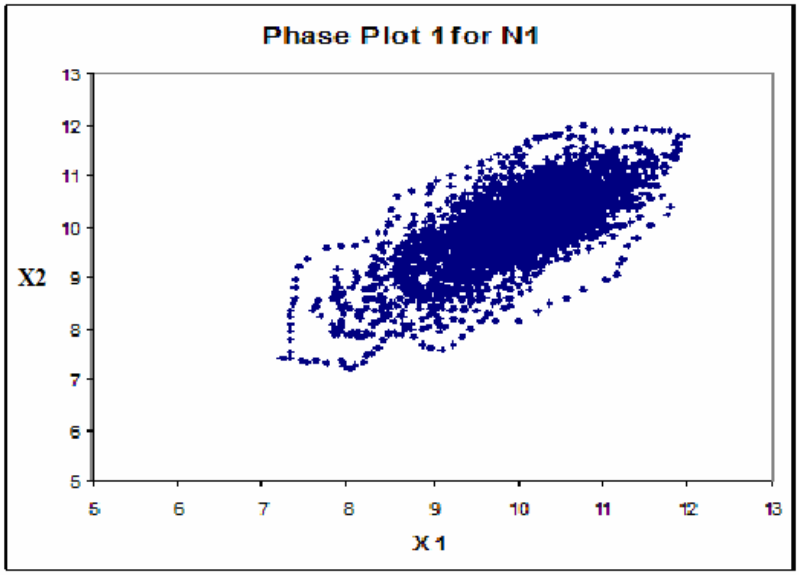


Figure 3.27 Phase plot of vector X1 vs. X2 for subject N1

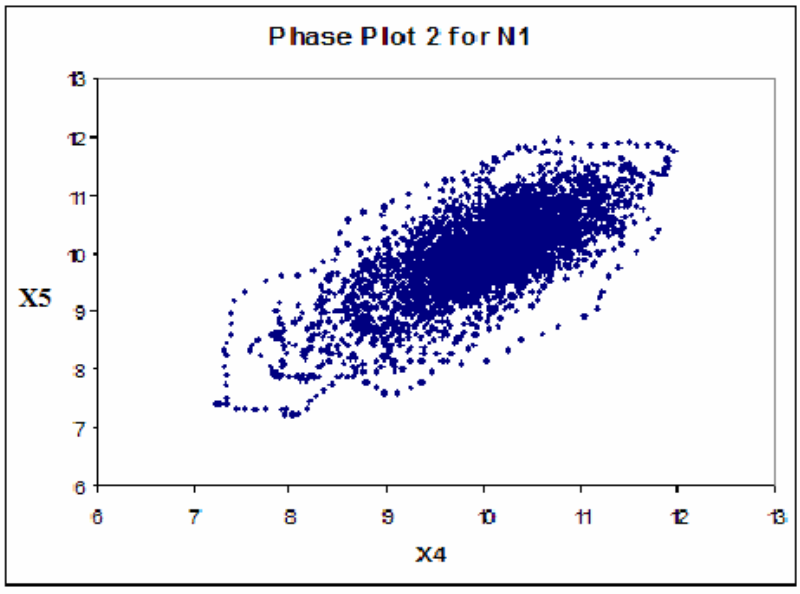


Figure 3.28 Phase plot of vector X4 vs. X5 for subject N1

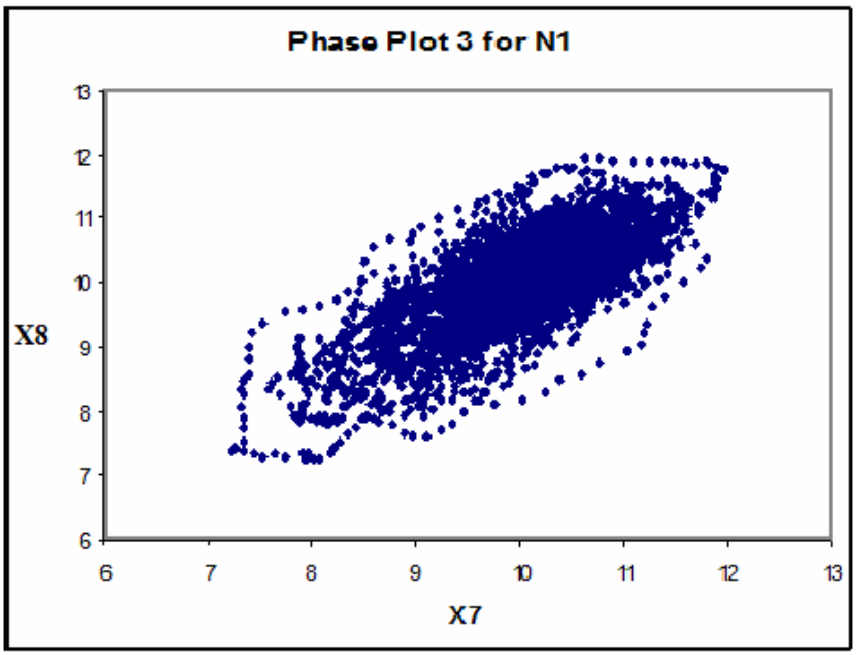


Figure 3.29 Phase plot of vector X7 vs. X8 for subject N1

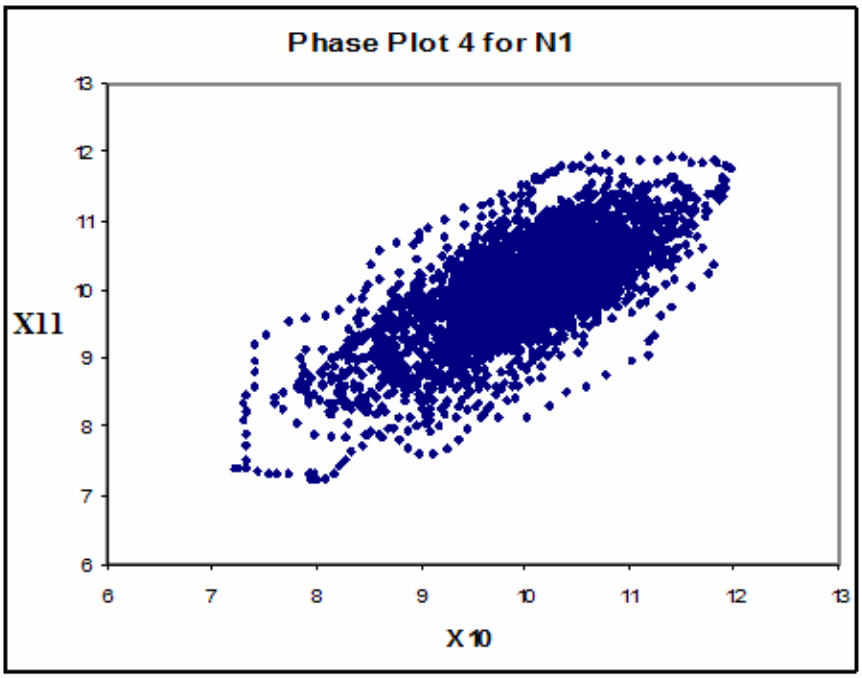


Figure 3.30 Phase plot of vector X10 vs. X11 for subject N1

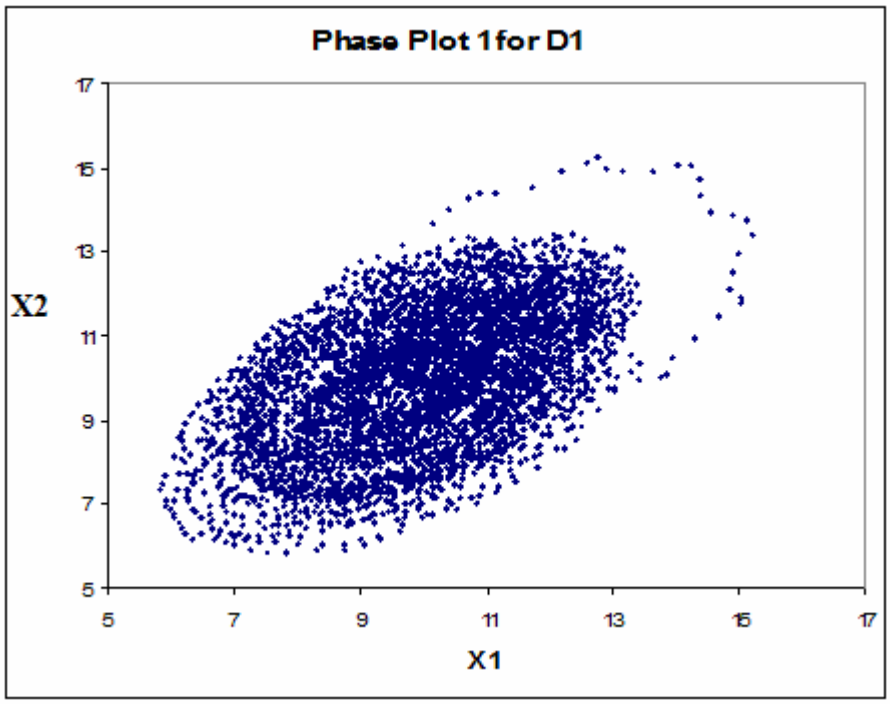


Figure 3.31 Phase plot of vector X1 vs. X2 for subject D1

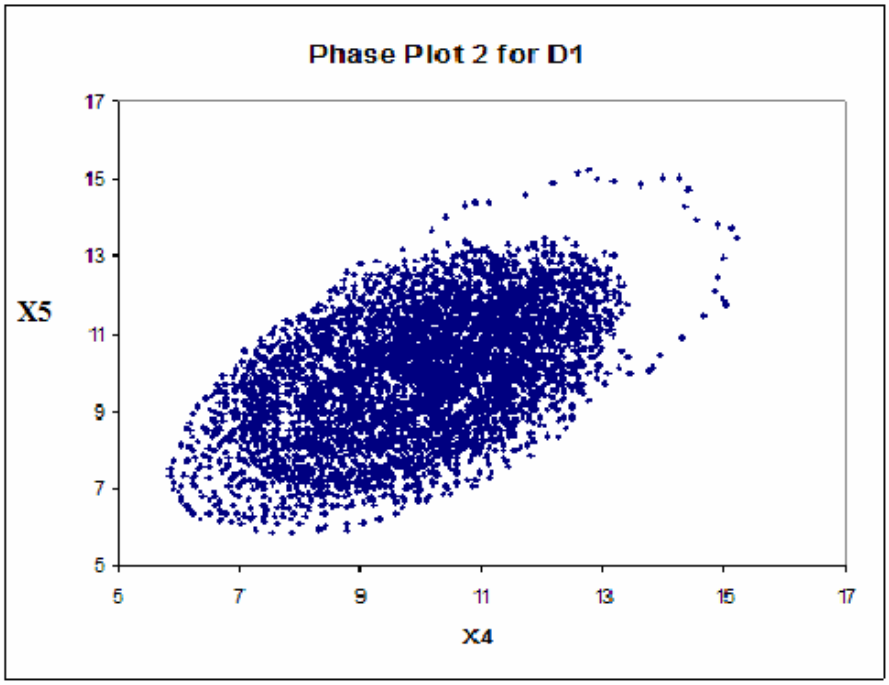


Figure 3.32 Phase plot of vector X4 vs. X5 for subject D1

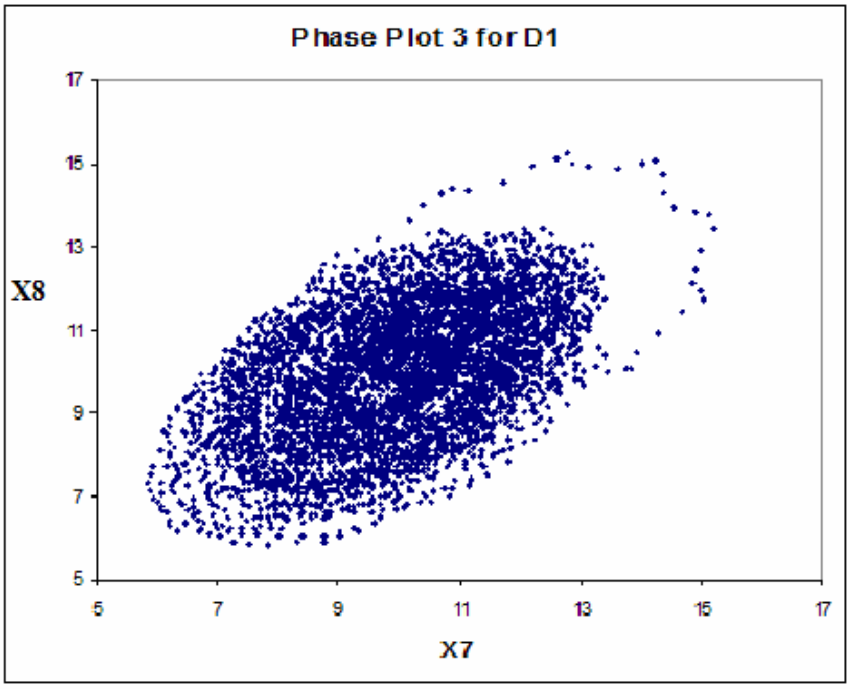


Figure 3.33 Phase plot of vector X7 vs. X8 for subject D1

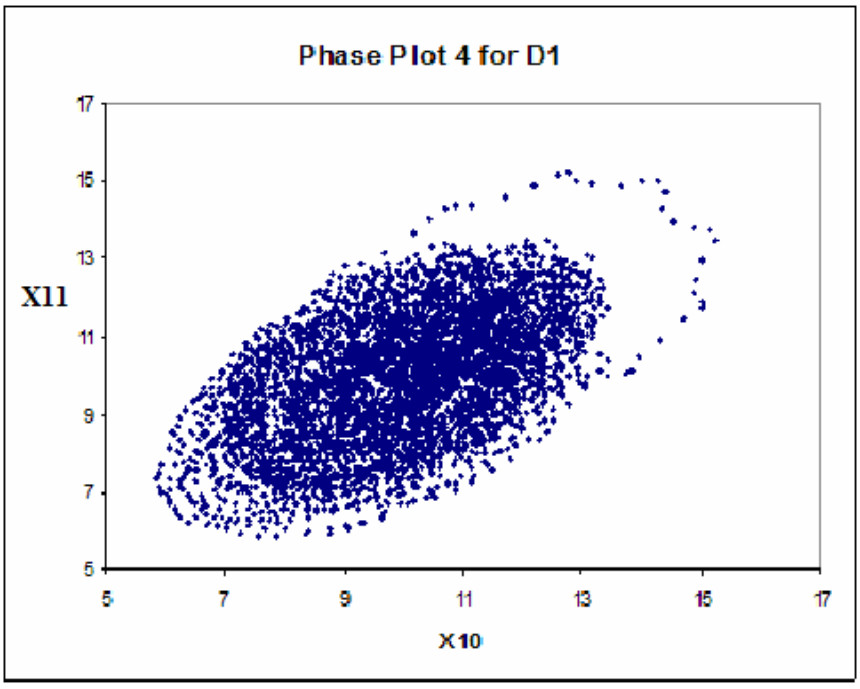


Figure 3.34 Phase plot of vector X10 vs. X11 for subject D1

The phase plots are go around themselves which implies that there is a lot of order and structure in the system. The phase plots of normal subjects appear more complex than those of the diseased subjects suggesting the loss or change of a variable in the vascular system of the diseased individuals.

The SVD was computed from Matlab and the singular values for normal and diseased subjects are shown in tables 3.10 and 3.11.

Table 3.10 Singular values for normal subjects

| Singular values | N1 | N2 | N3 | N4 | N5 | N6 |
|---|---|---|---|---|---|---|
| S1 | 2325.2 | 2327.7 | 2321.1 | 2324.3 | 2323.3 | 2321.6 |
| S2 | 67.907 | 113.76 | 28.989 | 198.94 | 151.26 | 153.03 |
| S3 | 59.295 | 110.65 | 27.606 | 195.38 | 149.94 | 145.03 |
| S4 | 52.638 | 73.578 | 27.549 | 115.9 | 115.4 | 131.91 |
| S5 | 49.086 | 64.693 | 26.996 | 97.277 | 78.237 | 129.62 |
| S6 | 36.737 | 37.943 | 20.023 | 69.115 | 51.671 | 117.03 |
| S7 | 23.924 | 24.351 | 13.797 | 54.403 | 41.292 | 110.38 |
| S8 | 16.983 | 15.415 | 10.018 | 50.421 | 31.999 | 99.43 |
| S9 | 11.993 | 9.2711 | 8.8605 | 46.088 | 29.471 | 88.732 |
| S10 | 9.391 | 7.8269 | 8.1289 | 44.956 | 28.302 | 84.28 |
| S11 | 7.5764 | 7.1132 | 8.0486 | 44.546 | 26.815 | 80.643 |

Table 3.11 Singular values for diseased subjects

| Singular values | D1 | D2 | D3 | D4 | D5 | D6 |
|---|---|---|---|---|---|---|
| S1 | 2322.8 | 2259.6 | 2322 | 2322.6 | 2326 | 2321.7 |
| S2 | 220.75 | 202.97 | 257.13 | 121.37 | 213.54 | 109.79 |
| S3 | 218.81 | 181.52 | 252.34 | 118.86 | 200.06 | 108.37 |
| S4 | 88.896 | 77.889 | 121.49 | 89.752 | 97.656 | 100.15 |
| S5 | 87.861 | 61.645 | 110.65 | 85.664 | 89.325 | 97.879 |
| S6 | 59.477 | 31.034 | 99.835 | 75.352 | 65.076 | 86.504 |
| S7 | 31.662 | 21.105 | 99 | 72.76 | 64.078 | 72.414 |
| S8 | 18.27 | 15.248 | 88.246 | 66.37 | 48.899 | 56.912 |
| S9 | 13.026 | 13.101 | 70.503 | 65.144 | 39.141 | 50.452 |
| S10 | 8.1784 | 10.837 | 61.853 | 63.17 | 34.664 | 44.129 |
| S11 | 5.2896 | 6.8948 | 55.818 | 41.979 | 33.797 | 37.164 |

The mean, SEM and CSEM were calculated for normal and diseased subjects. A two tailed t-test was performed as detailed in section 2.4. The results are tabulated in table 3.12.

Table 3.12 Mean, SEM and t-test values

| Singular Values | Mean | | SEM | | CSEM | t-test |
|---|---|---|---|---|---|---|
| | Normal | Diseased | Normal | Diseased | | |
| S1 | 2323.867 | 2312.45 | 0.996215 | 10.58873 | 10.63549 | -1.07345 |
| S2 | 118.981 | 187.5917 | 25.38312 | 24.00227 | 34.93439 | 1.963986 |
| S3 | 114.6502 | 179.9933 | 25.39192 | 23.10336 | 34.32951 | 1.903411 |
| S4 | 86.1625 | 95.97217 | 16.88173 | 6.020003 | 17.92298 | 0.547323 |
| S5 | 74.31817 | 88.83733 | 14.79803 | 6.603606 | 16.20461 | 0.89599 |
| S6 | 55.41983 | 69.54633 | 14.02955 | 9.73524 | 17.07639 | 0.827253 |
| S7 | 44.69117 | 60.16983 | 14.39947 | 11.79017 | 18.61056 | 0.831714 |
| S8 | 37.37767 | 48.99083 | 13.7797 | 11.52982 | 17.96711 | 0.646357 |
| S9 | 32.4026 | 41.8945 | 12.7472 | 10.169 | 16.30643 | 0.582096 |
| S10 | 30.4808 | 37.13857 | 12.33723 | 9.787564 | 15.74813 | 0.422765 |
| S11 | 29.1237 | 30.15707 | 11.95871 | 8.205916 | 14.50337 | 0.07125 |

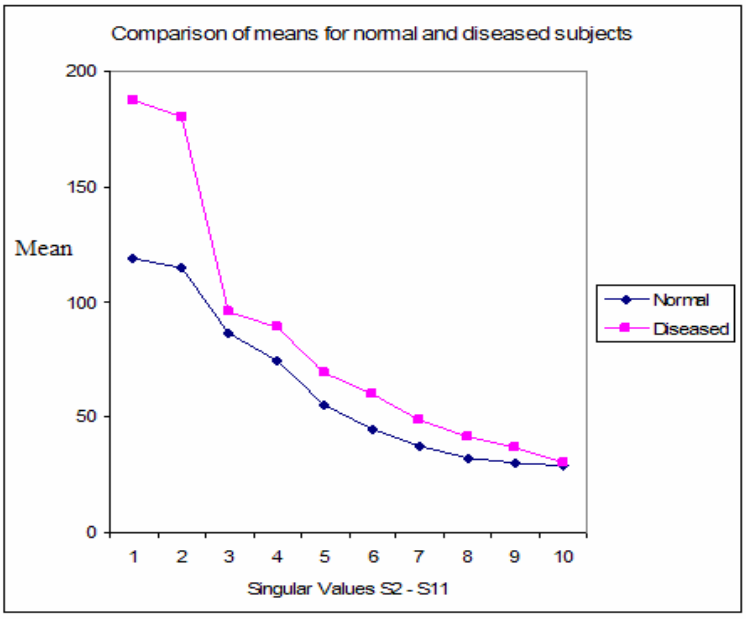


Figure 3.35 Comparison of means for normal and diseased subjects

The t-test did not yield significant results, but from figure 3.35 we observe that the difference in means between S3 and S4 for the diseased subjects is not proportional to that between the other singular values viz. S2 and S3 or S4 and S5, etc. as well as to those in the normal subject group. Also, if the trend line plateaus off, all the variables have been accounted for. In this case, the trend line does not approach zero but continues in a tangential fashion to the x-axis which implies that there many more variables influencing the vascular system that are still oblivious.

Taking this further, table 3.13 shows the product of the difference in singular values Δ(S3-S4) and Δ(S10-S11) and the ranks assigned to them.

Table 3.13 Rankings for observations of singular values in normal and diseased group

| Product of Δ(S3-S4) and Δ(S10-S11) for normal subjects | Product of Δ(S3-S4) and Δ(S10-S11) for diseased subjects | Ranks for normal subjects | Ranks for diseased subjects |
|---|---|---|---|
| 12.07979 | 375.2956 | 2 | 9 |
| 26.45829 | 408.5341 | 3 | 10 |
| 0.004577 | 789.6798 | 1 | 12 |
| 32.5868 | 616.8276 | 4 | 11 |
| 51.36098 | 88.78427 | 6 | 8 |
| 47.71744 | 57.2523 | 5 | 7 |
| $n_1 = 6$ | $n_2 = 6$ | $R_1 = 21$ | $R_2 = 57$ |

The Mann – Whitney statistic yields $U_{calculated} = 36$

and $U_{critical} = U_{0.05(2),6,6} = 35$

Since $U_{calculated} > U_{critical}$, it shows that the normal and diseased subject populations are different from each other. A two-tailed p-value of 0.003951 makes the test highly significant.

The standard deviation was computed for both subject populations and the F test was performed.

Table 3.14 Standard deviation and F-test results

| Singular Values | Standard Deviation | | $F(s_2/s_1)$ | $F(s_2/s_1)^2$ | Significance at $\alpha = 0.05$ |
|---|---|---|---|---|---|
| | Normal ($s_1$) | Diseased ($s_2$) | | | |
| S1 | 2.4402186 | 25.93698132 | 10.629 | 112.975 | significant |
| S2 | 62.17569 | 58.79332017 | 1.0575 | 1.11837 | not significant |
| S3 | 62.197259 | 56.59145153 | 1.0991 | 1.20793 | not significant |
| S4 | 41.351634 | 14.74593455 | 2.8043 | 7.86395 | significant |
| S5 | 36.247625 | 16.17546442 | 2.2409 | 5.02164 | not significant |
| S6 | 34.365238 | 23.84636964 | 1.4411 | 2.0768 | not significant |
| S7 | 35.271359 | 28.87990751 | 1.2213 | 1.4916 | not significant |
| S8 | 33.753232 | 28.24218568 | 1.1951 | 1.42835 | not significant |
| S9 | 31.224139 | 24.90884994 | 1.2535 | 1.57135 | not significant |
| S10 | 30.219923 | 23.97453665 | 1.2605 | 1.58886 | not significant |
| S11 | 29.292742 | 20.10030739 | 1.4573 | 2.12381 | not significant |

$$F_{calculated} > F_{critical} = F_{0.05\,(2),\,5,\,5} = 7.15$$

From table 3.14, we observe that the F-test provides good results and the normal and diseased groups are significantly different from each other for singular values S1 and S4. The normal group tends to cluster together while the diseased group is spread apart.

The singular values were fitted using polynomials as shown in figures 3.36 and 3.37 using JMP software. The normal subjects had low mean square error (MSE < 15) compared to diseased subjects (MSE > 15), but the degree of the polynomial varied for subjects of both categories between linear, quadratic and cubic.

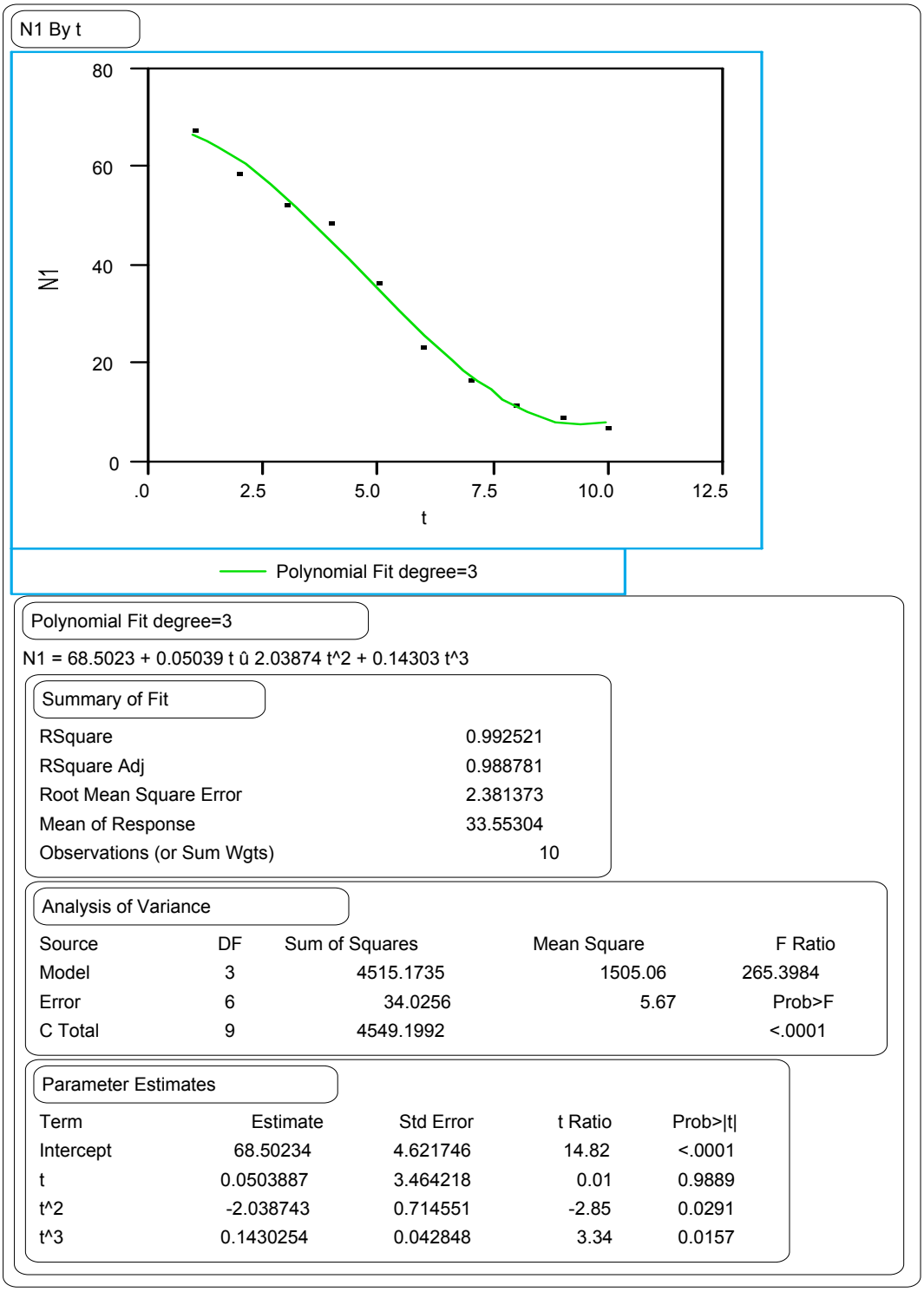


Figure 3.36 Polynomial curve fitting for subject N1

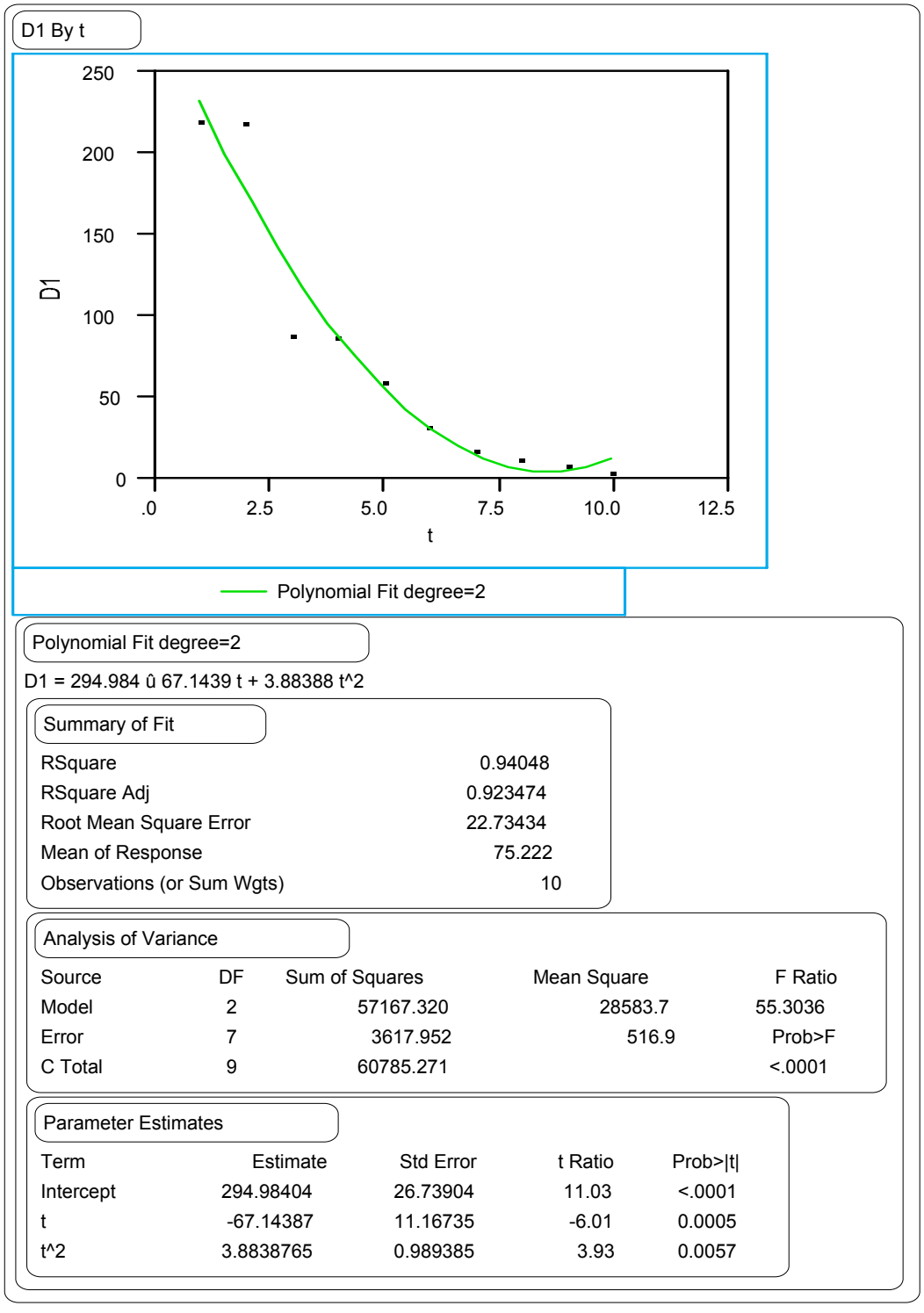


Figure 3.37 Polynomial curve fitting for subject D1

# CHAPTER 4

# DISCUSSION

The vascular system is composed of arteries which branch into arterioles, capillaries and then join together to form venules and veins. The arteries and arterioles provide peripheral vascular resistance and regulate blood flow. Regulation consists of a balance between vasoconstriction and vasodilatation. This balance maintains an average blood perfusion sufficient for all the needs of the cells, but the diameter of each artery and arteriole varies over time. When one measures the average perfusion for a given site, averaged over several minutes, one would obtain a constant value for a given region. That value is determined by the particular vascular and tissue anatomy at that site, as well as the blood perfusing the vessels. Average blood perfusion offers useful but limited amounts of information concerning the regulation of the peripheral vascular supply; however, the vasoconstriction and vasodilatation of the arteries and arterioles alter the observed vascular perfusion. This altered blood perfusion gives rise to variation of blood flow, observable by laser Doppler flow.

This study demonstrates that the complex pattern observed by laser Doppler flow of blood perfusion can be analyzed into discrete frequencies. The frequencies arise from the synchronized contraction and relaxation of these arteries and arterioles. The nature of the arterial vessel wall determines the features of flow variations of each of

the compartment and the presence of contractile fibers in the wall of the arterioles makes them undergo significant diameter changes.

The contractile nature of the arterioles gives rise to apparently rhythmic patterns. Curri has speculated that the rhythm may originate from pulsatile cardiac pressure or from the intrinsic relaxation-contraction cycles of arteries and arterioles known as vasomotion [19]. Chambers and Clark observed that small arterioles, down to the smallest branches showed spontaneous diameter changes with a periodicity of "several times a minute". They called this activity as vasomotion [20, 31].

Since vasomotion appears to originate in arterioles, it could become synchronized with the pathological states in many vessels [21]. Arterioles maintain peripheral vascular resistance, in the face of falling arterial blood pressure, which they achieve by vasoconstriction. They are responsible for allowing blood to flow to the distal tissue, which is achieved by vasodilatation. Some authors, using the technique of LDF, attribute the rhythmical activity to a local feedback mechanism where accumulation of metabolic products or depletion of oxygen causes the smooth muscles to contract or dilate the vessels. This rhythmatic flow is independent of heart and respiration rate with no relation between frequency and amplitude. The appearance of rhythmic activity varies between subjects, with different sites showing different frequencies [22].

## 4.1 Discussion of spectral analysis results

Analysis of LDF data in the past has not been of sufficient depth to make it a useful tool for probing the physiological mechanism causing vasomotion in the microvasculature or diagnosing abnormal (activated) from normal vasculature in the clinical setting. Most studies have identified one or at the most two frequencies [21]. Some studies have not used fast Fourier transforms and have failed to find the fine detail of frequencies as seen in our study [21]. Spectral analysis of relatively simple flow dynamics, as seen in the skin of the forehead, provides the details necessary to elucidate distinguishing vasculature features for mechanism and individual differences. Fagrell has postulated that the LDF signal is mainly generated by blood flow in the non-nutritional, sub-papillary vascular bed and only a very small portion (2-10%) is produced by capillary blood flow. In the skin of the hands and feet, more than 90% of the blood flows only through the sub-papillary vascular bed and less than 10% goes through the nutritional capillaries [23]; however our study utilized the skin of the forehead, which has a thickness of 40-50 micrometers, as opposed to the skin of the finger, which has a thickness of 200-400 micrometers [17]. Thus, our study is most likely to include an even mixture of nutritional and non-nutritional vessels.

Note that in figures 3.13 - 3.24 all plots show a significant number of distinct frequencies less than 0.4 Hz and the predominant frequencies are less than 0.2 Hz. For most people, their pulsatile frequency (related to the beating heart) is greater than 1.0 Hz; 72 beats/ min (a common pulse rate) yields a frequency of 1.2 Hz. Because higher frequencies, especially as a driving force ($d^2x/dt^2 + kx = F_o \cos \omega t$) impose their

frequency on higher harmonics in the system but not lower frequencies, vasomotion does not originate from the pulse. Griffith corroborated the independence of vasomotion from the pulse rate by showing the presence of vasomotion in isolated arteries undergoing constant infusion [24].

Another observation concerning our observed frequencies is the lack of a continuous series of integers as in we do not have a simple harmonic series (1, 2, 3, …). Continuing with this, we do not observe beats either. In each series of subjects, with the fundamental frequency assigned a value of 1, a frequency of 2 is clearly absent. If the frequency at 1 was the result of beat phenomenon, then one would observe frequency pairs of 2 and 3, or 3 and 4, or 5 and 6, etc. None of these combinations occur. Further, inspection of the raw data plots fail to reveal the typical pattern associated with beats. Thus, most of our observed frequencies are unique.

The raw data in figures 3.1 – 3.12 appear so complex that most observers would attribute it to noise, but spectral analysis demonstrates that they are composed of multiple individual frequencies which can be reconstructed according to equation 3.2. Most of the data is free of noise. We isolated frequencies from each of the subject's spectra even though the patterns looked unlike each other. Tables 3.1 – 3.6 show the various frequencies obtained from the spectral estimation of each of the subjects. Spectral analysis of the LDF signals revealed the presence of periodic components. For example (tables 3.1 – 3.3), the frequency of 0.0029297 Hz (T = 5.69 min) was seen in normal subjects N1 and N4 (absent in others) and the frequency of 0.0625 Hz (T = 0.27 min) was seen in all subjects (except N2). The frequency of 0.10352 Hz (T = 9.66 sec)

was observed subjects N1, N4 and N5 (absent in N2, N3 and N6). This presence of assorted but relative frequencies implies an inherent rhythm in the vascular system. Because spectral analysis demonstrates distinct frequencies that are integral and discrete (not continuous), the patterns seen in figures 3.1 – 3.12 are neither noise nor chaotic dynamics [25]. In fact, the spectra indicate that they are deterministic and periodic [26].

There are many primes and multiples of prime numbers that are found in the series of integers obtained by division with the resolution frequency (tables 3.1 – 3.6). The frequencies can be broken down into various series which have a different prime base (tables 3.7 and 3.8). Each prime number can be associated with a variable influencing the vascular system. All these variables are in constant interaction; basic primes are in the role of controlling variables and the higher order primes (integer multiples which have a prime number as their base) may behave as refining variables or may represent faster frequencies based on the primary frequency.

The skew of the series obtained from prime number 3 was different for normal and diseased individuals. Diseased subjects skewed towards the left side i.e. more faster frequencies > mean frequency while the normal subjects skewed towards the right side i.e. more slower frequencies < mean frequency. This shows that the skew can be used to discriminate between the two groups when used as a test in patients. It also leads to some important questions such as the reason for the appearance of faster frequencies, if they provide greater sustained vascular resistance and their relation to the inherent feedback mechanism.

Lewis found a frequency of 2.1 ± 0.4 (mean ± standard deviation) cycles per minute (cpm) or 0.035 Hz [21]. They also noted frequencies of 1 Hz every 5 to 7 minutes and they interpreted these results as beats. Colantuoni observed frequencies of 1-3 cpm [27]. The frequencies in our data were in the range 0.022-0.048 Hz, assuming a class interval of 95%. Our results are in agreement with earlier studies, but they show much finer detail without the necessity of invoking beats.

The significance of our findings is that firstly, the flow through the arterioles in the microcirculation exhibits complex behavior. Complex behavior is to be expected based on the anatomy and metabolic positive feedback found in the system. If one were to examine just one arteriolar network, one could see the structural complexity of the network. Each arteriolar network is composed of at least five levels of arterioles [28]. Further, each arteriolar network anastomoses with other arterioles at its hierarchal level. Beginning with the first arteriole, if each arteriole gives off three branches, then at level five, there would be 121 arterioles and the total number of arterioles in this network would be 121. Further, the venule retrieving blood from the capillary bed supplied by a given arteriole lies paired with their supplying arteriole providing a means for feedback regulation. This arrangement allows for metabolites in the venules to diffuse into the nearby arterioles where they can induce a response by the endothelial cells to synthesize and release nitric oxide [29]. The nitric oxide then causes vasodilation of the arteriole.

The presence of cardiac risk factors impairs endothelial-dependent dilation of resistance vessels. Endothelial-dependent vasodilator function is lost in a progressive and hierarchical fashion. Such impairment has been demonstrated in patients with

hypertension, diabetes mellitus or hypercholesterolemia. Endothelial dysfunction in patients with atherosclerosis is a systemic process, not necessarily confined to vessels that develop atherosclerosis, thus permitting noninvasive evaluation of endothelial function in readily accessible arteries [30]. Endothelial dysfunction plays a pivotal role in the pathogenesis and clinical manifestations of atherosclerosis because the normal endothelium has lost its ability to prevent abnormal vasoconstriction and to inhibit platelet aggregation and smooth muscle cell proliferation [32, 33]. Because endothelial dysfunction precedes the development of clinical atherosclerosis, it would be desirable to identify and treat endothelial dysfunction before atherosclerosis develops.

Impaired endothelial function has been documented in the past by impaired vasodilation to acetylcholine. Using high resolution ultrasound, the authors had demonstrated impaired flow-mediated vasodilation (FMD). This is an endothelium-dependent response of large peripheral arteries mediated by nitric oxide, in large arteries for patients with hypercholesterolemia (hyperlipidemia), children with homozygous homocystinuria, and CAD. Coronary risk factors interact to produce this endothelial dysfunction which may extend to the microvasculature [34].

The examination of the power spectra suggests that the diseased subjects have greater amplitudes at faster frequencies. The hypothesis was tested by summing the peaks occurring between frequencies 0.02 Hz - 0.07 Hz (X1) and 0.11 Hz – 0.16 Hz (X2) and taking their ratio (X1/X2). With 1.0 as the threshold, normal subjects typically had a ratio > 1.0 while the diseased subjects had a ratio < 1.0. By these criteria, an odds

ratio of 4 was obtained which implied that examination of peak height as a function of frequency has the potential to separate the normal and diseased groups.

The internal carotid artery is the major supplier of blood to the brain located in the neck. Stenosis of the carotid artery and plaque formation are the principle causes of cerebrovascular diseases which result in ischemia and stroke. Since our study measures the blood flow in the vessels of the forehead, it becomes equivalent to detecting any abnormalities in the general microvasculature.

## 4.2 Discussion of SVD and phase plane analysis results

Phase plane analysis is a qualitative method of analyzing a system. It allows making a connection between what is seen physically and mathematically (set of differential equations). Observation of the phase plots in figures 3.27 – 3.34 displays the elaborate structure and periodicity of the vascular system. The plots go around themselves which exhibits the mutual interaction of the variables; although every variable has the ability to act independently.

The phase plots of the normal subjects (figures 3.27 – 3.30) appear more complex than those of the diseased subjects (figures 3.31 – 3.34). This may be due to loss of one or more variables influencing the vascular system in the diseased subjects.

This theory of variables and their effect on the vascular system is substantiated by singular values obtained in tables 3.10 and 3.11. The fact that the singular values do not reach zero puts the least number of variables acting on the microvasculature at 5. The singular values are alike in both normal and diseased groups because the same

variables execute the necessary functions at the micro level, hence no significant t–test results. But, even though the means are same, the variances for the two groups (S1 and S4) are greatly different which is substantiated by the F-test. The disproportional difference between S3 and S4 in diseased subjects is confirmed by the Mann-Whitney test which points in the direction of a loss or change of one or more variables in their vascular system.

# CHAPTER 5

# CONCLUSIONS AND RECOMMENDATIONS FOR FUTURE WORK

## 5.1 Conclusions

The objective of analyzing vasomotion data was to establish its significance as a mechanism that is independent of any centralized control. Its uniqueness was evident from fact that the data we obtained from every subject was dynamic, complex and had absolutely no structure to it. Spectral analysis of the raw data revealed its deterministic and periodic nature.

Major activity was concentrated in the region of 0 Hz - 0.2 Hz distinguishing it from pulse. The presence of assorted but relative frequencies implied an inherent rhythm in the vascular system. The absence of a continuous series of integers means that the system is not harmonic. The data has no elements of beats either. The diseased subjects were demarcated from the normal subjects by having higher amplitudes at faster frequencies. Various series with different prime numbers at their bases were formulated. Diseased subjects skewed towards the left side i.e. more faster frequencies > mean frequency while the normal subjects skewed towards the right side i.e. more slower frequencies < mean frequency (for series 3). The techniques of SVD and phase plane analysis demonstrated the high level of structure and periodicity in the vascular

system along with providing insight into the number of variables acting on the vasculature.

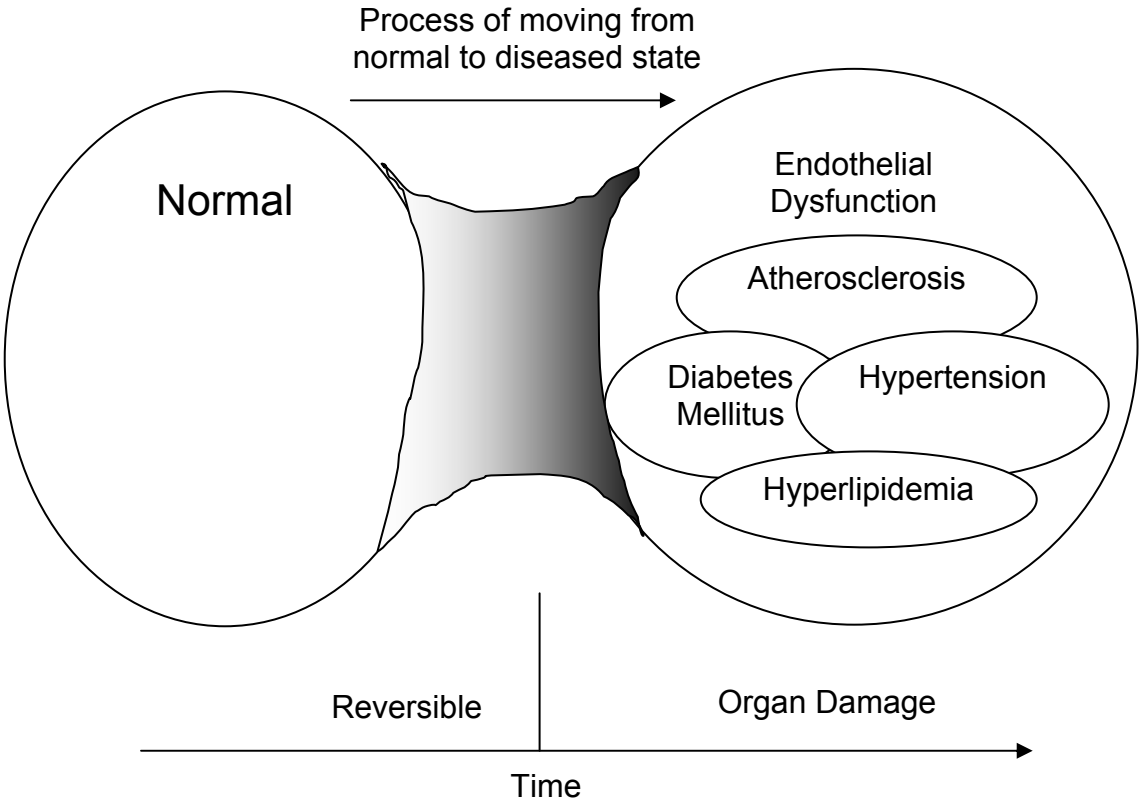


Figure 5.1 Progression of disease in an individual

The figure depicts the gradual progression of a vascular disease in an individual. By using the techniques of spectral analysis, SVD and phase plane analysis, the disease can be identified in the initial stages when it is reversible and complications of the disease, which lead to organ damage, can be prevented.

Spectral analysis has the potential to identify and separate structural patterns of blood flow, thus providing an alternate method of distinguishing between normal and diseased individuals. Due to the uniqueness of the blood flow pattern, it acts like a fingerprinting device. It can be used to ascertain any vascular disease before the individual is symptomatic.

## 5.2 Recommendations for future work

The results obtained from the study of vasomotion opens a wide arena to be investigated. The appearance of prime numbers and their frequency of occurrence can be examined in detail. Recurring patterns (and reverse patterns) in the LDF data need to be identified so that useful information about the vasculature can be studied. A physical model of the vascular system can be constructed to observe the dynamics of vasomotion.

The subjects in the present study were calm and relaxed with no movement. The effects of altering the state of the individual, as in exercising the subject vs. the normal subject can to be studied. Heating the probe (which is possible in PF3) and systematically warming the skin in a controlled manner are other options that can be considered. The influence of addition of chemicals such as acetylcholine (vasodilator), caffeine (vasoconstrictor), etc. to the vasculature can be analyzed. This would determine the state of the vascular system; if the system would change from periodic to quasiperiodic or chaotic.

The high level of structure and periodicity in the vascular system as seen by SVD and phase plane analysis can be interpreted by a system of differential equations. A model system of differential equations and its phase plane analysis can be set-up and the experimental data can be compared with it. A mathematical representation of the vascular system with differential equations can thus be achieved.

# APPENDIX A

# DATA ANALYSIS ALGORITHM

%Power_spectrum.m [35]

```
y = xlsread('subject.xls');                    % Obtaining normalized data from excel file
NFFT = 2^(nextpow2(length(y)));
                    % Next highest power of 2 >= to length(y) used to calculate the FFT
FFTY = fft(y,NFFT);
                    % Padding of fft with zeros so that length(FFTY) is equal to NFFT
N = ceil((NFFT+1)/2);                          % Calculation of number of unique points
FFTY = FFTY(1:N);              % Second half of fft discarded because fft is symmetric
Y = abs(FFTY);                                                  % Magnitude of fft of y
Y = Y/length(y);            % Scaling of fft so that it is not a function of the length of y
Y = Y.^2;                                                % Squaring of magnitude of FFTY
Y = Y*2;                % Multiply by 2 because second half of FFTY was thrown above
Y(1) = Y(1)/2;                                                % DC Component is unique
if ~rem(NFFT,2)
        Y(end) = Y(end)/2;              % Nyquist point included because NFFT is even
end
Fs = 8;                                                         % sampling frequency
f = (0:N-1)*Fs/NFFT;                % Evenly spaced frequency vector with N points
plot(f,Y);                                                      % Generation of plot
title('Power Spectrum of Subject');
xlabel('Frequency (Hz)');
ylabel('Power');
```

% Singular_Value_Decomposition.m

```
y = xlsread ('subjectsvd.xls');
[U, S, V] = svd(y,0);                          % S is the matrix of singular values
Y = y * V;
```

# APPENDIX B

## CONSENT FORM FOR SUBJECTS OF VASOMOTION STUDY

| Department of Veterans Affairs | **Dallas Veteran Affairs Medical Center Research Consent Form** |
|---|---|
| Date: | Page 1 of 7 |
| Subject Name: | |
| Title of Study: | Skin Blood Flow |
| Principal Investigator: | Martin H. Kroll, M.D. |
| Co-Investigator(s): | Manisha Shah, M.D. |
| Study Coordinators: | |

Before agreeing to take part in this research study, it is important that you read and understand the proposed research explained below. It describes the procedures, benefits, risks and discomforts of the study. It also describes other treatments that are open to you and your right to withdraw from the study at any time. It is important for you to understand that no promises can be made about the results of the study.

1. WHAT IS THIS RESEARCH STUDY ABOUT?

This study involves research on blood flow and its relationship to diseases of the heart and vessels. The purpose of this research is to relate the pattern of blood flow with such diseases as coronary heart disease, such as myocardial infarction, high blood pressure, heart failure, and diabetes. The expected duration of your participation is about 30 minutes. The approximate number of research subjects involved in this study is 80.

2. WHAT WILL HAPPEN DURING THE STUDY?

We will measure blood flow in the skin of the forehead using a technique known as laser Doppler flow (using the PF3 device from PERIMED). A red light is shone on the skin and the red cells in the vessels reflect the light back, indicating the amount of blood flow. The cable carrying the light is adhered to the skin using a gentle adhesive. The whole process takes about 30 minutes. One needs to remain still and quiet during this time.

3. WHAT ARE MY RISKS?

There are no risks due to this procedure. Unforeseen risks: A previously unknown problem could result from your taking part in this research. It is not possible to estimate the chances of such problems or how serious the problems could be.

Any new findings will be given to you that may affect your willingness to take part in this study. If new findings are discovered, you will be asked to sign a new (updated) informed consent form to document that new information provided in the updated Consent Form has been explained to you.

4. WILL THE RESEARCH BENEFIT ME OR OTHERS?

The only benefit is the increased knowledge related to your disease.

5. WHAT ARE MY ALTERNATIVES TO BEING A RESEARCH SUBJECT?

This study does not preclude standard diagnostic procedures.

6. WILL I GET PAID?

You will be paid $10 for the session. We need your name, social security number, and your address.

7. WILL I HAVE TO PAY?

No. Subjects do not pay for treatment associated with participation in a VA research program.

8. DOES BEING PREGNANT OR THE POSSIBILITY OF BEING PREGNANT PREVENT ME FROM TAKING PART?

No.

9. WHAT IF I GET INJURED?

The study doctors will make every effort to prevent injury that could result from this research. While the VA does not have to pay research subjects for injuries caused by research, it will provide needed medical treatment for injuries related to research according to Federal Law.
You do not give up any legal rights to payment for injuries caused by research by signing this form. The Federal Tort Claims Act is a way to request payment from the government for injuries caused by VA research. Study doctors at the VA will advise you about treatments open to you at the Dallas VA in case of bad effects of the research. You should report any problems to them promptly. The study doctors' phone numbers are at the end of this form.

10. ARE MY RESEARCH RECORDS SAFE FROM THE PUBLIC?
The study doctors keep your research records private in the same way as your other medical records. No one has access to your records except as required by law. You are, however, authorizing the Dallas VA Institutional Review Board (IRB), the Dallas VA Research and Development Committee and the members of the Dallas VA Research Office to inspect your medical and research records. These committees, people, and offices at the Dallas VAMC are responsible for overseeing human research studies.

By signing this form, you will allow the Veterans Health Administration (VHA) to provide Dr. Kroll and his research team access to the following health data about you:
age, gender, routine blood tests and lab results as well as the presence or absence of coronary artery disease, high blood pressure, heart failure, diabetes and renal failure.
If you do not sign this form, you will not be part of the study. This approval to use your health data will expire at the end of the research study which involves storing health data that may be used in future research. By signing this form, you agree to allow the health data collected in this study to be added to that database or used in future research.

VHA complies with the requirements of the Health Insurance Portability and Accountability Act of 1996 and all other laws that protect your privacy. We will protect your health data according to these laws. Despite these protections, there is a possibility that your health data could be used or disclosed in a way that it will no longer be protected. Our Notice of Privacy Practices (a separate document) provides more information on how we protect your health data. If you do not have a copy of the Notice, the research team will provide one to you.

If you choose to take part in the study, certain government agencies (such as the FDA or VA) may look at your research records. Your name as a subject in this study is private, and will not be included in any report prepared as a result of this study.

11. DO I HAVE TO TAKE PART IN THIS STUDY, OR CAN I WITHDRAW FROM THE STUDY?

Taking part in this study is voluntary and you may refuse to take part without penalty or loss of benefits to which you are otherwise entitled. You are free to withdraw your consent and stop taking part at any time. Not taking part in the study will in no way affect the quality of care you receive now or in the future from the VA. This will also not affect your right to take part in other studies. The study doctors will answer any questions you may have about the study.

You can also take back your authorization for the VHA or the study doctors to access or to share your health data with outside parties at any time. To stop taking part in the study or to take back your authorization, you should contact both:
1) Dr. Kroll or his representative listed at the bottom of this form, and
2) The IRB Administrator of the Dallas VA Medical Center [telephone: 214-857-0291; mail: Dallas VAMC, IRB Administrator (151) 4500 S. Lancaster Rd. Dallas, TX 75216.

If you decide to take back your authorization, you will be given a form to show your desire in writing. If you take back your authorization, you will not be able to continue to take part in the study. This will not affect your rights as a VHA patient.

If you take back your authorization, Dr. Kroll and his research team can keep using health data about you that has been collected. No health data will be collected after you take back the authorization. Your doctor may also take you out of the study without your consent for medical or administrative reasons.

12. WHOM SHOULD I CONTACT FOR QUESTIONS OR PROBLEMS?

If you have any questions about this study or have any bad effects of your treatment, you should call the study doctor, whose name and contact number appear on the last page of this form.

If you have any questions about your rights as a patient, complaints about your treatment or general concerns about the conduct of the research study, you may contact the Dallas VAMC Patient Representatives at 214-857-0482. The Patient Representative will guide you in resolving your question or complaint.

If you have a medical emergency you should immediately call 911 for assistance.

| | |
|---|---|
| Date: | |
| Subject Name: | |
| Title of Study: | Skin Blood Flow |
| Principal Investigator: | Martin H. Kroll, M.D. |
| Co-Investigator(s): | Manisha Shah, M.D. |
| Study Coordinators: | |

RESEARCH SUBJECT'S RIGHTS:

I have read or have had read to me all of the above. The study has been explained to me and all of my questions have been answered. If I have questions later, I understand I can contact Dr. Kroll. I have been told of the risks or discomforts and possible benefits of the study. I have been told of other choices of treatment open to me.

I understand that I do not have to take part in this study and my refusal to take part will involve no penalty or loss of rights to which I am entitled. I may withdraw at any time without penalty or loss of VA or other benefits to which I am entitled. The study doctor can take me out of the study at any time if it appears to be medically harmful to me, if I fail to follow directions for taking part in this study, if it is discovered that I do not meet the study requirements, or if the study is canceled.

In case there are medical problems or questions, I have been told I can call Dr. Kroll at 214-857-0578 during the day or at 800-725-4436 after hours.

I understand my rights as a research subject, and I voluntarily consent to take part in this study. I understand what the study is about and how and why it is being done. I authorize the use of my identifiable patient health information as described in this form. I will receive a signed copy of this consent form.

Subject's Signature Date

Signature of Subject's Representative* Subject's Representative (print)
*Only required if subject not competent.

| | |
|---|---|
| Date: | |
| Subject Name: | |
| Title of Study: | Skin Blood Flow |
| Principal Investigator: | Martin H. Kroll, M.D. |
| Co-Investigator(s): | Manisha Shah, M.D. |
| Study Coordinators: | |

I certify that I have reviewed the contents of this form with the person signing above, who, in my opinion, understood the explanation. I have explained the known side effects and benefits of the research.

Principal Investigator or designee (Signature) Date

Research Subject's Bill of Rights

1. Be informed of the nature and purpose of the research.
2. Be clearly told of the procedures to be followed in the medical research, and any drug or device to be used.
3. Be told of any discomforts and risks that might be expected from the research.
4. Be clearly told of any benefits that the patient might expect from the research.
5. Be clearly told of any other appropriate procedures, drugs, or devices that might be helpful to the patient, and their risks and benefits.
6. Be clearly told how to get medical treatment, if needed, after the research is finished if problems should arise.
7. Be given the chance to ask any questions about the research or the procedures involved.
8. Be clearly told that consent to take part in the medical research and/or release of identifiable patient health information may be taken back at any time. The patient may stop taking part in the medical research without any penalty or loss of VA or other benefits.
9. Be given a copy of the signed and dated written consent form.
10. Be given the chance to decide to consent or not to consent to a medical research study without any force, fraud, deceit, duress, coercion, or undue influence on the patient's decision.

REFERENCES

1. Holger N. & Christian A. (2003). Vasomotion: Mechanisms and Physiological Importance. Molecular Interventions, 3(2), 79-81.

2. Jones, T.W. (1852). Discovery that the veins of the bat's wing are endowed with rhythmical contractility and that onward flow of blood is accelerated by each contraction. Phil. Trans. Roy. Soc. Lond., 142, 131–136.

3. Schmidt, J.A., Borgstrom, P., Bruttig, S.P., Fronek, A. & Intaglietta M. (1993). Vasomotion as a flow-dependent phenomenon. In C. Allegra, Intaglietta & K. Messmer (Eds.), Progress in Applied Microcirculation, 20, (pp. 34-51). Basel: Karger.

4. Menger, M. D. & Messmer, K. (1993). Can laser Doppler flowmetry detect spontaneous arteriolar vasomotion? In C. Allegra, Intaglietta & K. Messmer (Eds.), Progress in Applied Microcirculation, 20, (pp. 27-33). Basel: Karger.

5. Seifert, H., Jager, K. & Bollinger, A. (1988). Analysis of flow motion by Laser Doppler technique in patients with peripheral arterial occlusive disease. Int. J Microcirc: Clin. Exp. 7, 223-236.

6. Braverman, I. M. & Schechner, J. S. (1991). Contour mapping of the cutaneous microvasculature by computerized laser Doppler velocimetry. Journal of Investigative Dermatology, 97, 1013-1018.

7. Salerud, E. G., Tenland, T., Nilsson, G. E. & Oberg, P. A. (1983). Rhythmical variations in human skin blood flow. Int. J Microcirc., Clin. Exp. 2, 91-102.

8. Johnson, P. C. & Smiesko, V. (1995). Overview of regulatory mechanisms in the microcirculation. In J. A. Bevan, G. Kaley, G. M. Rubanyi (Eds.), Flow-dependent regulation of vascular function. (pp. 178-213). New York: Oxford Univ. Press.

9. Griffith, T. M. (1995). Endothelium-derived relaxing factor and the control of flow in conduit and resistance arteries. In J. A. Bevan, G. Kaley, G. M. Rubanyi (Eds.), Flow-dependent regulation of vascular function. (pp. 178-213). New York: Oxford Univ. Press.

10. Lettinger, N. Et al. (1995). The effect of NO/EDRF and monocytes/macrophages on LDL-oxidation. Journal of Physiol. Pharmacol., 46, 385-408.

11. Holtz, J. (1996). Peripheral Circulation: Fundamental Concepts, Comparative Aspects of Control in Specific Vascular Sections and Lymph Flow. In R. Greger & U. Windhorst (Eds.), Comprehensive Human Physiology, 2. (pp. 1866-1867, 1966). New York: Springer Verlag Press.

12. Perimed Systems. Perimed PF 3 Laser Doppler Flowmeter Reference Manual.

13. Tompkins, W. J., (2002). Other Time- and Frequency- Domain Techniques. In W. J. Tompkins (Ed.), Biomedical Digital Signal Processing, (pp. 216-220). New Jersey: Pearson Education, Inc.

14. Albano, A. M., Mees, A. I., Guzman, G. C. & Rapp, P. E. (1987). Data requirements for reliable estimation of correlation dimensions. In H. Degn, A. V. Holden & L. F. Olsen (Eds.), Chaos in biological systems, (pp. 216-217). New York: Plenum Press.

15. Briggs, J. & Peat, F. D. (1989). Attractors and Reading Maps. In B. J. Hiley & F. D. Peat (Eds.), Turbulent mirror, (pp. 31-44). New York: Harper & Row Publishers.

16. Schoen, F. J. (2005). Blood Vessels. In V. Kumar, A. K. Abbas & N. Fausto (Eds.), Pathologic Basis of Disease, (pp. 511-529). Philadelphia: Elsevier Inc.

17. Nilsson, G. E., Tenland, T. & Oberg, P. A. (1980). A new instrument for continuous measurement of tissue blood flow by light beating spectroscopy. IEEE Trans. Biomed. Eng., 27(1), 2-9.

18. Anderson. (1981). The optics of human skin. Journal of Investigative Dermatology, 77, 13-19.

19. Curri, S. B. (1993). Vasomotility, Sphygmicity and Vasomotion. In C. Allegra, Intaglietta & K. Messmer (Eds.), Progress in Applied Microcirculation, 20, (pp. 8-9). Basel: Karger.

20. Chambers, R. & Zweifach, B. W. (1944). The topography and function of the mesenteric capillary circulation. The American Journal of Anatomy, 75, 173-205.

21. Lewis, D. H., Gustafsson, U., Wardell, K. & Nilsson, G. E. (1993). Flow motion in skeletal muscle. In C. Allegra, Intaglietta & K. Messmer (Eds.), Progress in Applied Microcirculation, 20, (pp. 59-66). Basel: Karger.

22. Guyton, A. C., Ross, J. M., Carrier, O. & Walker, J. R. (1964). Evidence for tissue oxygen demand as the major factor causing autoregulation. Circ. Res. 15(1), 60-68.

23. Fagrell, B. (1995). Advances in microcirculation network evaluation: An update. International Journal of Microcirculation, 1, 34-40.

24. Griffith, T. M. & Edwards, D. H. (1995). Complexity of chaotic vasomotion is insensitive to flow and pressure but can be regulated by external control. American Journal of Physiology, 269, H656- H668.

25. Berge, P., Pomeau, Y. & Vidal, C. (1984). Order within chaos, NY: John Wiley & Sons.

26. Schuster, H. G. (1989). The transition from quasiperiodicity to chaos. In W. Greulich (Eds.), Deterministic chaos, an introduction, (pp. 147-151). Weinheim: VCH Publishers.

27. Colantuoni, A., Bertuglia, S. & Intaglietta, M. (1984). Quantitation of rhythmic diameter oscillations in arterial microcirculation. American Journal of Physiology, 246, H508-H517.

28. Davis, M. J. & Gore, R. W. (1985). Pressure Distribution in the microvascular network of the hamster cheek pouch. Symposium on Microvascular networks: Experimental and theoretical studies, 197-209.

29. Segal, S. S. (2005). Regulation of blood flow in the microcirculation. Microcirculation, 12, 33-45.

30. Anderson, T. J., Gerhard, M. D., Meredith, I. T., Charbonneau, F., Delagrange, D., Creager, M. A., Selwyn, A. P., & Ganz, P. (1995). Systemic nature of endothelial dysfunction in atherosclerosis. American Journal of Cardiology, 75, 71B-74B.

31. Clark, E. R. & Clark, E. L. (1934). Observations on living arteriovenous anastomoses as seen in transparent chambers introduced into the rabbit's ear. The American Journal of Anatomy, 54, 229-286.

32. Moncada, S. (1993). The L-Arginine-nitric oxide pathway. N. Engl. J. Med., 329, 2002-2012.

33. Meredith, I. T. (1993). Role of impaired endothelium-dependent vasodilation in ischemic manifestations of coronary artery disease. Circulation 87(V), 56-66.

34. Neunteufl, T., Katzenschlager, R., Hassan, A., Klaar, U., Schwarzacher, S., Globar, D., Bauer, P. & Weidinger, F. (1997). Systemic endothelial dysfunction is related to the extent and severity of coronary artery disease. Atherosclerosis, 129, 111-118.

35. Website for MATLAB: www. Mathworks. com

36. Maitra, A. & Abbas, A. K. (2005). The Endocrine System. In V. Kumar, A. K. Abbas & N. Fausto (Eds.), Pathologic Basis of Disease, (pp. 1189-1201). Philadelphia: Elsevier Inc.

37. Adult Treatment Panel III Report. (2001). National Cholesterol Education Program, NHLBI. NIH Publ. # 01-3670. www. nhlbi. gov.

# BIOGRAPHICAL INFORMATION

Shruthi Raj was born in Bangalore, the Silicon Valley of India, on 10th July, 1980. She received her Bachelor of Engineering degree in Instrumentation Technology from M. S. Ramaiah Institute of Technology, Bangalore in August 2002 and joined the University of Texas at Arlington in spring 2003 for her Masters in Biomedical Engineering. Her current research interests are in vasomotion, bioinstrumentation and clinical technology.